Understanding the role of SATB1 in $CD4^+$ T cells by analysis of conditionally targeted mice generated by genetic engineering

Dissertation

zur

Erlangung des Doktorgrades (Dr. rer. nat.)

der

Mathematisch-Naturwissenschaftlichen Fakultät

der

Rheinischen Friedrich-Wilhelms-Universität Bonn

vorgelegt von

Daniel Sommer

aus Simmerath, Deutschland

Bonn, Dezember 2017

Angefertigt mit Genehmigung der Mathematisch-Naturwissenschaftlichen Fakultät
der Rheinischen Friedrich-Wilhelms-Universität Bonn

1. Gutachter: PD Dr. med. Marc Beyer
2. Gutachter: Prof. Dr. med. Joachim L. Schultze

Tag der Promotion: 09.11.2018
Erscheinungsjahr: 2018

Eidesstattliche Erklärung

Hiermit versichere ich, dass die vorliegende Arbeit ohne unzulässige Hilfe Dritter und ohne die Benutzung anderer als der angegebenen Quellen angefertigt wurde. Die aus fremden Quellen direkt oder indirekt übernommenen Gedanken sind gemäß §6 der Promotionsordnung vom 17.06.2011 als solche kenntlich gemacht.

Teile dieser Arbeit (Abschnitt 3.1.1) wurden bereits in Form eines wissenschaftlichen Artikels im Journal Nature Communications mit der Hilfe der angegebenen Autoren veröffentlicht:
Sommer, D., Peters, A., Wirtz, T., Mai, M., Ackermann, J., Thabet, Y., Schmidt, J., Weighardt, H., Wunderlich, F.T., Degen, J., Schultze, J.L., and Beyer, M., **Efficient genome engineering by targeted homologous recombination in mouse embryos using transcription activator-like effector nucleases.**
Nat Commun, 2014. 5: p. 3045.

Die Charakterisierung des SATB1-KI Modells und ein Teil der Analyse des SATB1-Flex KO Modells wurden in Zusammenarbeit mit Maren Köhne während der Erstellung ihrer Masterarbeit durchgeführt.

Bonn, 14.12.2017

Daniel Sommer

Acknowledgements

In the following section I want to express my deep gratefulness to all, who made this thesis possible.

First, I want to thank PD Dr. Marc Beyer, my first supervisor, for giving me the chance to work in this exciting project, for his constant support and his ideas, as well as the constructive scientific discussions throughout the project.

Furthermore, I thank Prof. Dr. Joachim Schultze for giving me the opportunity to work in his lab, for his scientific advice during the project and for serving as my second supervisor in this thesis.

A lot of appreciation goes to Dr. Joachim Degen, PD Dr. Heike Weighardt, PD Dr. Thomas Wunderlich, Philip Hatzfeld and Justus Ackermann, for sharing their knowledge and providing me with technical support in the genetic engineering part of this project.

Moreover, I thank all present and former members of the Genomics and Immunoregulation group, too many to mention all their names here, for the great time and their friendly support in and outside the institute, with special thanks to the people directly involved in the project, Maren Köhne, Maren Schell, Tristan Wirtz, Annika Peters, Yasser Thabet, Wolfgang Krebs, Timm Weber, Lisa Schmidleithner and Ann-Kathrin Baumgart.

Finally, I want to thank my family, my girlfriend Alisa Görgen and, especially, my grandfather Helmut Pauls, to whom this thesis is dedicated, for their support and their encouragement over the last years. Without them, this thesis would not have been possible.

Abstract

Special-AT-rich-binding protein 1 (SATB1) is a nuclear protein providing higher order chromatin organization and regulation of gene expression, especially in T cells. In regulatory T cells, SATB1 is repressed to maintain T_{reg} cell phenotype and function, whereas expression of SATB1 is associated with effector T cell responses. However, the overall impact of SATB1 on peripheral T cell function is still poorly understood, mainly due to a lack of appropriate *in vivo* models, as removal of SATB1 in mice has detrimental effects on T cell development and survival of the model organism. To address this issue and to gain a comprehensive picture of the function of SATB1 in peripheral $CD4^+$ T cells, two mouse models were generated during this thesis, which allow for spatiotemporally controlled removal (SATB1-Flex KO) and induction (SATB1-KI) of the *Satb1* gene specifically in peripheral $CD4^+$ T cells. One of these mouse models was generated by a novel genome engineering approach, whereby we could demonstrate that TALEN-assisted gene targeting can facilitate the site-directed integration of even complex targeting constructs into the genome, thus allowing a facile generation of complex genetically modified mouse models.

Analysis of the SATB1-Flex KO model revealed new insights into the biological function of SATB1 in $CD4^+$ T cell function, as it showed a yet unknown impact of SATB1 on the phenotypic switch from non-pathogenic to pathogenic TH17 cells, while the differentiation into the classical effector T cell subsets TH1, TH2 and non-pathogenic TH17 was not impaired by the removal of SATB1.

In contrast to that, the approach to evaluate the function of SATB1 in T_{reg} cells using the SATB1-KI model is not suitable, as the apparent reprogramming of T_{reg} cells hypothesized from a subset of exFoxp3 cells identified in this model is probably due to unspecific Cre-activity, rather than a SATB1-mediated effect. However, further analysis of the origin of these exFoxp3 cells might enable new insights into the role of SATB1 and Foxp3 during T_{reg} cell development in the thymus.

Zusammenfassung

Special-AT-rich-binding protein 1 (SATB1) ist ein nukleäres Protein, das vor allem in T-Zellen für die Organisation der Chromatinstruktur und die Regulation von Genexpression zuständig ist. Die Expression von SATB1 wird in regulatorischen T-Zellen unterdrückt, um den T_{reg}-Phänotyp und die T_{reg}-Funktion aufrecht zu erhalten. Im Gegensatz dazu wird die Expression von SATB1 in $CD4^+$ T-Zellen mit Effektor T-Zellfunktion assoziiert. Allerdings ist die generelle Funktion von SATB1 in peripheren T-Zellen noch nicht klar, was hauptsächlich auf einem Mangel an geeigneten *in vivo* Modellen zurückzuführen ist, da der Gesamt-Knock-out von SATB1 in Mäusen zu einer Blockade der T-Zellentwicklung und zum vorzeitigen Tod des Modellorganismus führt. Um diese Probleme zu umgehen und damit ein umfassendes Bild der *in vivo* Funktion von SATB1 in peripheren $CD4^+$ T-Zellen zu erhalten, wurden in dieser Arbeit zwei Mausmodelle generiert, die eine Entfernung (SATB1-Flex KO) bzw. eine Induktion (SATB1-KI) des *Satb1* Gens spezifisch in peripheren $CD4^+$ T-Zellen ermöglicht.

Eines dieser Mausmodelle wurde dabei mit der TALEN-Technologie, einer neuartigen Gentechnikmethode, hergestellt. Damit demonstrierten wir, dass das TALEN unterstützte Gene Targeting die lokusspezifische Integration von komplexen Targeting-Konstrukten begünstigt und somit eine erleichterte Herstellung von komplexen gentechnisch veränderten Mausmodellen ermöglicht.

Die Analyse des SATB1-Flex KO Modells ergab neue Einblicke in die biologische Funktion des SATB1 Proteins in $CD4^+$ T-Zellen, da sie einen bisher unbekannten Einfluss von SATB1 auf die Differenzierung von nicht-pathogenen in pathogene TH17-Zellen zeigte, während die Differenzierung in die klassischen T-Zell Subtypen TH1-, TH2- und nicht-pathogene TH17-Zellen nicht beeinträchtigt wurde. Im Gegensatz dazu war die Überexpression von SATB1 in T_{reg}-Zellen mit dem SATB1-KI Modell nicht geeignet, um die Funktion von SATB1 in T_{reg}-Zellen zu untersuchen, da die beobachtete Entstehung von exFoxp3 Zellen vermutlich nicht durch SATB1-vermittelte Reprogrammierung von T_{reg}-Zellen, sondern durch unspezifische Cre-Aktivität des verwendeten Foxp3-YFP-Cre Modells hervorgerufen wurde. Dennoch könnten weitere Analysen zur Herkunft dieser exFoxp3 Zellen neue Erkenntnisse über die Rolle von SATB1 und Foxp3 in der Entwicklung von regulatorischen T-Zellen im Thymus liefern.

Table of Content

List of Figures

List of Tables

Abbreviations

APC	Antigen presenting cell
BAC	Bacterial artificial chromosome
Bp	base pair
CD	Cluster of differentiation
cDNA	Complementary DNA
CDS	Coding sequence
Cre	Causes recombination
CRISPR/Cas9	Clustered-regularly-interspaced-short-palindromic-repeats/CRISPR-associated-protein-9
CTLA4	Cytotoxic T lymphocyte antigen 4
DN	double-negative
DP	double-positive
DSB	Double-strand break
DTA	Diphtheria toxin A-subunit
E_2	17β-estradiol
EAE	Experimental autoimmune encephalomyelitis
ER	Estrogen receptor
ERT1 and 2	Mutant estrogen receptors
ES cell	Embryonic stem cell
Flex	Flip-excision
floxed	Flanked by lox sites
Foxp3	Forkhead box protein 3
FRT	Recombination sites for Flp recombinase
GANC	Gancyclovir
GITR	Glucocorticoid-induced TNFR-related protein
HR	Homologous recombination
HSP	Heat-shock protein
IFN-γ	Interferon gamma
IL	Interleukine
IPEX	Immune dysregulation, polyendocrinopathy, enteropathy, X-linked
IRES	Internal ribosomal entry site
Kb	kilo base pairs
KI	knock-in
KO	knock-out
LBD	Ligand-binding domain
loxP	locus of X-over in P1
MAR	Matrix associating regions
MEF	Mouse embryonic fibroblast
MHC	Major histocompatibility complex
mLN	Mesenteric lymph node

NHEJ	Non-homologous end-joining
NLS	Nuclear localization signal
NMTS	Nuclear matrix targeting sequence
PCR	Polymerase chain reaction
pLN	Peripheral lymph node
PP	Peyer´s patches
pT_{reg}	Peripherally induced regulatory T cells
qPCR	Quantitative polymerase chain reaction
RVD	Repeat-variable di-residues
SATB1	Special-AT-rich-binding protein 1
SATB1-Flex KO	$SATB1^{fl/fl}$ x $CD4^{+/CreERT2}$ mice treated with tamoxifen
SATB1-Flex WT	$SATB1^{fl/fl}$ x $CD4^{+/CreERT2}$ mice treated with olive oil
SATB1-KI	$Foxp3^{YFP\text{-}Cre/Y}$ x $ROSA26^{SATB1\text{-}GFP/+}$ mice
SATB1-WT	$Foxp3^{YFP\text{-}Cre/Y}$ x $ROSA26^{+/+}$ mice
SP	single-positive
ssODN	small single-stranded oligodeoxynucleotides
TALE(N)	Transcription activator-like effector (nuclease)
T_{conv}	Conventional T cell
TCR	T cell receptor
tdTomato	$Foxp3^{YFP\text{-}Cre/Y}$ x $ROSA26^{LSL\text{-}tdTomato/+}$ mice
T_{eff}	Effector T cell
TGF-β	Transforming growth factor β
TH1	T helper 1
TH17	T helper 17
TH2	T helper 2
T_{mem}	Memory T cell
T_{naive}	Naive T cell
T_{reg}	Regulatory T cell
tT_{reg}	Thymic regulatory T cells
TTS	TALEN targeting site
UTR	Untranslated region
WT	Wild-type
ZFN	Zinc finger nuclease

1 Introduction

1.1 CD4$^+$ T helper cells as important and diverse players in the immune system

The vertebrate immune system is a highly-sophisticated system, which protects the host from a wide variety of pathogens by a dense interplay between its two arms, the innate and adaptive immune system [1]. While the cells and components of the innate immune system recognize evolutionary conserved patterns on pathogens or endogenous ligands and provide an immediate identification and clearance of infection, lymphocytes as the major cellular component of the adaptive immune system are able to identify a much wider range of pathogen-derived antigens due to their wide variety of antigen receptors. Thereby the adaptive immune system provides a second line of defense and ensures eradication of pathogens breaching the barrier of innate immunity.

CD4$^+$ T cells represent one of the most diverse cell types of the adaptive immune system with a wide variety of functions ranging from activation and recruitment of other immune cells for effective pathogen eradication to suppression of immune responses for the establishment of immune tolerance. This diverse functional repertoire is on the one hand based on the antigen-specific activation of CD4$^+$ T cells via their T cell receptors (TCRs), which recognize the corresponding peptide-antigen presented by antigen-presenting cells (APCs), such as dendritic cells, macrophages and B-cells, via the major-histocompatibility-complex class II (MHC-II) molecule. On the other hand, it is defined by the capability of activated CD4$^+$ T cells to differentiate into different T helper cell subsets in response to the surrounding cytokine milieu, which are specialized in promoting a distinct immune function. Furthermore, as other lymphocytes, CD4$^+$ T cells are also able to differentiate into a subset of memory cells after clearance of a primary response, which allows rapid establishment of a proper immune response upon encountering a secondary infection with the same pathogen.

Besides their role in protection against infectious agents, the different CD4$^+$ T cell subsets are also associated with different immune-related diseases, such as autoimmunity, allergies and cancer (for review see [2, 3]. Thus, the identification and understanding of the molecular mechanisms regulating the diversity of CD4$^+$ T cells are of high importance to generate appropriate strategies against these diseases, which makes CD4$^+$ T cells an interesting target for research.

1.1.1 Development of CD4$^+$ T cells in the thymus

To generate mature CD4$^+$ T cells with a diverse TCR repertoire, which recognize various peptide antigens, T cells develop in a complex and selective process in the thymus. In a process called somatic recombination the genes for the two protein chains, which form the final TCR (α- and β-chain), are randomly assembled from a pool of gene segments, yielding a unique TCR on each mature T cell leaving the thymus. As this assembly is a random process, developing thymocytes undergo a positive and negative selection process during their development to remove cells harboring non-functional receptors and receptors directed against self-antigens, which would cause severe autoimmunity (for review see [4, 5]). Thereby thymocytes interact with peptide-MHC complexes presented by different types of thymic epithelial cells and APCs and receive signals through their TCR. Cells, which receive too weak (positive selection) and too strong (negative selection) signals, respectively, die by apoptosis and are removed from the system.

TCR assembly, as well as positive and negative selection are not performed in a single step, but occur over different developmental stages in different parts of the thymus: in an initial step precursor cells enter the cortex of the thymus and start rearranging the TCR β-chain. As these cells do not express the T cell co-receptors CD4 and CD8, this developmental stage is called the double-negative (DN) stage. Once a functional β-chain has been formed, the TCR α-chain is assembled, which is accompanied by expression of the T cell co-receptors CD4 and CD8 (double-positive (DP) stage). At this DP stage, the assembled TCR undergoes positive selection. Furthermore, depending on its affinity to peptides presented either by MHC class I or II molecules, a lineage decision is made, whether the cell develops into the CD4 single-positive (SP) or CD8 SP T cell lineage, which is accompanied by removal of the other co-receptor. After lineage commitment, SP thymocytes enter the thymic medulla to undergo negative selection. Cells surviving this selection subsequently leave the thymus as mature CD4$^+$ or CD8$^+$ T cells.

While CD8$^+$ T cells leave the thymus as naive T cells, CD4$^+$ T cells can either develop into naive T cells (T_{naive}), which further differentiate into different effector T cell subsets (T_{eff}) upon activation in the peripheral lymphoid organs, or into regulatory T cells (T_{reg}), which promote immunosuppression in the periphery (for a detailed description of T_{eff} and T_{reg} cell subsets see paragraph 1.1.2 below). According to current concepts these differential outcomes of thymic CD4$^+$ T cell development

mainly depend on different TCR affinities, in which CD4 SP precursor cells with no affinity to self-peptides develop into T_{naive} cells. In contrast to that T_{reg} cells develop from precursor cells with intermediate affinity to self-peptides, which survived negative selection by successfully competing for the availability of the cytokine interleukin-2 (IL-2) and, to a lesser extent, IL-7 and IL-15 [6-8]. Although this general concept of TCR avidity and cytokine competition is well accepted, the details how the T_{reg} cell program is elicited are still controversially discussed. Some studies showed that TCR signaling in response to self-peptide recognition leads to an upregulation of the IL-2 receptor α-chain (CD25), which in consequence promoted IL-2 signaling and with it survival of the cell and initiation of the T_{reg} cell program by inducing the expression of the T_{reg} cell lineage-defining transcription factor Foxp3 [7, 8] (see paragraph 1.1.2 below). In contrast to that Tai *et al.* [6] recently reported that TCR signaling in response to self-peptide recognition directly induced Foxp3 expression, which in consequence promoted a pro-apoptotic program. To prevent apoptosis, these $Foxp3^+$ T_{reg} precursor cells have to compete for a limited amount of IL-2, whereby surviving cells develop into mature T_{reg} cells, while cells losing this competition undergo apoptosis and are removed from the system.

Despite the controversial discussion, both concepts seem to be valid, as the respective $Foxp3^-CD25^+$ and $Foxp3^+CD25^-$ precursor T cell subsets are present in the thymus.

1.1.2 $CD4^+$ T cell subsets

After leaving the thymus mature naive $CD4^+$ T cells circulate through the blood to the peripheral lymphoid organs. Upon recognizing peptide antigens presented by APCs via their TCR and co-stimulation via CD28 (for review of CD28 co-stimulation see e.g. [9]) $CD4^+$ T_{naive} cells are activated and subsequently differentiate into T_{eff} cells. Depending on environmental factors, such as the cytokine milieu, T_{naive} cells can differentiate into different T helper cell subsets, each having distinct functions during an immune response (Figure 1.1).

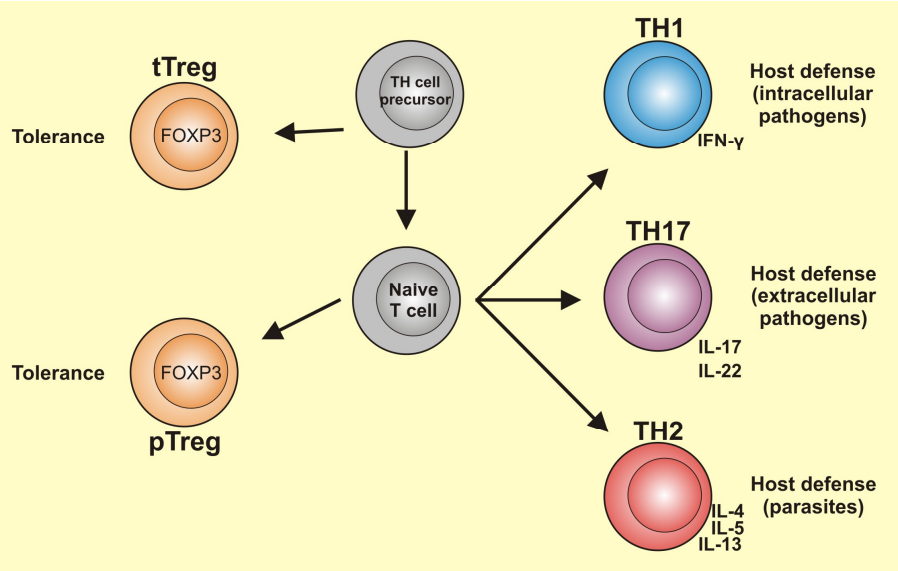

Figure 1.1 T helper cell subsets
SP TH precursor cells in the thymus differentiate either into naive or regulatory T cells (tT_{reg}) depending on TCR avidity and cytokine availability and leave the thymus as mature cells. In the periphery, naive T cells further differentiate into various effector cell subsets or into peripheral T_{reg} cells (pT_{reg}) promoting host defence or tolerance, respectively. Differentiation is elicited by stimulation of the cells through TCR and CD28 and defined by the surrounding cytokine milieu.

These subsets can be identified on the one hand by key transcription factors mainly involved in differentiation and maintenance of the respective subset and on the other hand by the cytokines generated after differentiation.

T helper 1 and 2 (TH1 and TH2), initially described by Mosmann *et al.* in 1986 [10], were the first two helper T cell classes known. TH1 cells are formed in the presence of interleukin 12 (IL-12) and interferon gamma (IFN-γ), which stimulate the induction of the transcription factor T-bet, the master regulator of TH1 differentiation [11], and the production of IFN-γ. Thereby TH1 cells promote activation of innate immune cells, especially macrophages, which subsequently are able to lyse engulfed pathogens, thus, providing protection against obligate intracellular pathogens.

TH2 cells are the T cell subset mainly responsible for eradication of parasites, such as helminths and nematodes, as they are involved in eosinophil, basophil and mast cell recruitment [12]. The cytokines produced by TH2 cells are IL-4, IL-5, IL-10 and IL-13, with IL-4 also being required for differentiation of naive cells into TH2 cells [13]. IL-4 induces the transcription factor Gata-3, which is the master regulator for TH2 differentiation [14].

Besides the two classical T_{eff} cell subsets a third subset has been described, which was called T helper 17 (TH17) cell subset, according to the main cytokine produced by these cells, IL-17 [15]. The function of TH17 cells is the eradication of extracellular

pathogens by recruitment of neutrophils to the site of infection and the induction of antimicrobial peptides (for review see [16]). The cytokines promoting TH17 differentiation along with TCR and co-stimulation are IL-6 and transforming growth factor β (TGF-β) [17]. These signals, acting in concert, induce an up-regulation of the orphan nuclear receptor RORγt, the master transcription factor for TH17 cells [18]. After an infection has been cleared, the effector T cell subsets shrink by apoptosis and a pool of memory T cells (T_{mem}) is established to provide a rapid response upon a secondary infection with a pathogen. In the mouse $CD4^+$ T_{mem} cells can be distinguished from T_{naive} by the expression of the surface molecule CD44 [19].

Besides effector T cell subsets promoting inflammatory responses as described above, there is an additional T cell subset, which is mainly involved in maintaining self-tolerance and immune homeostasis by acting as immune suppressors. These T_{reg} cells were first described by Sakaguchi *et al.* in 1995 [20] and promote immunosuppression mainly via production of inhibitory cytokines, metabolic disruption, such as IL-2 deprivation, and modulation of dendritic cell function and maturation, as well as cytolysis of the targeted cell (for review see e.g. [21]).

T_{reg} cells are characterized by the central lineage-defining transcription factor forkhead box protein 3 (Foxp3), which is essential for the induction of the T_{reg} cell phenotype in the thymus as well as for its maintenance in the periphery [22].

The importance of Foxp3 for the generation and maintenance of T_{reg} cells is further supported by the human disease IPEX (immune dysregulation, polyendocrinopathy, enteropathy, X-linked) and its murine analogue, the scurfy mouse model, which both harbor non-functional *Foxp3* mutations and are characterized by an hyperproliferation of $CD4^+$ T lymphocytes, as well as extensive multi-organ infiltration and severe autoimmunity [23, 24].

In addition to Foxp3, T_{reg} cells are characterized by the expression of the surface molecules CD4 and CD25, cytotoxic T lymphocyte antigen 4 (CTLA4) and glucocorticoid-induced TNFR-related protein (GITR) [25, 26].

As already mentioned (paragraph 1.1.1), T_{reg} cells develop in the thymus from developing thymocytes. These cells are called natural or thymic regulatory T cells (tT_{reg}) [27]. However, in addition to these thymically derived cells, T_{reg} cells can also differentiate from naive T cells in the periphery upon antigen contact in the presence of T_{reg} cell promoting conditions, such as cytokines (TGF-β), low-dose-antigen or

suboptimally stimulated APCs [28]. Cells derived from this pathway are known as peripherally induced regulatory T cells (pT_{reg}) [27].

1.1.3 Stability of $CD4^+$ T cell subsets

While $CD4^+$ T cell subsets were initially regarded as separate and irreversibly differentiated lineages, in recent years the concept of plasticity among the different T cell subsets, which proposes a certain degree of flexibility between the T helper subsets, has become more popular through experimental evidence supporting this plasticity between TH cell subsets.

Amongst the T helper cell subsets, TH17 cells are probably the most plastic ones. As shown by fate mapping experiments in mice [29], TH17 cells induce the production of IFN-γ during the course of chronic inflammation, indicating that cells committed to the TH17 subset can change their phenotype in response to the surrounding inflammatory environment. In line with this observation, another study identified IFN-γ-producing TH17 cells in patients suffering from Crohn´s disease [30], suggesting that the phenotypic changes of TH17 cells under chronic inflammation are also present in humans.

In addition to plasticity between TH17 and TH1 cells, Cosmi *et al.* [31] reported the presence of a population of cells in human blood, which expressed IL-17 and IL-4. Although these TH17/TH2 cells were very rare, they were significantly enriched in the blood of patients suffering from chronic asthma.

Furthermore, a study by Kastirr *et al.* [32] further supported the existence of the interplay and conversion of TH17 and TH1 cells. In this study, the conversion of TH17 into pathogenic TH17/TH1 cells was prohibited by IL-21. Additionally, IL-21 lead to the production of IL-10 and to the development of a regulatory phenotype.

Besides TH17 cells, the plasticity of T_{reg} cells has been extensively investigated over the last years. However, in contrast to TH17 cells, plasticity in T_{reg} cells is still less accepted and controversially debated. Zhou *et al.* [33] were the first, who proposed an instable T_{reg} cell phenotype, as they showed with fate mapping experiments that a substantial percentage of all T_{reg} cells found in the periphery had lost Foxp3 and produced effector cytokines (exFoxp3 T_{reg} cells). However, other studies demonstrated that these exFoxp3 cells were not derived from bona fide T_{reg} cells under homeostatic conditions [34], but might be the result of a promiscuous expression of Foxp3 during thymic development in cells, which had discontinued T_{reg} cell development and had developed into T_{naive} cells instead [35]. In contrast, Bailey-

Bucktrout *et al.* [36] showed in an induced autoimmune encephalomyelitis model (EAE) that bona fide T_{reg} cells were indeed unstable under inflammatory conditions. This study finally resulted in the currently accepted general model of T_{reg} cell plasticity, in which T_{reg} cells are generally stable under homeostatic conditions, but preferentially pT_{reg} cells can lose Foxp3 expression and gain effector function during an inflammatory response, which is reversed with the resolution of the inflammation. However, despite this compromise, the debate about T_{reg} cell plasticity is still ongoing and a lot of work is still necessary to clarify the stability of T_{reg} cells.

Finally, the plasticity of TH1 and TH2 cell subsets has also been heavily investigated over the last years. Whereas earlier studies had shown that both subsets were irreversibly defined lineages with repression of cytokine profiles and genes contributing to the opposing lineage to maintain their effector T cell program even under changing environmental conditions [37, 38], a more recent study [39] assessing global epigenetic changes yielded different results: Although some cytokine loci were indeed epigenetically silenced, other genes, especially transcription factors, were not clearly repressed, but in a poised state, which might contribute to $CD4^+$ T cell plasticity. Furthermore, other studies [40, 41] detected cells with TH1 and TH2 cell properties, which were even able to generate long-term memory cells harboring both fates. These data supported that TH1 and TH2 can be co-expressed in the same cell.

Taken together these studies show that plasticity exists across all currently known $CD4^+$ T cell subsets. Moreover, these studies indicate that T cell plasticity seems to play an important role in immune responses [40], as well as in immunological diseases, such as autoimmunity and allergy [30, 31, 36]. Thus, further knowledge about the role of T cell plasticity in the context of these diseases, as well as the underlying molecular mechanisms and target proteins could help to understand the development of these diseases and could provide novel treatment options, such as reprogramming of self-reactive effector cells into tolerizing regulatory T cells. Furthermore, reprogramming of regulatory T cells inhibiting effective immune responses could help in the treatment of neoplastic diseases, as it has been shown in several studies that T_{reg} cells can migrate to the tumor microenvironment and inhibit effective anti-tumor responses (for review see e.g. [42]).

1.2 Generation of genetically modified murine model organisms by gene targeting

Mice are widely used model organisms in immunology and other fields of biomedical research to simulate human diseases and to analyze the function of genes *in vivo*. One of the reasons for the extensive use of mice as model organisms is the ability to precisely modify the murine genome in a process known as gene targeting, which had been discovered by Thomas and Capecci in 1987 [43]. The importance and the demand to generate genetically modified mice can be seen by the fact that since its first description gene targeting of the murine genome has been distributed to most biomedical laboratories and has led to the foundation of large consortia with high-throughput gene targeting facilities aiming at the mutation of all protein coding and non-coding genes for *in vivo* analysis [44-46].

Gene targeting for the generation of murine models is based on the finding that exogenous DNA can be integrated site-specifically into the genome of mammalian cells by homologous recombination (HR) [47-49], a cell-intrinsic DNA repair pathway (for review see [50]), as well as the discovery that embryonic stem cells (ES cells) can be cultured *in vitro* [51] and later on injected into blastocysts to yield chimeric animals able to propagate the genetic alterations to their offspring [52].

Based on these findings a general concept to generate gene targeted mice was developed [53], which, with small modifications, is still used today as standard technique (Figure 1.2): after transferring a targeting construct containing a resistance gene as well as sites homologous to the desired integration site into pluripotent ES cells, the construct will integrate into the genome by homologous recombination after the formation of a DNA double-strand break (DSB), thereby leading to the disruption of the open reading frame of the targeted gene (Figure 1.2 upper left panel). In a next step, cells harboring the targeting construct in their genome are positively selected by antibiotic selection, followed by negative selection with gancyclovir (GANC). This second selection step is necessary to enrich for targeted ES cell clones, as most positively selected clones show random integration of the targeting construct [43]. Due its location outside of the homology regions, the *HSV-tk* gene, which encodes for the GANC susceptibility, will be retained in the case of random integration of the targeting construct, making cells susceptible to GANC, while homologously recombined clones will lose the *HSV-tk* gene, thus staying resistant to GANC [53] (Figure 1.2 lower left panel).

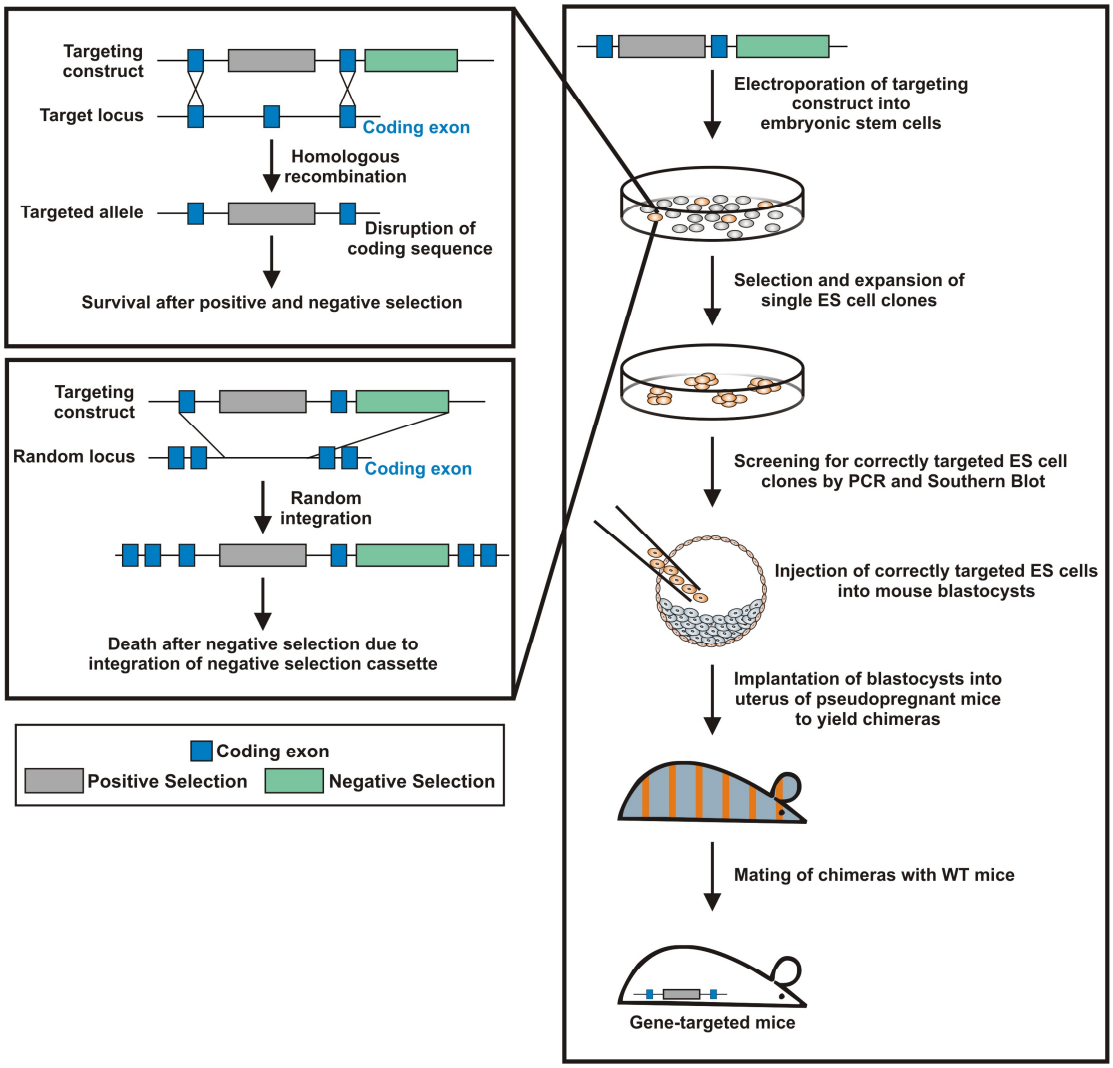

Figure 1.2 General workflow for the generation of targeted mice by homologous recombination in murine embryonic stem cells
A targeting construct containing genes for positive and negative selection as well as sites homologous to the desired integration site is electroporated into pluripotent ES cells, which will lead to integration of the construct into the genome, either by homologous recombination (upper left panel) or by random integration (lower left panel). Homologous recombination will lead to integration of the resistance gene for positive selection thereby disrupting the open reading frame of the targeted gene and rendering the cells resistant for the subsequent positive selection step. In addition, the negative selection gene is not integrated by homologous recombination, thus keeping the cell resistant to negative selection. In contrast, random integration will lead to insertion of both selection genes, thereby making cells susceptible to negative selection, which will reduce the number of randomly integrated cell clones. ES cell clones surviving the selection process are screened for correct integration of the targeting construct at the desired locus by PCR and Southern blot analysis. Correctly targeted clones are injected into blastocysts and the injected blastocysts are implanted into pseudo-pregnant foster mice, resulting in chimeric offspring. Chimeras can be easily identified by a mixed coat color since the injected ES cells encode for a different coat color than the recipient blastocysts. Finally, chimeras are crossed to WT animals to obtain a founder mouse, which can be used for the establishment of a new targeted mouse line.

As negative selection with *HSV-tk* and GANC requires an additional selection step, the diphtheria toxin A-subunit (DTA) is used as an alternative approach [54]. Here the encoded protein itself is toxic to the cell, so that there is no need for the addition

of a chemical agent. Thus, negative selection takes place simultaneously with the positive selection.

After the selection process, the ES cell clones are analyzed by classical molecular biology approaches, e.g. Southern blot and PCR analysis to confirm correct targeting of the desired locus, followed by injection of correctly targeted ES cell clones into blastocysts and implantation of the injected blastocysts into pseudo-pregnant foster mice. The resulting chimeric offspring, which can be easily identified by a mixed coat color due to the fact that the injected ES cells encode for a different coat color than the recipient blastocysts, are then crossed to wild-type (WT) animals. If germ cells of these chimeras originate from the injected ES cells, the targeted gene will be transmitted through the germ line to the next generation, giving rise to a founder mouse, which can be used for the establishment of a new targeted mouse line.

1.2.1 Conditional gene targeting with the Cre/loxP system

Although the initial approach of gene targeting enabled new insights into gene function and biological processes, it has some limitations. Due to the disruption of the targeted gene in all tissues and from the beginning of embryonic development, embryonic lethality or early death of the animal might be the consequences, if the disrupted gene was required for developmental processes, thus, precluding the analysis of gene function at later developmental stages or the establishment of a homozygously targeted knock-out (KO) mouse line. Furthermore, analyses of gene abrogation in a certain tissue or cell type might be altered by bystander effects of surrounding cells also suffering from the genetic defect. To circumvent these problems advanced methods, known as conditional gene targeting, have been developed, allowing spatial and temporal alteration of a gene of interest [55].

One of the most important systems for conditional gene targeting is the Cre/loxP system.

Cre (**c**auses **re**combination) is a site-specific recombinase of the bacteriophage P1 and recognizes a 34 base-pair (bp) sequence, known as loxP (**lo**cus of **X**-over in **P**1) and consisting of two 13 bp inverted repeats and an eight bp spacer region, which is used for the strand exchange during the recombination reaction [56]. To perform Cre-mediated recombination two Cre molecules bind to the inverted repeat regions of a loxP site, forming a dimer at each site. This dimer subsequently forms a tetramer by interaction with a second Cre-loxP dimer, thereby building a recombination synapse. In this synapse one strand of each loxP site is cleaved by a conserved tyrosine

residue (Tyr324) in the 8 bp spacer region to form a covalent phosphotyrosine bond at the 3´end of the double-strand break, as well as a free hydroxyl group at its 5´ end. This hydroxyl group consequently reacts with the phosphotyrosine of the other loxP site to form a phosphodiester bond, which ligates the two DNA ends together in a Holliday junction like structure. The repetition of this process with the respective complementary strands finally leads to dissolution of the recombination synapse and the release of the two newly recombined DNA molecules.

Although the actual recombination reaction is always constant, the consequences for the Cre-recombined loci or DNA molecules vary depending on the orientation of the loxP sites to each other, with their directionality being determined by the 8 bp spacer sequence within the loxP site (Figure 1.3): while Cre-mediated recombination of loxP sites arranged in opposite directions on the same DNA molecule will lead to an inversion of the intermediary DNA [57] (Figure 1.3b), their orientation in the same direction will result in an excision of the interjacent DNA as circular molecule and a single loxP site remaining in the genome [58] (Figure 1.3a).

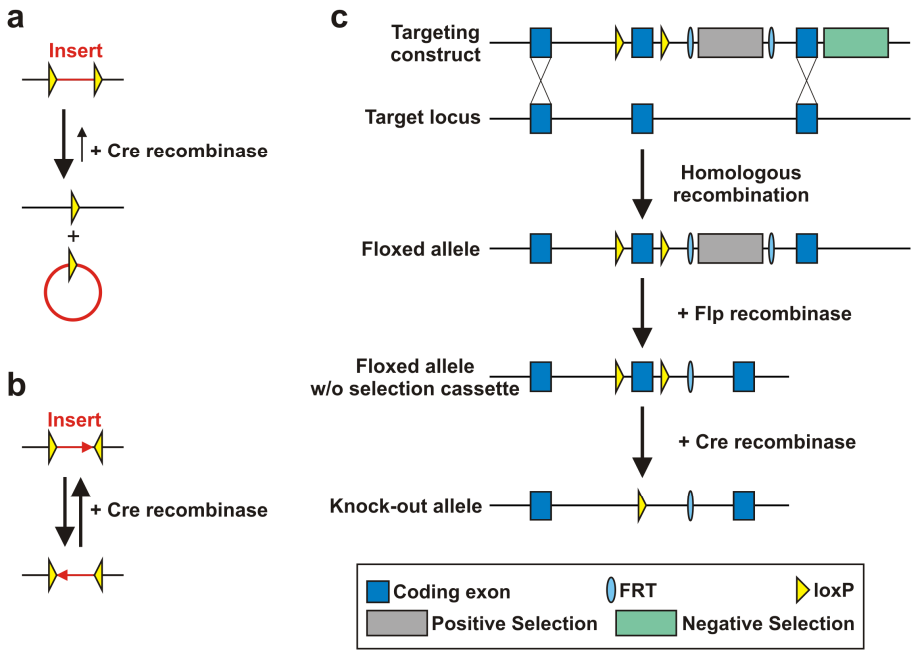

Figure 1.3 Cre-mediated recombination
(a and b) Varying outcomes of Cre-mediated recombination depending on the orientation of loxP sites. loxP sites arranged in parallel lead to excision of the intervening DNA (a), while orientation of loxP sites in opposite directions causes reversible inversion of the intervening DNA (b). (c) Generation of a conditional knock-out allele by gene targeting and subsequent removal of the gene by Cre-mediated recombination (for details of the removal of the selection cassette by Flp recombinase see paragraph 1.2.1.4).

Since the intermediary DNA in the latter case is excised from the genome and due to the fact that this excision reaction is favored over the integration reaction [59], this

system is very suitable for the removal of genes from the genome and thus has emerged as the method of choice for conditional gene targeting.

To enable conditional gene targeting by the Cre/loxP system, the target region in the genome has to be flanked by lox sites (“floxed”) arranged in the same orientation, which requires classical gene targeting by homologous recombination (Figure 1.3c). The floxed allele can then be conditionally removed by Cre-mediated recombination *in vitro* and *in vivo*. For the latter case, expression of Cre recombinase can be restricted to certain cell types, tissues or developmental stages, as described in the following paragraph.

1.2.1.1 Spatiotemporal Cre-mediated recombination

The most common approach to restrict Cre recombinase expression to certain cell types or developmental stages in the mouse is the generation of genetically modified mice expressing Cre recombinase under the control of a tissue or cell type specific promoter. These mice can be crossed to any mouse line harboring a floxed allele, which will result in offspring with a gene deletion only in those cell types or tissues expressing the Cre recombinase. Gu *et al.* [60] demonstrated the functionality and usefulness of this approach by limiting the gene inactivation of DNA polymerase-β (*polβ*) to the T cell lineage, thereby circumventing the embryonic lethality of the complete *polβ* knock-out and allowing the analysis of *polβ* deficiency in the T cell lineage. For this purpose, they crossed a mouse harboring a floxed *polβ* gene with a transgenic mouse line expressing Cre recombinase under the control of the proximal promoter of the *lck* gene [61].

Most tissue/cell-type specific Cre lines are generated by random insertion of Cre-encoding constructs into the genome using microinjections of the DNA into the pro-nucleus of a fertilized oocyte. For this approach, different types of constructs can be used. While Orban *et al.* [61] used a strategy based on a Cre construct containing only the proximal part of the *lck* promoter, others made use of bacterial artificial chromosomes (BAC), commercially available DNA vectors carrying large (approx. 200-400 kb) human or murine genomic fragments. The Cre open reading frame is inserted into a BAC encoding the gene, to which Cre expression should be restricted. The advantage of this approach compared to the use of plasmid based constructs is that due to the size of the BAC the expression of the construct is less affected by the surrounding integration sites and that even distant regulatory elements of the Cre-driving gene are integrated into the genome (for review see [62]). This subsequently

leads to an expression of the Cre recombinase, which reflects the expression of the Cre-driving gene in the respective tissue/cell-type more truthfully.
As an alternative to random integration, Cre recombinase carrying constructs are also integrated site-specifically into the locus of the tissue/cell-type specific gene via gene targeting. Thereby the endogenous gene will either be destroyed due to the integration of the Cre open reading frame [63], or a bicistronic gene will be generated by insertion of the Cre open reading frame downstream of the coding sequence of the endogenous gene and separating both cistrons with an internal ribosomal entry site (IRES) [64].

1.2.1.2 Posttranslational control of Cre-mediated recombination

In addition to the transcriptional control of Cre recombinase in murine model organisms (paragraph 1.2.1.1), Cre-mediated recombination can also be controlled on posttranslational level by fusion of Cre recombinase to the ligand-binding domain (LBD) of the estrogen receptor (ER) and addition of its synthetic ligand 4-hydroxytamoxifen [65]. In absence of its ligand, Cre-mediated recombination is prevented, as the LBD-Cre fusion protein is kept in the cytosol by heat-shock proteins (HSP). Upon ligand binding, however, the fusion protein is released from HSP binding and translocated to the nucleus enabling Cre-mediated recombination. Since wild-type LBDs also recognize the natural ER ligand 17β-estradiol (E_2), which accordingly leads to high background Cre-activity in absence of the synthetic ligand, mutant LBDs, termed ERT1 and ERT2, were developed. These mutant LBDs do not recognize E_2, but show high affinity to 4-OH tamoxifen and high recombination rates, when fused to Cre recombinase [66].
Thus, the CreERT1/2 system enables an additional level of conditional gene targeting, since due to the application of an exogenous agent (tamoxifen) it allows the specification of the time point of Cre-mediated recombination. Furthermore, combining this posttranslational control of Cre recombination with approaches to restrict Cre expression to certain cell-types or tissues (see paragraph 1.2.1.1) enables further specificity, as here Cre recombination can be induced time- and site-specifically.

1.2.1.3 Use of the Cre/loxP system beyond simple gene deletion

Besides its use as a sole deleting agent, the Cre/loxP system is also utilized for other purposes of gene modification in mice, such as the conditional induction of

transgenes [67]. For this purpose, a construct containing a strong promoter and the coding sequence of the transgene is integrated into the genome. To allow conditional overexpression, promoter and coding sequence are separated by a floxed transcriptional stop cassette consisting of several polyadenylation signals, which suppresses expression of the transgene. Upon Cre-mediated recombination this stop cassette is removed and expression of the transgene is enabled. Thus, by crossing such transgenic mouse lines with an appropriate Cre-line spatiotemporal induction of the transgene can be achieved.

Analogous to the generation of tissue/cell-type specific Cre-lines, these conditional overexpression mouse lines can also be generated by gene targeting rather than by random transgenesis, which results in the integration of the overexpression construct at a defined site in the genome. However, due to the integration of the promoter and the transcriptional stop cassette the targeted locus will ultimately be destroyed. Thus, to prevent adverse events resulting from the destruction of the original locus, gene targeting of such overexpression constructs is typically performed at the *Rosa26* locus, a locus for which no known adverse events upon destruction have been reported [68]. Furthermore, the *Rosa26* locus serves as an appropriate environment for the integration of transgene-encoding constructs, as it is expressed in all tissues of the murine embryo and the adult mouse, thus reducing the risk of epigenetic silencing of the integrated construct [68, 69].

In addition to deletion and induction of genes the Cre/loxP system can also be used for gene replacement, in which an existing gene is exchanged with another one, such as a reporter gene or a variant of the endogenous gene. For this purpose, Schnütgen *et al.* [70] developed an approach, known as flip-excision (Flex), which is based on the inversion capabilities of Cre-mediated recombination at loxP sites arranged in opposite directions to each other (Figure 1.3b). However, since this inversion is a reversible process and thus would not result in a stable gene exchange, the Flex approach uses two pairs of heterotypic lox sites (a wild-type and a mutated form of loxP). As the different lox variants only interact with homotypic, but not with heterotypic lox sites, this arrangement leads to a stable inversion reaction in a two-step process (Figure 1.4a): in a first step, Cre-mediated recombination is performed via one of the two lox pairs, leading to an inversion of the interjacent DNA, as well as a rearrangement of the lox sites, in which one lox site is flanked by two homotypic lox sites orientated in the same direction. Due to this arrangement of lox sites, this floxed

heterotypic lox site and one of the flanking lox sites will be deleted in a second step of Cre-mediated recombination, which finally results in an inverted gene segment with two heterotypic lox sites. As these two heterotypic lox sites cannot further interact with each other, Cre-mediated recombination is prevented, which results in an irreversibly inverted gene segment.

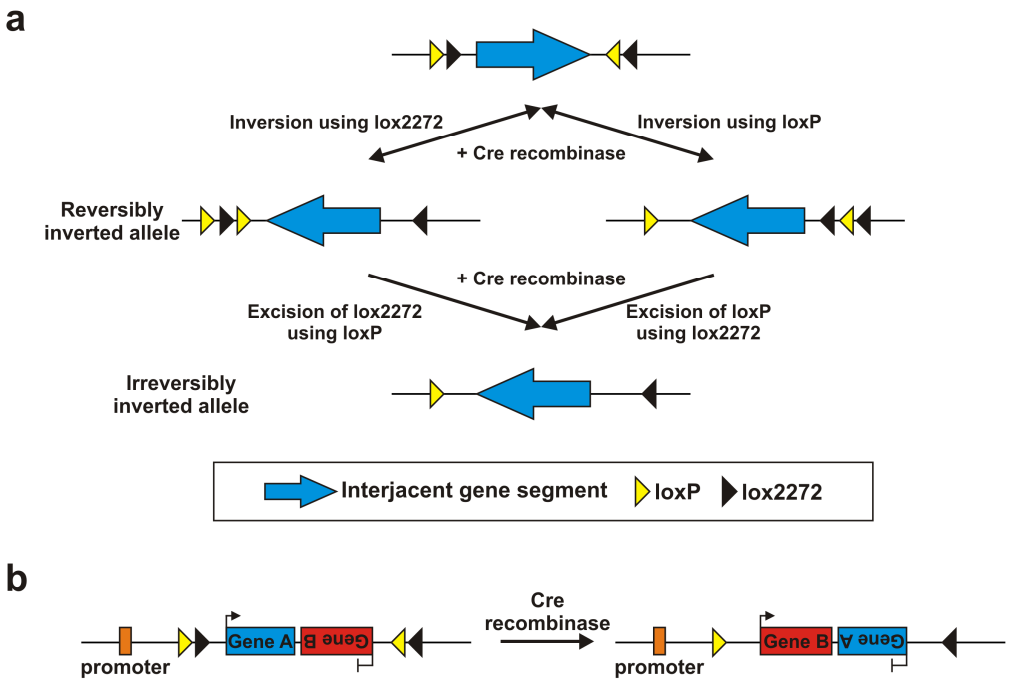

Figure 1.4 Exchange of gene segments using the Flex-system
(a) General mechanism of Cre-mediated irreversible inversion of a gene segment. (b) Irreversible replacement of Gene A with Gene B.

Thus, by performing gene targeting with a construct harboring this Flex cassette as well as the targeted gene segment (Gene A) followed by the replacing gene (Gene B) in inverse orientation, this allows for an irreversible replacement of Gene A with Gene B (Figure 1.4b).

1.2.1.4 Flp/FRT system

A further recombination system used in conditional gene targeting is the Flp/FRT system, which uses a recombinase and recognition site derived from the yeast *Saccharomyces cerevisiae*. Similar to Cre recombinase, Flp recombinase recognizes recombination sites (FRT sites) with two 13 bp repeat regions and an eight bp core region [71], which is used for the directionality of the FRT site as well as for the strand exchange reaction. In contrast to Cre, however, it has been shown that the recombination efficiency of this 34 bp minimal FRT site can be increased, when flanked by an additional Flp binding site, which finally yields a 48 bp FRT sequence.

Furthermore, in contrast to Cre, wild-type Flp recombinase is more thermolabile, thus making it unsuitable for use in mammalian organisms [72]. To circumvent this problem Flpe, a mutated form of the wild-type Flp recombinase harboring four amino acid exchanges, has been developed, which shows higher thermostability and higher recombination efficiencies in mammalian cells compared to wild-type Flp recombinase [73].

However, although the Flp/FRT system has been improved and adapted for the use in mammalian systems, it is rarely used in murine model systems for the conditional deletion of genes. Instead, in most cases Flp/FRT is only used for the removal of selection cassettes from genes conditionally targeted with a loxP flanked cassette (Figure 1.3c).

1.2.2 Improvement of gene targeting by TAL effector nucleases

Despite its benefits for biomedical research, classical gene targeting via homologous recombination still has some limitations, which impede the generation of genetically modified mouse models for every gene or disease. The major drawback of this approach is the low efficiency of homologous recombination, which in consequence requires generation and screening of a huge number of ES cell clones to obtain a sufficient number of correctly targeted clones for further processing. In line with this, Thomas *et al.* [49] reported a ratio of one correctly targeted clone in 1000 clones analyzed in their initial gene targeting approaches. Some loci, such as the murine Y chromosome, are even not targetable at all by homologous recombination [74, 75]. Furthermore, the low efficiency of homologous recombination has long precluded the generation of mice harboring more than one genetic modification on the same chromosome, as several rounds of gene targeting and cell culture would be required to obtain the respective clones.

To overcome these obstacles, genetically engineered site-specific nucleases, such as zinc finger nucleases (ZFN), transcription activator-like effector nucleases (TALENs) and the clustered-regularly-interspaced-short-palindromic-repeats/CRISPR-associated-protein-9 (CRISPR/Cas9) system, have been identified and developed over the last decade (for review see [76]).

Despite their different origins, their different structures and their different modes of DNA recognition, these nuclease systems share the same principle, the introduction of DNA double-strand breaks at desired sites in the genome.

Due to the induction of a DSB, the DNA repair machinery of the cell is activated and DSBs are either repaired by non-homologous end-joining (NHEJ), a mechanism, which ligates the two ends of the break together without using a repair template (for review see [77]), or by homologous recombination.

NHEJ-mediated repair is very error-prone and often leads to the introduction of small insertions or deletions at the site of the DSB, which result in mutations in the affected gene. Thus, by introducing site-directed DSBs into exons of a gene by engineered nucleases, mutations, such as frameshifts or nonsense mutations, can be introduced into a gene, which will consequently result in a targeted gene disruption.

In addition to simple gene mutations, engineered nucleases can also support the insertion of targeting constructs into the genome by homologous recombination, when an appropriate repair template containing regions homologous to the sequences surrounding the DSB is administered together with the engineered nucleases.

The first attempts of using engineered nucleases for gene targeting were very limited, as they solely relied on ZFN technology, which is technically challenging and strictly protected by intellectual property rights [78]. However, the discovery of TALENs and the CRISPR/Cas9 system as alternatives to ZFNs has dramatically accelerated the use of engineered nucleases for genome engineering, as these systems are freely available for academic use and their assembly is much easier compared to ZFNs (for a detailed review of the CRISPR/Cas9 system see e.g. [79]).

TALENs originate from virulence factors of the plant pathogen *Xanthomonas spp.*, which can bind to specific sites in the plant genome to control expression of the host´s genes [80]. Boch *et al.* [80] discovered that the DNA binding capacity of TAL effectors (TALEs) was based on repetitive subunits (repeats) consisting of 33-35 amino acids, each recognizing a single DNA base. Base-specificity is thereby determined by the amino acid residues at the 12^{th} and 13^{th} position of each repeat, which are termed repeat-variable di-residues (RVD). Furthermore, this study revealed the possibility to generate artificial TALEs to target desired regions in the genome by sequential assembly of appropriate repeat units.

Based on these findings Christian *et al.* demonstrated the generation of TALE nucleases (TALENs), which they used to induce DSBs at specific target sites [81]. For this purpose, they adopted the molecular architecture of ZFNs and fused a monomer of the FokI endonuclease to a TALE domain, which in turn was recruited to

the desired target site to initiate the DSB. As the FokI endonuclease is only active as a dimer, a second TALEN binding on the reverse strand in close proximity to the first one was additionally required to provide the second FokI monomer and generate the DSB.

Since this first proof of principle, this concept has been improved by several other groups and many different protocols for efficient and easy assembly of TALENs have been developed [82-89].

Furthermore, TALENs have been successfully applied in murine gene targeting. Wang *et al.* (2013) for instance reported successful TALEN-mediated targeting of two genes located at the Y chromosome, as well as insertion of a GFP expression cassette at these loci, which had not been possible using classical gene targeting [75]. Others reported an increase in gene targeting efficiency, which allowed them to skip the laborious ES cell culture and to perform gene targeting directly in oocytes [90-92]. Li *et al.* [91] even reported targeting of up to three genes per oocyte. While these studies focused on the TALEN-mediated introduction of mutations via the NHEJ DNA repair pathway, Wefers *et al.* [92] showed that TALEN-assisted gene targeting in oocytes could also be used to insert exogenous DNA into the genome via homologous recombination. Interestingly, they used small single-stranded oligodeoxynucleotides (ssODN) as repair templates instead of large plasmid based targeting constructs, which lead to a further simplification of the gene targeting approach, as the repair template could be generated by oligo synthesis rather than by labor-intensive cloning attempts. However, another study [93] also reported successful TALEN-assisted integration of a plasmid-based targeting construct with long homology arms analogous to classical gene targeting constructs. Although this larger targeting construct was only used for the introduction of a point mutation, which had also been achieved with the injection of ssODNs by Wefers *et al.* [92], the study by Jones and Meisler provided proof-of-principle that TALENs can also increase the homology directed integration of a larger plasmid-based targeting construct in oocytes. Taken together, these findings established a basis for the TALEN-assisted introduction of larger changes into the genome, which relies on such plasmid-based targeting constructs.

1.3 Special-AT-rich-binding protein 1 (SATB1)

Regulation of T cell development and differentiation has been mainly attributed to external signals, such as cytokines, and transcription factors. However, in the last years, chromatin organization has been identified as another level of regulation. The term chromatin organization in this context comprises different levels of modifications, which regulate the accessibility of chromatin regions for the transcriptional machinery, such as histone modifications or the change of the three-dimensional structure of chromatin by formation of chromatin loops (for review see [94]).

One of the proteins involved in the organization of chromatin is special AT-rich binding protein 1 (SATB1), a nuclear protein, which has been discovered by Dickinson *et al.* in 1992 by screening proteins derived from a human testis cDNA library for their ability to bind to matrix associating regions (MAR) [95].

MARs are DNA sequences located upstream of gene loci and regulatory elements, such as the immunoglobulin heavy chain enhancer [95] and serve as binding sites for the nuclear matrix to chromatin, thus providing higher-order chromatin organization and contribution to gene regulation [96]. MARs lack specific consensus sequences, but contain a certain sequence context, termed ATC sequences, which consists of only adenines, thymines and cytosines on one strand, but no guanines [97]. SATB1 was reported to have high affinity to such sequences [95].

Although *Satb1* had been identified in cDNA derived from testis, it could be shown that it is highly expressed in the mouse thymus and to some degree in the brain [95]. The latter observation is supported by the fact that SATB1 KO mice die 4 weeks after birth from neurological defects [98]. Alvarez *et al.* could further show that SATB1 is predominantly expressed in thymocytes and regulates about 2 % of all expressed genes in these cells, which was the first indication that a MAR binding protein can act as a global regulator in a specific cell lineage and demonstrated that SATB1 is highly important for the development of T cells. This important role for T cell development is further supported by the observation that SATB1-deficient mice lack functional T cells, due to an arrest of thymocyte development at the DP stage [96, 98, 99] and have an impaired TCR rearrangement due to abrogated *Rag1* and *Rag2* expression [100]. Moreover, it was recently shown that SATB1 is essential for the differentiation of DP thymocytes into SP lineages as well as the differentiation of CD4 SP cells into

tT_{reg} cells, as it activates lineage-specifying genes after positive selection by the activation of enhancers [101, 102].

Structurally the SATB1 protein consists of four different domains [103]:

With its dimerization domain, also known as PDZ-like domain, SATB1 can homodimerize, which is required for optimal DNA binding [104]. In addition, SATB1 interacts with other proteins via the PDZ-like domain [105, 106]. Both, the MAR binding domain and the homeodomain are necessary for DNA binding. Moreover, the homeodomain strengthens DNA binding.

The nuclear matrix targeting sequence (NMTS) of SATB1 is necessary for binding of the protein to the nuclear matrix [103], so that SATB1 serves as a linker between nuclear matrix and chromatin.

In addition to these domains, Seo *et al.* (2005) and Nakayama *et al.* (2005) described the presence of a nuclear localization signal (NLS) domain between amino acids 20 to 40 leading to transport of the protein into the nucleus [96, 103].

The linker function of SATB1 and its cage-like distribution in thymocyte nuclei support the initial idea of a higher order chromatin organization and gene regulation by SATB1 [107]. Currently two models are proposed, how SATB1 can regulate gene expression (Figure 1.5): the first model was derived from a study, where SATB1 was shown to be involved in the expression of the genes of the murine TH2 locus after activation of TH2 cell clones [108]. According to the results of this study, SATB1 folds chromatin into loops with MARs being located at their bases, thereby making chromatin accessible to the transcription machinery and facilitating the communication between regulatory sequences, such as promoters, enhancers and locus control regions [109], by bringing them into close proximity. In the second model, SATB1 is involved in the epigenetic control of gene expression as it can bind histone modifying enzymes, such as histone acetylases and deacetylases, as well as other proteins to form activator and repressor complexes, thereby regulating gene expression [105, 106, 110].

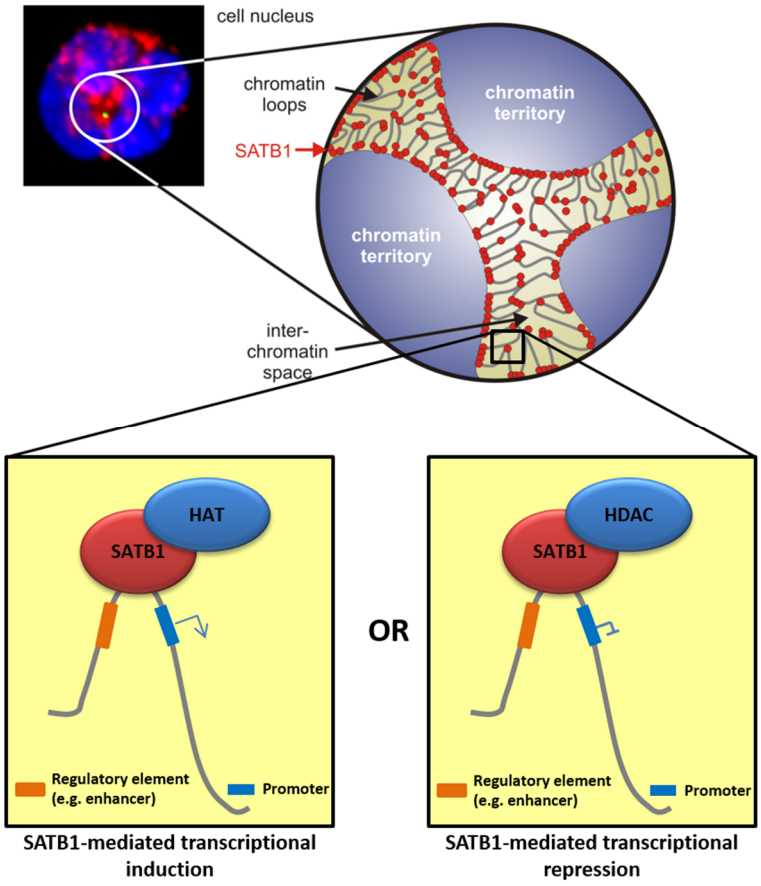

Figure 1.5 Regulation of gene expression by SATB1
SATB1 shows a cage-like distribution in the nucleus of the cell due to its binding to chromatin and to the nuclear matrix (upper panel). With this linker function SATB1 provides higher order chromatin organization by folding chromatin into loops, which is used for regulation of gene expression in different ways: (1) the chromatin is anchored to the nuclear matrix, which makes the chromatin accessible to the transcription machinery (not shown); (2) the loop structure brings regulatory sequences, such as promoters and enhancers, into proximity, thereby facilitating the communication between these sequences (lower panel); (3) SATB1 serves as landing platform for histone modifying enzymes, to form activator and repressor complexes, which regulate gene expression on epigenetic level (lower panel). HAT: histone acetyltransferase; HDAC: histone deacetylase.

Besides its role in thymocyte and brain development, SATB1 is also involved in the effector cell differentiation of peripheral $CD4^+$ T cells (Figure 1.6).

Cai *et al.* showed that besides chromatin folding, SATB1 is also required for the expression of the TH2 cytokines IL-4, IL-5 and IL-13 and consequently for TH2 cell activation [108]. In line with this, Ahlfors *et al.* reported that SATB1 is involved in the early phase of TH2 differentiation in human peripheral blood T cells [111]. Furthermore, our own results showed that SATB1 is upregulated on transcriptional and protein level after polyclonal stimulation of human conventional $CD4^+$ T cells (T_{conv}) via CD3 and CD28 [112]. Moreover, when preventing this stimulation-dependent upregulation of SATB1 using siRNA-mediated knock-down of *SATB1*, the

cells secreted significantly lower amounts of inflammatory cytokines, such as IFN-γ (Yasser Thabet, unpublished data).

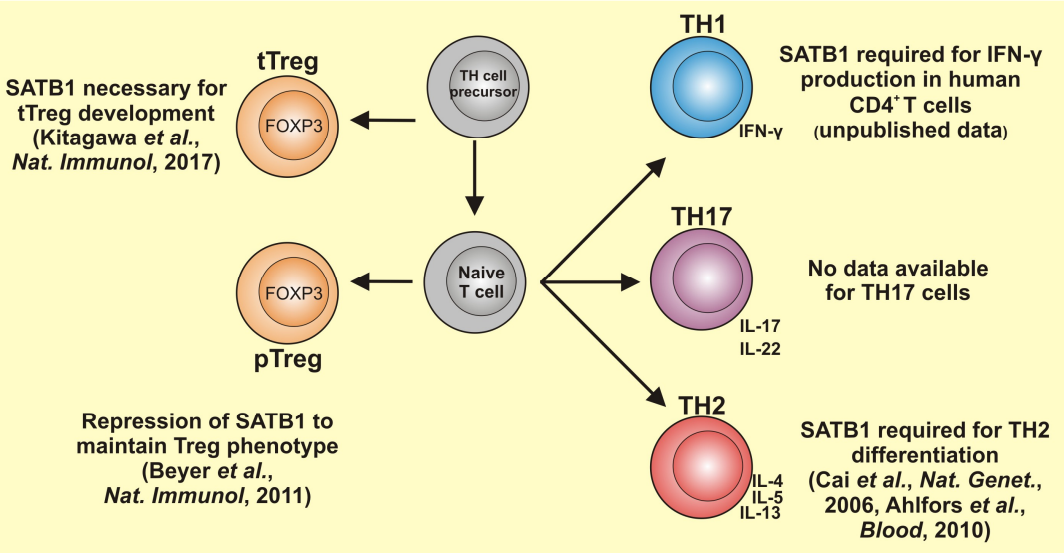

Figure 1.6 Involvement of SATB1 in different T helper subsets
Different studies have shown an involvement of SATB1 in the development of TH2 cells, as well as T_{reg} cell development and maintenance. Furthermore, our own unpublished data demonstrated a reduction of IFN-γ production in human $CD4^+$ T cells, indicating that SATB1 is required for TH1 differentiation in humans. In contrast to TH1, TH2 and T_{reg} cell development the involvement of SATB1 in TH17 cell differentiation has not been addressed so far.

In addition to its role during effector T cell differentiation, we recently showed that SATB1 is repressed in T_{reg} cells by Foxp3 and that this repression was critical for maintaining the T_{reg} cell phenotype and function by preventing the induction of effector T cell programs in T_{reg} cells [113].

1.4 Aim of the project

Despite the intense research performed on the role of SATB1 in $CD4^+$ T cells, conclusive data on the general mode of action of SATB1 in peripheral T cells is still sparse, as the currently available studies suffer from the drawback that they were either generated using *in vitro* systems or *in vivo* systems relying on intense manipulation of $CD4^+$ T cells *in vitro*. Furthermore, the available studies only deal with the major T helper subsets TH1, TH2 and T_{reg}, while so far nothing is known about the function of other subsets, such as TH17 (see Figure 1.6).

The lack of sufficient *in vivo* data in this context is mainly due to the detrimental effects on T cell development in the thymus after the *in vivo* of deletion of *Satb1* [98], which on the one hand makes the assessment of SATB1 function in peripheral $CD4^+$ T cells difficult and on the other hand indicates that genetically modified mouse

models are necessary that can specifically alter the expression of *Satb1* in peripheral $CD4^+$ T cells to study the role of SATB1 in peripheral $CD4^+$ T cells *in vivo*.

Thus, the aim of this project was to generate appropriate mouse models to address the role of SATB1 in peripheral T cells and perform the necessary experiments to properly test this *in vivo*.

Therefore, we wanted to generate two conditional mouse models for the spatiotemporal removal and overexpression of SATB1. The conditional SATB1 knock-out mouse should be used to remove SATB1 specifically in naive peripheral $CD4^+$ T cells to test their potential to differentiate into effector cells after *Satb1* gene deletion. In contrast, with the conditional SATB1 overexpressing mouse model we should be able to overexpress SATB1 specifically in T_{reg} cells to assess whether T_{reg} cells indeed lose their regulatory phenotype after the release of SATB1 from the Foxp3-mediated repression *in vivo*. Thus, by combining the data gained from these two complementary mouse models we should be able to get a comprehensive understanding of the *in vivo* role of SATB1 for peripheral $CD4^+$ T cells.

2 Materials and Methods

2.1 Materials

2.1.1 Equipment

Table 2.1 List of Equipment and corresponding manufacturers

Device	Manufacturer
Accu Jet Plus	Brand
AG285 Analytical balance	Mettler Toledo
BD FACS Aria III	BD Bioscience
BD™ LSR II Flow Cytometer System	BD Bioscience
BioDoc Analyzer	Biometra
Centrifuge 5810R	Eppendorf
Centrifuge 5815R	Eppendorf
Centrifuge Allegra X 15R	Beckman Coulter
Centrifuge Avanti J-26 XP	Beckman Coulter
Centrifuge Rotina 420	Hettich
CO2 Incubator CB210	Binder
ConcentratorPlus	Eppendorf
DynaMag™-2	Invitrogen
Eclipse TS100 (light microscope)	Nikon
Electrophoresis System Mini-Protean	BioRad Laboratories
Ergo One Pipettes	Starlab
Laminar Flow Hood	BDK Luft & Raumtechnik GmbH
Light Cycler® 480	Roche
Magnet MACS Multi Stand	Miltenyi Biotech
Multipette Plus	Eppendorf
Neubauer counting chamber	Superior Marienfeld
PerfectBlue™ Gel System	Peqlab
Pipet-Lite XLS Adjustable Spacer (20-300 µl)	Mettler Toledo
Power Supply PowerPac HC	BioRad Laboratories
QuadroMACS Separator	Miltenyi Biotech
Roller Mixer SRT9D Stuart	Bibby Scientific
SevenEasy (pH-meter)	Mettler Toledo
Spectrophotometer NanoDrop 2000	Thermo Scientifc
Thermocycler Professional Basic Gradient	Biometra
Thermocycler T3000	Biometra
Thermomixer comfort	Eppendorf
X-Ray film developer Curix 60	AGFA

2.1.2 Consumables

Standard plastic ware for cell culture and molecular biology was purchased from Greiner Bio-One, Sarstedt and Star Lab. Consumables for special purposes are listed in Table 2.2.

Table 2.2 List of special consumables

Name	Manufacturer
BD Falcon Cell strainer (70 µm and 100 µm)	BD Bioscience
Easy Strainer (70 µm and 100 µm)	Greiner Bio-One
Hybond N+ nylon membrane	GE Healthcare
MACS Columns LS	Miltenyi Biotec
Sephadex G50 Columns	GE Healthcare

2.1.3 Kits

Table 2.3 List of kits and corresponding manufacturers

Name	Manufacturer
GeneJet Plasmid Miniprep	Thermo Fisher Scientific
$CD4^+$ T cell Isolation Kit II mouse	Miltenyi Biotec
DNA Isolation Kit for Cells and Tissues	Roche
Foxp3/Transcription Factor Staining Buffer Set	eBioscience
Megaprime DNA Labeling Kit	GE Healthcare
miRNeasy Micro Kit	Qiagen
mMESSAGE mMACHINE® T7 ULTRA Kit	Ambion
Mouse TH1/TH2 10 plex Kit	eBioscience
NucleoBond Xtra Maxi Plus	Macherey-Nagel
NucleoSpin Tissue Kit	Macherey-Nagel
QIAquick Gel Extraction Kit	Qiagen
QIAquick PCR Purification Kit	Qiagen
QuikChange Lightning Multi Site-Directed Mutagenesis Kit	Agilent Technologies
ReliaPrep gDNA Tissue Miniprep Kit	Promega
RNeasy MinElute Cleanup Kit	Qiagen
Surveyor Mutation Detection Kit for Standard Gel Electrophoresis	Transgenomics
TNT Quick Coupled Transcription/Translation System	Promega
TOPO TA Cloning Dual Promoter Kit	Thermo Fisher Scientific
Transcriptor First Strand cDNA Synthesis Kit	Roche

2.1.4 Reagents

Standard laboratory chemicals were purchased from AppliChem, Merck, Roth and Sigma-Aldrich. Special reagents are listed in Table 2.4.

Table 2.4 List of chemicals and reagents

Name	Manufacturer
6x DNA Loading dye	Thermo Fisher Scientific
Agarose (UltraPure)	Thermo Fisher Scientific
Ampicillin	AppliChem
Bovine serum albumine (BSA)	Sigma-Aldrich
Brefeldin A Solution	eBioscience
Cell Stimulation Cocktail	eBioscience
Dimethylsulfoxide (DMSO)	Sigma-Aldrich
Dulbecco's Modified Eagle Medium (DMEM)	PAA Laboratories
Dulbecco's Phosphate Buffered Saline (PBS)	Sigma-Aldrich
Dynabeads Mouse T-Activator CD3/CD28	Thermo Fisher Scientific
eFluor450	eBioscience
eFluor670	eBioscience
Fetal Calf Serum (ES cell tested)	PAA Laboratories
Fetal Calf Serum (FCS)	Sigma-Aldrich
G-418 (Geneticin)	PAA Laboratories
HEPES buffer solution	PAA Laboratories
High Fidelity PCR Master	Roche
IL-12	ImmunoTools
IL-2	Chiron
IL-4	ImmunoTools
IL-6	ImmunoTools
Kanamycin	AppliChem
Leukemia Inhibitory Factor (LIF)	In-house preparation (Prof. W. Kolanus, Univeristy of Bonn)
Liquid counting beads	BD Bioscience
Live/Dead Fixable Near-IR dye	Thermo Fisher Scientific
Maxima SYBR Green qPCR Master Mix	Thermo Fisher Scientific
Mitomycin C	Sigma-Aldrich
Monensin Solution	eBioscience
Non-essential amino acids	Gibco
Penicillin/Streptomycin	Gibco
QuikHyb Rapid Hybridization Solution	Agilent Technologies
RPMI 1640 with L-Glutamine	PAA Laboratories
RPMI 1640 without Phenol Red	PAA Laboratories
Sodium pyruvate	Gibco
Tamoxifen	Sigma-Aldrich
TGF-β	PeproTech
Trypsin-EDTA	Gibco
TurboFect Transfection Reagent	Thermo Fisher Scientific
β-Mercaptoethanol (50 mM)	Gibco

2.1.5 Culture media and buffers

Table 2.5 List of cell culture media and the corresponding components

Medium	Components	Final concentration
1x/2x freezing medium	FCS (ES-cell tested) DMSO	90 % / 80 % 10 % / 20 %
ES cell culture medium (ES-DMEM)	DMEM FCS (ES-cell tested) Glutamax Non-essential amino acids Sodium pyruvate β-Mercaptoethanol LIF Penicillin/Streptomycin	1x 20 % 1 % 1 % 1 % 0.1mM 0.3 % 1 %
LB medium/agar (pH 7.5)	Yeast extract Trypton NaCl (Agar)	0.5 % 1 % 0.5 % (1.5 %)
MEF cell culture medium (F-DMEM)	DMEM FCS (ES-cell tested) Non-essential amino acids Sodium pyruvate Penicillin/Streptomycin	1x 20 % 1 % 1 % 1 %
NIH3T3 cell medium	DMEM FCS Glutamax Penicillin/Streptomycin	1x 10 % 1 % 1 %
SOC medium	Yeast extract Trypton NaCl KCl $MgCl_2$ $MgSO_4$ Glucose	0.5 % 2 % 10 mM 2.5 mM 10 mM 10 mM 20 mM
T-cell medium	RPMI 1640 with L-Glutamine FCS Glutamax β-Mercaptoethanol Sodium pyruvate Non-essential amino acids HEPES Penicillin/Streptomycin	1x 10 % 1 % 55 µM 0.5 mM 1 % 5 mM 1 %

Table 2.6 List of buffers and the corresponding components

Buffer	Components	Final concentration
20x SSC buffer (pH 7)	NaCl Trisodium citrate dihydrate	3 M 0.3 M
Denaturation buffer	NaCl NaOH	1.5 M 0.5 M
Injection buffer (pH 7.4)	Tris EDTA	10 mM 0.25 mM
MACS Buffer (pH 7.2)	PBS BSA EDTA	1x 0.5 % 2 mM
Neutralization buffer (pH 7.5)	Tris NaCl	0.5 M 1.5 M
Red blood cell lysis buffer (pH 7.2-7.4)	Ammonium chloride Potassium hydrogen carbonate EDTA	155 mM 10 mM 0.1 mM
TAE buffer (pH 8.0)	Tris-acetate EDTA	40 mM 1 mM

2.1.6 Enzymes

Table 2.7 List of enzymes and the corresponding manufacturers

Name	Manufacturer
GO Taq Polymerase	Promega
Pfu Polymerase	Thermo Fisher Scientific
Phusion Hot Start II Polymerase	Thermo Fisher Scientific
Restriction Endonucleases	Thermo Fisher Scientific, New England Biolabs
Shrimp Alkaline Phosphatase	New England Biolabs
T4 Ligase	Thermo Fisher Scientific
T7 Endonuclease I	New England Biolabs
Taq Polymerase	Sigma-Aldrich

2.1.7 Primers

Table 2.8 Primers used for mutation of the TALEN targeting sites of pSATB1-Flex

Location	Sequence (5´-3´)
TALEN 1 binding site	ATGGGGCAGGCATAACTATAGATCTCCATCCACTTATAACGTCTTCTTTTC
TALEN 2 binding site	CTTTTCCAGTTCTGGCAGGTGCTTTTTAAGACAGTGACTGAGTATGG

Table 2.9 List of primers for mutation screening and genotyping PCRs

Sequence (5´-3´)	Binding direction/site	PCR reaction	Annealing temp. [°C]
TGCTGAGGTTTCCGTCCATAAC	fwd	T7/Surveyor-Assay PCR[1]	62.5
TGTGCTCCCAAGCCTTCCTC	rev		
AGCCCCCAGATCGCATGCCT	fwd	TnT-assay PCR[1]	55
AAACAGGAGCCTTCGCTGGACTGC	rev		
TGCTGAGGTTTCCGTCCATAAC	fwd	Genotyping PCR I[2]	62.5
TGTGCTCCCAAGCCTTCCTC	rev		
AGGACATGGACCTGACATGAGAAC	fwd	Genotyping PCR II[1]	64.6
CTAACAATACGGAGTGCTGTGTCTGT	rev		
GGCTAACTGAAACACGGAAGGAG	internal		
AGCCTGCTTTCTGGGTGCCAT	fwd	5´ homology PCR[2]	64.6
TGGGTCGATGGTGATGCTTGGC	rev		
CGAAGTTATGTCCCTCGAAGAGGTTC	fwd	3´homology PCR[2]	64.6
GGTGTGCGACCATTGTTCAGGAG	rev		
CCAAAGTCGCTCTGAGTTGTTATC	fwd	ROSA26-genotyping PCR[3]	56
GGAGCGGGAGAAATGGATATG	rev		
GCGAAGAGTTTGTCCTCAACC	internal		
CAAGCTGACCCTGAAGTTCATCTG	fwd	3´homology PCR (ROSA26)[2]	64.6
TCAGTGGCTCAACAACACTTGGTC	rev		

fwd: primer binding site on direct strand; rev: primer binding site on reverse strand; internal: primer binding site located in the recombinant allele/targeting construct, but not in WT genome. [1]PCR performed with Phusion Hot Start II polymerase (Thermo Fisher Scientific); [2]PCR performed with GO Taq polymerase (Promega); [3]PCR performed with Sigma Taq polymerase (Sigma-Aldrich).

2.1.8 Plasmid vectors

Table 2.10 List of commercially available plasmid vectors

Plasmid	Distributor/manufacturer
pTriEx4 Neo	Merck Millipore
pJ241-Flex (Plasmid #18925)	Addgene
TALE toolbox (Kit # 1000000019)	Addgene

2.1.9 Mouse lines

Table 2.11 List of mouse lines and their origin

Mouse line	Origin
B6D2F1 x C57BL/6J	Jackson Laboratory
B6(Cg)-Tyrc-2J/J	Jackson Laboratory
CD4-Cre	Jackson Laboratory
CD4-CreERT2	Prof. Thorsten Buch, Institute of Laboratory Animal Science, University of Zurich
Foxp3-YFP-Cre	Prof. Alexander Rudensky, Memorial Sloan Kettering Cancer Center, New York
$RAG2^{-/-}$	House for experimental therapy, University Hospital Bonn
ROSA26-tdTomato	Prof. Thomas Wunderlich, Institute of Genetics, University of Cologne

2.1.10 Antibodies

Table 2.12 List of antibodies for T cell stimulation and *in vitro* differentiation

Antigen	Clone	Manufacturer
CD3	145-2C11	Biolegend
CD28	37.51	Biolegend
IFN-γ	R4-6A2	Biolegend
IL-4	11B11	Biolegend

Table 2.13 List of fluorescent-dye conjugated antibodies for flow cytometry

Antigen	Fluorophore	Clone	Manufacturer
CD3	Pacific Blue BV421 BV510 BV650	17A2 17A2 145-2C11 17A2	Biolegend Biolegend BD Biosciences Biolegend
CD4	APC-Cy7 PerCP-Cy5.5 BV510 PE-Cy7	RM4-5	Biolegend
CD8	Pacific Blue BV650 APC	53-6.7	Biolegend
CD25	APC-Cy7 Alexa Fluor 647 PE-Cy7	PC61	Biolegend
CD44	Pacific Blue BV605	IM7	Biolegend
CD62L	PE-Cy7 APC-eFluor 780	MEL-14	BD Biosciences eBioscience
FOXP3	PE PerCP-Cy5.5 PE-eFlour 610	MEF-14 FJK-16s FJK-16s	Biolegend eBioscience eBioscience
IFN-γ	PE/Cy7	XMG1.2	eBioscience
IL-4	APC	11B11	eBioscience
IL-17A	PE	eBio17B7	eBioscience
Ki-67	PE-eFluor 610	SolA15	eBioscience
SATB1	Alexa Fluor 647	14/SATB1	BD Bioscience

2.1.11 Software

Table 2.14 List of software and the corresponding developers

Name	Developer
BD FACS Diva	BD Biosciences
Flow Jo V7.6.5/ V10	Tree Star
Light Cycler 480 SW 1.5	Roche
Sigma Plot 10.0	Systat Software
Corel Draw X3/X4	Corel Corporation
Vector NTI Advance 11	Invitrogen
FCAP Array v2.0.1	Soft Flow
TAL Effector Nucleotide Targeter 2.0	School of Integrative Plant Science, Cornell University, Ithaca, New York [114].

2.2 Methods

2.2.1 Molecular biology

2.2.1.1 Cloning of plasmid vectors

For the cloning of plasmid vectors a general protocol consisting of restriction digestion of amplified PCR products and plasmid backbone vectors (1), ligation of the respective digestion fragments (2), as well as transformation of the ligated product into chemo-competent bacteria (3) and isolation of plasmid DNA from single bacterial clones harboring the ligated vector (4) was performed.

Restriction digest was performed using commercially available enzymes and buffer solutions (Thermo Fisher Scientific and New England Biolabs). Therefore, 1 – 2.5 µg of PCR product and plasmid DNA, respectively, were mixed with 2 µl of 10x reaction buffer and 1 µl of each restriction enzyme in 20 µl reaction volume, followed by incubation according to the manufacturer´s protocol. Depending on the amount of digested DNA required, the reaction was scaled up.

To prevent re-ligation, linearized vectors were 5´-dephosphorylated by addition of 1 U shrimp alkaline phosphatase (New England Biolabs) to the digested sample after the restriction reaction, followed by incubation for 20 min at 37 °C. Afterwards phosphatase was heat-inactivated by incubation at 65 °C for 10 min.

Digested vectors and PCR products were separated by agarose gel electrophoresis, the respective bands were cut out of the gels and purified using the QIAquick Gel Extraction Kit (Qiagen) according to the manufacturer´s protocol and eluted with 30 µl of ddH_2O.

The purified fragments were ligated by mixing 50 ng of backbone vector with an appropriate amount of insert to yield a backbone-to-insert molar ratio of 1:3. Additionally, 1 U of T4 ligase (Thermo Fisher Scientific) and 2 µl of 10x reaction buffer were added to the reaction in a final volume of 20 µl. The reaction was incubated at RT for 1 hour or 16 °C overnight.

Subsequently, the ligation products were transformed into chemo-competent *E. coli*. For each transformation 10 µl of the ligation reaction were added to 100 µl of competent cells, which had been thawed on ice shortly before transformation. Bacteria were incubated for 30 min on ice, followed by incubation at 42 °C for 45 sec and cooling on ice for 1 min immediately afterwards. Next, 400 µl of SOC medium pre-warmed at 37 °C were added and bacteria were incubated for 1 h at 37 °C at

constant shaking. Afterwards 50 to 200 µl of bacterial cultures were transferred to LB agar plates containing the respective antibiotics for positive selection and the plates were incubated overnight at 37 °C (bacterial cultures containing pROSA26-STOP-SATB1 vector were incubated at 30 °C) until bacterial colonies were observable. Single colonies were then expanded by inoculating cultures containing 3 ml LB medium with the respective antibiotic and overnight incubation at 37 °C (or 30 °C for pROSA26-STOP-SATB1). 2 ml of these cultures were subjected to plasmid purification using the GeneJET Plasmid Miniprep Kit (Thermo Fisher Scientific) according to the manufacturer's protocol (elution in ddH_2O), as well as insert verification by restriction digestion (as described above) and Sanger sequencing. Sanger sequencing was done by GATC Biotech. Samples were prepared for sequencing according to instructions given by GATC Biotech.

After insert verification plasmids were used for downstream experiments. If large amounts of plasmid DNA were needed, 250 ml LB cultures were inoculated with 10 µl of the respective Mini culture and incubated overnight at 37 (or 30) °C, followed by plasmid isolation with the NucleoBond Xtra Maxi Plus Kit (Macherey-Nagel) according to the manufacturer´s instructions.

2.2.1.1.1 Generation of targeting vectors

The cloning strategy for the generation of the pSATB1-Flex targeting construct was developed in cooperation with Dr. Joachim Degen, Genetic Resources Center, University of Bonn. The construct was generated together with Tristan Wirtz and generation is described in detail in his Master thesis [115]. Briefly, the construct was assembled by generating and subsequently combining three intermediate vectors (pDTA-5´&3´HR, pBSK:Satb1WT-frt-Neo and pBSK:flexGFPmit) using standard cloning techniques as described in paragraph 2.2.1.1 above. The pDTA-5´&3´HR vector was generated by inserting the Flex cassette from the pJ241-Flex vector obtained from Addgene into a vector containing the DTA cassette for negative selection. Additionally, 5´ and 3´ homologous regions, which were amplified by PCR, were inserted upstream and downstream of the Flex cassette to yield the finished intermediate construct. The pBSK:Satb1WT-frt-Neo was generated by insertion of the *Satb1* exon 2 and intronic sequences upstream of this exon, both amplified by PCR, and a FRT-flanked neomycin cassette. For the generation of the third intermediate vector (pBSK:flexGFPmit) a fusion construct and the *Satb1* 3´UTR were inserted into the pBSK vector backbone. The fusion construct consisted of parts of the intron

upstream of the *Satb1* exon 2 including the splice site, 5´UTR and the start codon of *Satb1* exon 2 as well as a sequence encoding the eGFP open reading frame. Finally, the three intermediate vectors were combined to yield the final pSATB1-Flex targeting construct.

The pROSA26-STOP-SATB1 targeting construct was generated by inserting the *Satb1* open reading frame amplified by PCR into the STOP-eGFP-ROSA-CAG vector (obtained from Prof. Thomas Wunderlich, Institute of Genetics, University of Cologne) via AscI restriction sites using standard cloning techniques (see paragraph 2.2.1.1 above). Cloning was performed by Yasser Thabet, University of Bonn.

2.2.1.1.2 Generation of the pTriEx-SATB1-Flex test vector

The pTriEx-SATB1-Flex vector was generated by inserting the Flex cassette of the pSATB1-Flex vector into the pTriEx 4 Neo vector (Merck Millipore) downstream of the eukaryotic CMV promoter using standard cloning techniques as described in paragraph 2.2.1.1. Therefore, the pSATB1-Flex was digested with PmeI and MfeI to yield compatible ends to the pTriEx 4 Neo backbone, which was digested with EcoRI and PvuII.

2.2.1.2 Polymerase chain reaction (PCR)

PCR products generated for cloning into plasmid vectors with sizes smaller than 3 kb were amplified with Pfu polymerase (Thermo Fisher Scientific), whereas for products larger than 3 kb the High-Fidelity Master mix (Roche) was used. The reaction setups and thermocycler programs for both polymerase systems are given below:

Table 2.15 Reaction setup for PCRs performed with Pfu poymerase

Component	Volume [µl]
DNA Template (10 ng – 100 ng)	X
Forward Primer (10µM)	0.5
Reverse Primer (10 µM)	0.5
dNTPs (10 mM each)	0.5
10 x reaction buffer	2.5
Pfu DNA polymerase (2.5 U/µl)	0.5
H_2O (PCR-grade)	ad 25

X: DNA amount ranged from 10 ng for plasmid DNA up to 100 ng for genomic DNA

Table 2.16 PCR cycler settings for PCRs performed with Pfu poymerase

Step	Temperature [°C]	Time [s]
1. Initial denaturation	95	120
2. Short denaturation	95	30
3. Annealing	X	30
4. Elongation	72	X
5. 34 repetitions of steps 2 to 4		
6. Final elongation	72	600

X: Annealing temperatures were individual for each primer pair used and experimentally assessed and are given in Table 2.9. Elongation time: 2 kb/min

Table 2.17 Reaction setup for PCRs performed with High Fidelity PCR Master mix

Component	Volume [µl]
DNA Template (10 ng – 100 ng)	X
Forward Primer (10µM)	0.5
Reverse Primer (10 µM)	0.5
2 x High Fidelity PCR Master mix	10
H_2O (PCR-grade)	ad 20

X: DNA amount ranged from 10 ng for plasmid DNA up to 100 ng for genomic DNA

Table 2.18 PCR cycler settings for PCRs performed with High Fidelity PCR Master mix

Step	Temperature [°C]	Time [s]
1. Initial denaturation	94	120
2. Short denaturation	94	10
3. Annealing	X	70
4. Elongation	72	X
5. 10 repetitions of steps 2 to 4		
6. Denaturation	94	15
7. Annealing	X	30
8. Elongation	72	X
9. 20 repetitions of steps 6 to 8		
10. Final elongation	72	420

X: Annealing temperatures were individual for each primer pair used and experimentally assessed and are given in Table 2.9. Elongation time: 1 kb/min

PCRs used for genotyping or analysis of TALEN-induced mutations were performed either with Phusion Hot Start II polymerase (Thermo Fisher Scientific), GO Taq (Promega) or Taq polymerase (Sigma-Aldrich) according to the following reaction setups and thermocycler programs:

Table 2.19 Reaction setup for PCRs performed with Phusion Hot Start II poymerase

Component	Volume [µl]
DNA Template	X
Forward Primer (10µM)	0.5
Reverse Primer (10 µM)	0.5
dNTPs (10 mM each)	0.4
5 x Phusion HF reaction	4.0
Phusion Hot Start II polymerase (2.0 U/µl)	0.2
H_2O (PCR-grade)	ad 20

X: DNA amount ranged from 10 ng for plasmid DNA up to 100 ng for genomic DNA

Table 2.20 PCR cycler settings for PCRs performed with Phusion Hot Start II poymerase

Step	Temperature [°C]	Time [s]
1. Initial denaturation	98	30
2. Short denaturation	98	10
3. Annealing	X	30
4. Elongation	72	X
5. 34 repetitions of steps 2 to 4		
6. Final elongation	72	300

X: Annealing temperatures were individual for each primer pair used and are given in Table 2.8Table 2.9. Elongation time: 30 s/kb.

Table 2.21 Reaction setup for PCRs performed with GO Taq poymerase

Component	Volume [µl]
DNA Template	X
Forward Primer (10µM)	0.5
Reverse Primer (10 µM)	0.5
Internal Primer (10 µM)	0.5
dNTPs (10 mM each)	0.5
5 x Flexi green reaction buffer	5.0
$MgCl_2$ (25mM)	2.0
GO Taq polymerase (5.0 U/µl)	0.15
H_2O (PCR-grade)	ad 25

X: DNA amount ~100 ng for genomic DNA

Table 2.22 PCR cycler settings for PCRs performed with GO Taq poymerase

Step	Temperature [°C]	Time [s]
1. Initial denaturation	95	150
2. Short denaturation	95	30
3. Annealing	X	30
4. Elongation	72	X
5. 34 repetitions of steps 2 to 4		
6. Final elongation	72	300

X: Annealing temperatures were individual for each primer pair used and are given in Table 2.8Table 2.9. Elongation time: 1 min/kb

Table 2.23 Reaction setup for PCRs performed with Taq poymerase

Component	Volume [µl]
DNA Template	X
Forward Primer (10µM)	0.5
Reverse Primer (10 µM)	0.5
Internal Primer (10 µM)	0.5
dNTPs (10 mM each)	0.5
10 x reaction buffer	2.5
$MgCl_2$ (25mM)	2.5
Sigma Taq polymerase (0.025 U/µl)	0.125
H_2O (PCR-grade)	ad 25

X: DNA amount ~100 ng for genomic DNA

Table 2.24 PCR cycler settings for PCRs performed with Taq poymerase

Step	Temperature [°C]	Time [s]
1. Initial denaturation	94	300
2. Short denaturation	94	30
3. Annealing	X	60
4. Elongation	72	X
5. 34 repetitions of steps 2 to 4		
6. Final elongation	72	300

X: Annealing temperatures were individual for each primer pair used and are given in Table 2.8Table 2.9. Elongation time: 1 kb/min

2.2.1.3 Generation of TAL Effector Nucleases

TALENs targeting the murine *Satb1* locus were designed and analyzed for off-targets using the TAL Effector Nucleotide Targeter 2.0 online tool [114]. TALEN assembly was performed with the TALE toolbox obtained from Addgene (Kit # 1000000019) according to the published protocol [88]. After the Golden gate II reaction, the assembled TALEN plasmids were transformed into *Stbl3 E. coli* cells, followed by inoculation of Mini cultures with single colonies and plasmid isolation, as described in paragraph 2.2.1.1. Correct assembly of TALEN plasmids was verified by Sanger sequencing (GATC Biotech) using the primers recommended by Sanjana *et al.* [88].

Sequence-verified TALEN plasmids were further expanded by inoculating 250 ml cultures (see paragraph 2.2.1.1), followed by plasmid isolation and either used directly for downstream experiments or as template for the generation of TALEN mRNAs by *in vitro* transcription.

For *in vitro* transcription TALEN plasmids were linearized by restriction digest with XmaI, followed by purification of the linearized plasmid by agarose gel electrophoresis and DNA cleanup (see paragraph 2.2.1.1). *In vitro* transcription was

performed with the mMESSAGE mMACHINE T7 ULTRA Kit (Ambion) according to the manufacturer´s recommendations. Transcribed TALEN mRNAs were purified using the RNeasy MinElute Cleanup Kit (Qiagen) following the manufacturer´s protocol and mRNAs were eluted with 14 µl sterile water. 1 µl of each transcribed and purified mRNA sample was subjected to agarose gel electrophoresis to verify successful *in vitro* transcription.

2.2.1.4 Mutagenesis of the pSATB1-Flex targeting construct

The TALEN targeting site in the pSATB1-Flex vector was mutated using the QuickChange Lightning Multi Site-Directed Mutagenesis Kit (Agilent Technologies) according to the manufacturer´s instructions. Single colonies of transformed XL10-Gold bacteria were expanded and plasmids were isolated as described in paragraph 2.2.1.1 Successful mutation of the targeting construct was verified by Sanger sequencing (see paragraph 2.2.1.1).

2.2.1.5 Assessment of TALEN activity with the transcription/translation system (TnT assay)

To test TALEN functionality *in vitro*, the assembled TALEN plasmids targeting the *Satb1* locus were translated *in vitro* into protein (1 µg per plasmid) using the Quick Coupled Transcription/Translation system (Promega) according to the manufacturer´s instructions. Subsequently, a 3 kb PCR fragment encoding the TALEN targeting site (TTS) was added to the reaction mix, followed by incubation for 60 min at 37 °C to allow TALEN-mediated cleavage of the DNA fragment. TALEN-mediated cleavage was stopped by addition of 5 µl proteinase K and incubation for 10 min at 50 °C. DNA was purified using the QIAquick PCR purification Kit (Qiagen) and cleavage of the DNA fragment was analyzed by agarose gel electrophoresis. Transcription/Translation reactions lacking TALEN plasmids and TTS-PCR fragment, respectively, served as controls.

2.2.1.6 Assessment of TALEN activity *in vivo* with the T7 endonuclease I assay

To assess the activity of the TALENs targeting the *Satb1* locus *in vivo*, NIH3T3 cells were transfected with TALEN-encoding plasmids. Therefore, NIH3T3 cells were seeded into six-well plates at densities of 2x 10^5 cells per well approximately 24 h before transfection. Cells were transfected with 4 µg of the respective TALEN plasmids per well using Turbofect Transfection Reagent (Thermo Fisher Scientific)

according to the manufacturer´s protocol. 24 to 48 h after transfection cells were harvested and DNA was isolated using the NucleoSpin Tissue Kit (Macherey-Nagel) according to the manufacturer´s recommendations. From the DNA samples, a region of 606 bp containing the *Satb1* TALEN-targeting site was amplified by PCR (see paragraph 2.2.1.2) and subjected to the T7 endonuclease I assays. Genomic DNA from NIH3T3 cells transfected with an eGFP encoding plasmid served as non-mutated control.

800 ng of each PCR amplicon were mixed with 2 µl of 10x NEB 2 buffer (New England Biolabs) in a 20 µl reaction volume and incubated at 95 °C for 5 min, 95 °C to 85 °C at -2 °C/s and 85 °C to 25 °C at -0.1 °C/s to allow annealing of complementary but mismatched strands. Subsequently, 1 µl T7 endonuclease I (New England Biolabs) was added to the reaction and samples were incubated at 37 °C for 60 min to digest the annealed PCR products at the sites of mismatch. Cleavage of T7 endonuclease I-treated PCR products as marker for TALEN-induced mutations was subsequently assessed by agarose gel electrophoresis.

2.2.1.7 Analysis of TALEN-induced *Satb1* mutation in founder mice

To identify TALEN-mediated mutation of the *Satb1* locus in founder mice originating from oocyte injections, DNA was isolated from tail biopsies taken from these mice using the ReliaPrep gDNA Tissue Miniprep Kit (Promega) and subjected to the Surveyor Nuclease assay and sequence determination by Sanger Sequencing. For the Surveyor nuclease assay, a DNA fragment containing the Satb1 TTS was amplified by PCR (see paragraph 2.2.1.2) from the isolated genomic DNA samples. Without further purification, the PCR samples were melted and re-annealed to form heteroduplex DNA according to the protocol given in the Surveyor Mutation Detection Kit for Standard Gel Electrophoresis (Transgenomics). Afterwards the re-annealed samples (20 µl each) were supplemented with 2.2 µl $MgCl_2$ (0.15 M), 1 µl Enhance S solution and 1 µl Surveyor nuclease (Transgenomics), followed by incubation at 42 °C for 60 min and analysis of Surveyor nuclease-mediated cleavage by agarose gel electrophoresis.

Samples positive in this assay were further confirmed by sequencing of the TTS. Therefore, genomic DNA from founder mice was amplified with the same PCR used for the Surveyor assay and products were cloned into the pCRII-TOPO vector using the TOPO TA Cloning Dual Promoter Kit (Thermo Fisher Scientific) according to the manufacturer´s protocol. Bacterial clones derived from this cloning reaction were

expanded in 3 ml cultures and plasmids purified from these cultures were subjected to Sanger sequencing (see paragraph 2.2.1.1) using M13 forward and reverse primers.

2.2.1.8 Assessment of correct integration of the targeting vector by Southern blot analysis

For Southern blot analysis of ES cells, DNA was isolated from ES cells grown in one well of a six-well plate using the DNA Isolation Kit for Cells and Tissues (Roche) according to the manufacturer´s instructions. Southern blot analysis of the founder mouse was performed by isolating DNA from the liver of one descendant of the founder mouse. Therefore, one liver lobe was cut into small pieces and lysed with the DNA Isolation Kit for Cells and Tissues (Roche) according to the manufacturer´s instructions. After lysis, DNA was precipitated by addition of 0.7 volumes of Isopropanol. Precipitated DNA was not harvested by centrifugation, but was collected with a pipette tip to prevent shearing of the high molecular weight DNA. The collected DNA was washed twice by immersing the pipet tip into 70 % ethanol, followed by air-drying of the DNA. Dried DNA was then dissolved in nuclease-free H_2O for 10 min at 50 °C, followed by overnight incubation at 4 °C.

20 - 25 µg of isolated genomic DNA of each clone was digested with 50 U of the respective restriction enzyme (Figure 3.15 and Figure 3.34) overnight at 37 °C in a final reaction volume of 50 µl. The digested genomic DNA samples were separated on a 0.8 % agarose gel in 1 x TAE buffer overnight at 30 V. Subsequently, the gel was incubated in 0.25 M HCl for 8 min to depurinate the DNA. After a short wash in H_2O, DNA was denatured by incubating the gel two times for 15 min in denaturation buffer, followed by another short wash in H_2O. The gel was then neutralized by two incubation steps in neutralization buffer for 15 min. Afterwards, DNA was transferred overnight to a Hybond N+ membrane by capillary blotting in 20x SSC buffer. After blotting, the nylon membrane was washed shortly in 2x SSC and dried at room temperature, followed by UV-crosslinking with 70,000 µJ/cm^2.

The crosslinked membrane was shortly washed in 5x SSC and then incubated in 10 ml of hybridization buffer (QuikHyb Rapid Hybridization Solution, Agilent) for 45 min at 68 °C. Afterwards, denatured radioactively labeled probe (see paragraph 2.2.1.8.1) was added to the hybridization solution and the membrane was incubated for 90 min at 68 °C. Subsequently, the membrane was washed with SSC buffers containing 0.1 % SDS to remove unspecifically bound probes. Thereby stringency was increased

with each washing step by reducing the SSC concentration from 2x SSC/0.1 % SDS to 0.1x SSC/0.1 % SDS. Decrease in radioactivity was tracked with a Geiger-Müller counter to stop washing before removal of specifically bound probes. Finally, the signal was visualized by incubating the membrane on an X-ray film in the dark for 48 h. X-ray films were developed and digitally scanned.

2.2.1.8.1 Radioactive labeling of probes

5´ and 3´ Probes were generated by PCR (see paragraph 2.2.1.2), while the eGFP probe was generated by restriction digest of the pENTR4-eGFP vector with NotI and EcoRV. Probes were radioactively labeled by random-primer labeling using the Megaprime DNA Labeling Kit (GE Healthcare). Thereby, 150 ng of each probe and 7 µl radioactively labeled ^{32}P-dCTP (10 µCi/µl) were used in the reaction. Labeled probes were purified with Sephadex-G50 columns (GE Healthcare) according to the manufacturer´s protocol.

The purified probe was denatured by incubation for 10 min at 99 °C and subsequently cooled on ice for 5 min. 2 µl of each probe were used for quantification of labeling efficiency by liquid scintillation counting. The remaining probes were added to the respective membranes.

2.2.1.9 Assessment of Satb1 expression by qPCR

For assessment of *Satb1* mRNA expression, RNA was isolated from freshly purified T cells lysed in 1 ml Qiazol lysis reagent (Qiagen) using the miRNeasy Micro Kit (Qiagen) according to the manufacture´s protocol and RNA concentration was determined using the NanoDrop2000 photometer. Complementary DNA (cDNA) was generated by reverse transcription of 30 - 50 ng RNA with random hexamer primers in a 20 µl reaction volume using the Transcriptor First Strand cDNA Synthesis Kit (Roche) following the manufacturer´s instructions. Finally, the generated cDNA was diluted 1:10 by addition of 180 µl of nuclease-free H_2O.

Quantitative PCR (qPCR) was performed with the Maxima SYBR Green qPCR Master Mix (Thermo Fisher Scientific) and the LightCycler 480 II (Roche) according to the following reaction setup and cycling conditions:

Table 2.25 Reaction setup for qPCR

Reagent	Volume [µl]
cDNA	2
Forward Primer (10 µM)	0.75
Reverse Primer (10 µM)	0.75
Maxima SYBR Green qPCR Master Mix (2x)	10
Nucleas-free H_2O	6.5

Table 2.26 PCR cycler settings for qPCR

Step	Temperature [°C]	Time [s]
1. Initial denaturation	95	600
2. Short denaturation	95	15
3. Annealing	60	30
4. Elongation	72	30
5. 44 repetitions of steps 2 to 4		

Crossing points of each sample as well as relative expression of *Satb1* to murine beta 2-microglobulin were calculated using the LightCycler 480 II software using the $2^{-\Delta\Delta CT}$ method.

2.2.2 Generation of gene targeted mice

2.2.2.1 Generation of gene targeted mice from ES cells

JM8A3 ES cells (obtained from Prof. Dr. Thomas Wunderlich, Institute of Genetics, University of Cologne) were generally cultured on a mouse embryonic fibroblast (MEF) feeder layer (see paragraph 2.2.2.1.1) at 37 °C and 5 % CO_2 with a daily change of ES cell culture medium (ES-DMEM) and splitting 1:3 every three days or earlier, if necessary. For transfection with the targeting construct, ES cells cultured on one 10 cm dish were harvested by trypsinization at 37 °C for 3-5 min, addition of ES cell medium to stop trypsinization and centrifugation for 3 min at 200 x g. The pellet was resuspended in 400 µl RPMI medium without phenolred, the cells were transferred to a 0.4 cm electroporation cuvette and 40 µg of the linearized targeting vector (see paragraph 2.2.2.1.2) dissolved in 400 µl RPMI without Phenolred was added. Electroporation was performed with an exponential pulse at 230 V and 500 µF capacity, followed by incubation for 10 min at RT. Cells were resuspended in 40 ml ES-DMEM and transferred to four 10 cm dishes with Mitomycin C treated feeder cells. On day one, the medium was exchanged with normal ES-DMEM. From day two, cells were cultured in ES-DMEM supplemented with 150 µg/ml of G-418 with a

daily exchange of the medium to select for cells harboring the targeting construct in their genome. On days 9 to 10, the cells were washed once with 10 ml PBS, covered with 10 ml PBS and single clones were picked with a P200 pipette. Picked clones were subsequently transferred to one well of a 96-well plate containing 100 µl ES-DMEM per well and were separated by repeated pipetting to obtain single cell suspensions. Cells were then transferred to a 48-well plate containing Mitomycin C treated feeder cells and 500 µl ES-DMEM per well and were incubated at 37 °C and 5 % CO_2 with daily exchange of ES-DMEM (without G418). When ~ 80 % confluency was reached (approximately after three to five days), cells were trypsinized with 100µl Trypsin-EDTA per well for three to five minutes at 37 °C, followed by stopping of trypsinization with 500 µl ES-DMEM per well. 200 µl of this suspension were transferred to a new 48-well plate coated with 0.1 % gelatin for 1 h at 37 °C and cells were grown for DNA isolation at 37 °C and 5 % CO_2 with daily exchange of medium until confluency was reached. The remaining 400 µl of cell suspension were mixed with 400 µl of 2x freezing medium and the plate was frozen at -80 °C in an isopropanol bath.

After confluency was reached, cells grown on gelatin were harvested by trypsinization and DNA was isolated using the QIAamp DNA Mini Kit (Qiagen) according to the manufacturer´s instructions. Correct integration was assessed using the respective genotyping PCRs (see paragraph 2.2.1.2 as well as Figure 3.12 and Figure 3.33). Clones positive in the genotyping PCRs were thawed and seeded on one well of a 48-well plate coated with Mitomycin C treated feeder cells (only ES cell clones electroporated with ROSA26-STOP-SATB1). When confluent (approximately every 3 to 4 days) cells were transferred to larger wells (24-well, 12-well and 6-well plates) and cultured with the volumes of medium given in Table 2.27.

Table 2.27 Volumes of reagents used for ES cell culture in different culture vessels

Cell culture vessel	Volume of 0,1% gelatin [ml]	Volume of ES-DMEM [ml]	Volume of PBS for washing [ml]	Volume of Trypsin-EDTA [ml]	Volume of ES-DMEM to stop trypsinization [ml]
48-well	0.1	0.5	0.5	0.1	0.5
24-well	0.25	1.5	1	0.25	1
12-well	0.5	2.5	2	0.5	2
6-well	1	7	3	1	4
6 cm	3	4	5	2	6
10 cm	6	10	10	5	15

When confluency was reached on 6-well plates, cells were harvested and one third of each clone was seeded onto a new 6-well coated with feeder cells and cultured for another 3 to 4 days, followed by harvesting of cells and isolation of DNA for Southern blot analysis, as described in paragraph 2.2.1.8. The remaining suspension was harvested by centrifugation (200 x g for 3 min), resuspended in 1x freezing medium and frozen at -80 °C. For long-term storage, frozen cells were transferred to -196 °C after 24 h at -80 °C.

Clones positive in Southern blot analysis were thawed, seeded onto a 6-well plate coated with feeder cells and cultured at 37 °C and 5 % CO_2 until confluency was reached (approximately three days). Confluent wells were harvested, transferred to a 6-cm dish and cultured for two to three days until confluency was reached. One third of the confluent 6-cm dish culture was seeded onto a new feeder cell-coated 6-cm dish and further cultured. The remaining two thirds of the cell suspension were harvested by centrifugation, resuspended in 1 ml ES-DMEM and transferred on ice to the Genetic resource center, University of Bonn, for blastocyst injections into B6-albino (B6(Cg)-Tyrc-^{2J}/J) blastocysts. Blastocyst injections were performed according to in-house protocols and injected blastocysts were implanted into pseudo-pregnant foster mice. Chimeric founders originating from these injections were further bread to C57BL/6J mice and offspring was analyzed by PCR for the presence of the targeted allele (see paragraph 2.2.1.2 and Figure 3.35).

2.2.2.1.1 Cultivation and preparation of MEF feeder cells

Mouse embryonic fibroblasts were obtained from Prof. Thomas Wunderlich, Institute of Genetics, University of Cologne, as zero generation embryonic fibroblasts (EF0). EF0 cells had been generated from day 13.5 embryos by removing the head and the red tissue and cultivating the remaining cells. Adherent cells were regarded as EF0 cells and frozen at -80°C.

One vial of EF0 cells was thawed and cells were cultured on three 15-cm dishes coated with 0.1 % gelatin at RT for 1 h (or overnight at 4 °C) for three days (37 °C, 5 % CO_2). Cells were harvested by trypsinization with 5 ml Trypsin-EDTA for 3 min at 37 °C, followed by stopping of trypsinization with 15 ml of fibroblast cell culture medium (F-DMEM) and centrifugation at 200x g for 3 min. Cells from each 15-cm culture were seeded onto three new gelatin-coated 15-cm dishes. After the first splitting, cells were first generation fibroblast cells (EF1). This process was repeated twice to obtain third generation fibroblasts (EF3), which were used as feeder layer

cells for ES cell culture. To prevent overgrowth of the ES cell cultures by feeder layer cells, EF3 cells were treated with Mitomycin C. Therefore, F-DMEM was exchanged on the third day of EF3 culture with F-DMEM supplemented with 10 µg/ml Mitomcyin C, followed by incubation at 37 °C and 5 % CO_2 for 4 h. Cells were then washed three times with 15 ml PBS to remove Mitomycin C and harvested by trypsinization and centrifugation. Harvested cells were either directly used for coating ES cell culture dishes or were resuspended in 3 ml of 1 x freezing medium and distributed onto three 1 ml freezing vials, followed by freezing at -80°C for later use. The number of cells from 1 freezing vial was sufficient for coating of one 10 cm plate, two 6 cm or one 6-,12-,24-, 48- and 96-well plate.

2.2.2.1.2 Preparation of the targeting construct for electroporation

40 µg of pSATB1-Flex and the pROSA26-STOP-SATB1 targeting constructs were linearized by restriction digest with KpnI and AsiSI, respectively, according to the standard restriction digestion protocol given in paragraph 2.2.1.1 with an upscaling of reagent volumes to adapt the reaction to the higher amount of plasmid DNA. The linearized construct was subsequently purified by isopropanol/ethanol precipitation, the dried pellet was dissolved in 400 µl RPMI medium without Phenolred and subjected to ES cell transfection.

2.2.2.2 Generation of gene targeted mice by oocyte injections

Oocyte injections were performed at the House of Experimental Therapy, University Hospital Bonn, in accordance with the German legislation governing animal studies following ‘The Principles of Laboratory Animal Care’ [116]. Protocols for injections were reviewed and approved by the Animal Care Commission of North Rhine Westfalia, Germany (permit number: 8.87-50.10.31.09.042).

Satb1 TALEN mRNAs were prepared as described in paragraph 2.2.1.3 and equal amounts of each TALEN mRNA were mixed. The mixture was then diluted to 2x working concentrations in injection buffer (0.25mM EDTA, 10mM Tris, pH 7.4). The pSATB1-Flex targeting construct was linearized and purified as described in paragraph 2.2.2.1.2 and the pellet was resuspended in injection buffer at 10 ng/µl. Equal volumes of TALEN and targeting vector solutions were united to yield the final injection solutions with two different TALEN mRNA concentrations (10 ng/µl and 5 ng/µl) and a fixed concentration of pSATB1-Flex targeting vector (5 ng/µl). The differentially concentrated injection solutions were injected into the male pronucleus

of single-cell mouse embryos (B6D2F1 x C57BL/6J) in M2 medium (Sigma) using a Piezo-driven micromanipulator, followed by incubation for 4 h at 37 °C. Injections were performed at the House of Experimental Therapy, University Hospital Bonn. Non-lytic embryos were selected and transferred into the oviducts of pseudo-pregnant foster mothers and offspring was analyzed by genotyping PCRs and Southern blot analysis to assess correct integration of the targeting construct, as well as Surveyor assays and Sanger sequencing to assess mutation of the *Satb1* locus.

2.2.3 Mice

2.2.3.1 General characteristics of mice used for experiments

Mouse lines used in this thesis were housed under specific pathogen-free conditions at the Genetic Resources Center, University of Bonn, and used in accordance with the German legislation governing animal studies following 'The Principles of Laboratory Animal Care' [116]. If not specified for the respective experiment, mice were between eight weeks to three months of age. Mice in experimental and control cohorts were always age and sex matched. When possible, littermates were used in experimental and control cohorts.

2.2.3.2 Tamoxifen administration

Tamoxifen was dissolved at a final concentration of 40 mg/ml in olive oil and stored at -20 °C until use. Before use, the solution was thawed and warmed to 37 °C. Tamoxifen was administered to mice by oral gavage, whereby a gavage needle is inserted into the esophagus of the conscious animal and tamoxifen is directly delivered into the stomach via a syringe. Each mouse received two doses of tamoxifen (8 mg each) at days 0 and 3 and mice were analyzed on day 7.

2.2.4 Isolation and analysis of murine T cells

2.2.4.1 T cell isolation from lymphoid organs

For the isolation of murine T cells, thymus, spleen, peripheral lymph nodes (pLN), mesenteric lymph nodes (mLN) and/or Peyer's Patches (PP) were removed from mice sacrificed by cervical dislocation and subsequently passed through a 70 µm or 100 µm cell strainer. While cells from thymus, pLNs and mLNs, as well as PPs were directly used for downstream analysis, such as analysis by flow cytometry, spleen

samples required further processing to remove erythrocytes from the cell suspensions. Therefore, cells were resuspended in 1 ml red blood cell lysis buffer per spleen, followed by incubation at room temperature (RT) for 2 min under gentle shaking. Lysis was stopped by adding 30 ml PBS, followed by passing the cell suspensions through a 70 µm or 100 µm cell strainer to remove residual debris. Cell suspensions were centrifuged (300x g, 10 min) to remove stopping solution and resuspended in a volume of PBS appropriate for further processing of the sample, e.g. flow cytometric analysis or sorting.

2.2.4.2 Purification of T cells by magnetic and flow cytometry-based cell sorting

To yield highly pure $CD4^+$ T cell subsets, splenocytes isolated as described in paragraph 2.2.4.1 were first subjected to magnetic cell sorting with the $CD4^+$ T cell isolation kit II (Miltenyi Biotec) to enrich for $CD4^+$ T cells. Therefore, splenocytes were resuspended in 20 µl MACS buffer and 5 µl biotin-conjugated antibody cocktail per 1x 10^7 cells and incubated in the dark (4 °C, 15 min), whereby non-$CD4^+$ T cells are labeled with the biotinylated antibodies. After the incubation, 15 µl MACS buffer and 10 µl anti-biotin MicroBeads per 1 x 10^7 cells were added, followed by a second incubation in the dark (4 °C, 20 min) to allow binding of the beads to biotin-antibody labeled cells. Then cells were washed with MACS buffer (300x g, 10 min) to remove unbound antibodies and beads were resuspended in MACS buffer at 0.5 ml per 1x 10^8 cells, but not in less than 0.5 ml MACS buffer. The cell suspension was loaded onto a LS Column, which had been equilibrated with MACS buffer and attached to a MACS Separator magnet by passing the cells through a 30 µm nylon mesh pre-separation filter. The column was washed once with 3 ml of MACS buffer and the flow through containing the enriched $CD4^+$ T cells was collected.

For further purification of $CD4^+$ T cell subsets, enriched $CD4^+$ T cells were subjected to flow cytometry based sorting using a FACS Aria III cell sorter (BD Biosciences). Enriched $CD4^+$ T cells were resuspended in PBS at 2.5x 10^6 cells per 100 µl and appropriate fluorochrome-labeled antibodies at a 1:200 dilution, followed by incubation in the dark (4 °C, 30 min). Cells were washed with PBS (200x g, 10 min) and resuspended in T cell medium, followed by sorting of the respective cell populations (see Table 2.28).

Table 2.28 Cell populations purified by flow cytometry-based cell sorting

Mouse line	T cell population	Surface marker
SATB1$^{+/fl}$ x CD4$^{Cre/+}$	SATB1-GFP^{+} and SATB1-GFP^{-}	CD3^{+}CD4^{+}CD25^{-}GFP^{+}/ GFP^{-}
SATB1-Flex KO/WT	T_{naive}	CD3^{+}CD4^{+}CD25^{-}CD44^{-} CD62L^{+} GFP^{+}/ GFP^{-}
SATB1-KI/WT	T_{conv}	CD3^{+}CD4^{+}CD25^{-}YFP^{-}GFP^{-}
SATB1-KI	T_{reg}	CD3^{+}CD4^{+}CD25^{+}YFP^{+}GFP^{+}
SATB1-KI	exFoxp3	CD3^{+}CD4^{+}CD25^{-}YFP^{-}GFP^{+}
SATB1-WT	T_{reg}	CD3^{+}CD4^{+}CD25^{+}YFP^{+}GFP^{-}

2.2.4.3 *In vitro* proliferation assays

T_{naive} cells isolated from spleens of SATB1-Flex KO and WT mice and purified as described in paragraph 2.2.4.2 were stained with the membrane intercalating dye eFluor450 (eBioscience) by incubating 1 x 10^7 cells per ml (but at least 0.5 ml) in PBS supplemented with 10 µM eFluor450 protected from light (RT, 20 min). The staining reaction was stopped by addition of 4-5 volumes of T-cell medium and cells were washed three times with T-cell medium to remove residual non-intercalated dye.

Labeled cells were then stimulated by culturing in T cell medium at 1x 10^6 cells per ml for 48 h (37 °C, 5 % CO_2) in presence of soluble anti-CD28 (2 µg/ml) and plate-bound anti-CD3, which had been bound to the plate in advance by incubating the plate with 100 - 200 µl anti-CD3 antibody (5 µg/ml in PBS) for 2 h at RT or overnight at 4 °C. Finally, cell proliferation was assessed using a BD LSR II flow cytometer (BD Biosciences) and evaluated with Flow Jo 7.6.5 software.

2.2.4.4 *In vitro* suppression assays

T_{conv} cells isolated from spleens of SATB1-WT mice and purified as described in paragraph 2.2.4.2 were stained with the membrane intercalating dye eFluor670 (eBioscience) by incubating 1x 10^7 cells per ml (but at least 0.5 ml) in PBS supplemented with 5 µM eFluor670 protected from light (37 °C, 10 min). The staining reaction was stopped by addition of 4-5 volumes of FCS, followed by incubation on ice for 5 min and two washing steps with T-cell medium to remove residual non-intercalated dye. 1x 10^5 labeled T_{conv} cells were then co-cultured with the respective T_{reg} and exFoxp3 cells from SATB1-KI and SATB1-WT mice, respectively, at T_{conv} : T_{reg}/exFoxp3 ratios of 1:0, 1:1, 2:1, 4:1, 8:1 and 16:1 for 72 h at 37 °C and 5 % CO_2.

Additionally, to stimulate T_{conv} cells anti-CD3/anti-CD28-coated beads (Dynabeads Mouse T-Activator CD3/CD28, Thermo Fisher Scientific) were added to the T-cell culture in a T_{conv} : bead ratio of 3:1. The final volume of the assay was 200 µl per condition. Labeled T_{conv} cells cultured alone without beads served as unstimulated control. After 72 h T_{conv} cell proliferation as marker for T_{reg}/exFoxp3 cell suppressive activity was assessed by flow cytometry with a BD LSR II flow cytometer and evaluated with Flow Jo 7.6.5 software.

2.2.4.5 *In vitro* differentiation of naive T cells

For *in vitro* differentiation, T_{naive} cells isolated from spleens of SATB1-Flex KO and WT mice and purified as described in paragraph 2.2.4.2 were stimulated with plate-bound anti-CD3 and soluble anti-CD28 (see paragraph 2.2.4.3) in a 96-well plate (max. volume 200 µl) at 1 x 10^5 cells/well for five days at 37 °C and 5 % CO_2 in presence of respective TH subset-promoting cytokines as well as anti-IL-4 and anti-IFN-γ antibodies, as shown in Table 2.29:

Table 2.29 T cell medium supplements for *in vitro* differentiation of TH1, TH2 and TH17 cells

	TH1	TH2	TH17
IL-2	100 U/ml	100 U/ml	-
IL-4	-	5 ng/µl	-
IL-12	5 ng/µl	-	-
TGF-β	-	-	1 ng/µl
IL-6	-	-	20 ng/µl
anti-IL-4	10 µg/µl	-	-
anti-IFN-γ	-	10 µg/µl	10 µg/µl

To evaluate TH subset differentiation, cultured cells were subjected to intracellular cytokine staining (see paragraph 2.2.4.82.2.4.7) after five days and subsequently cytokine production was assessed by flow cytometry with a BD LSR II flow cytometer and evaluated with Flow Jo V10 software.

2.2.4.6 $RAG2^{-/-}$ adoptive colitis model

Naive T cells isolated from spleens of SATB1-Flex KO and WT mice and purified as described in paragraph 2.2.4.2 were intravenously injected into the tail vein of five- to six-month-old $RAG2^{-/-}$ mice at 1 x 10^6 T_{naive} cells per $RAG2^{-/-}$ mouse (injections were performed by M. Schunk, AG Förster). $RAG2^{-/-}$ mice injected with PBS without T_{naive} cells served as vehicle control. $RAG2^{-/-}$ mice were weighed prior to injection and afterwards 3 times per week. Furthermore, mice were assessed for signs of colitis,

such as loose stools and behavioral changes. 21 days after injection, mice were sacrificed by cervical dislocation and mLNs, spleen and large intestine were isolated. Cells from mLNs and splenocytes were analyzed by flow cytometry to determine absolute numbers of $CD4^+$ T cells in the respective organs, as well as IL-17, IFN-γ and Foxp3 expression in these cells (see paragraphs 2.2.4.7 and 2.2.4.8). Isolated colons were flushed with PBS using a syringe to remove stool, followed by determination of colon length.

2.2.4.7 Analysis of murine T cells by flow cytometry

For surface antigen staining, cells resuspended in PBS were incubated with the respective fluorochrome-conjugated antibodies at a 1:200 dilution in the dark (4 °C, 20 min). Afterwards cells were washed with PBS to remove unbound antibody and either directly analyzed by flow cytometry or subjected to intracellular staining using the Foxp3/Transcription Factor Staining Buffer Set (eBioscience) according to the manufacturer's protocol. Unspecific binding sites were blocked by addition of CD16/CD32 antibody cocktail (obtained from Zeinab Abdullah, University Hospital Bonn) at a 1:200 dilution and incubation in the dark (RT, 15 min) before addition of the fluorochrome-conjugated antibodies. After blocking of unspecific binding sites, antibodies against intracellular proteins as well as the respective isotype control antibodies were directly added at the respective dilutions (see Table 2.30), followed by incubation in the dark (RT, 30 min).

Table 2.30 Dilutions of antibodies for intracellular immunostaining

Antigen	Final dilution
Foxp3	1:80
IFN-γ	1:200
IL-4	1:200
IL-17A	1:200
Ki-67	1:200
SATB1	1:66

After the final washing step, cells were resuspended in PBS and analyzed by flow cytometry on a LSR II or BD FACS Aria III flow cytometer. Data evaluation was performed using FlowJo v10 software. Absolute cell numbers were determined by flow cytometry by adding 20 µl liquid counting beads (BD Bioscience) per sample prior to the staining procedure. Beads were assessed by flow cytometry together with

the stained cells and absolute cell numbers were determined according to the manufacturer´s protocol.

2.2.4.8 Intracellular cytokine staining

Intracellular cytokine staining was performed with $CD4^+$ T cells obtained from *in vitro* differentiation and whole cell suspensions from mLNs of $RAG2^{-/-}$ mice from the adoptive colitis model to determine T_{eff} cytokine production as marker for effector T cell subsets.

Therefore, cells (either one well per condition from *in vitro* differentiation or one fourth of each mLN from the adoptive colitis model) were stained with CD3 and CD4 antibodies as described in paragraph 2.2.4.7 . Cells were then cultured in a 24-well plate in 1 ml of T cell medium supplemented with 1x Monensin, 1x Brefeldin and 1x cell stimulation cocktail (eBioscience) at 37 °C and 5 % CO_2 for 4 h. Cells from each experimental condition cultured under the same conditions without cell stimulation cocktail served as control. Subsequently, cells were washed with PBS and stained with Live/Dead Fixable Near-IR dye (Thermo Fisher Scientific) diluted 1:1000 in PBS at 4 °C for 15 min. After stopping the live/dead stain by washing with PBS, cytokines were stained using the Foxp3/Transcription Factor Staining Buffer Set (eBioscience), as described in paragraph 2.2.4.7 with antibodies directed against IFN-γ, IL-17 and/or IL-4 (see Table 2.30 for dilutions). Finally, cells were analyzed by flow cytometry on a BD LSR II or BD FACS Aria III flow cytometer. Data evaluation was performed using FlowJo V10 software.

2.2.4.9 Determination of T_{eff} cytokine production of T_{reg} and exFoxp3 cells

T_{reg} cells and exFopx3 cells from SATB1-KI mice as well as T_{reg} cells from SATB1-WT mice were cultured together with anti-CD3/anti-CD28 coated beads (Dynabeads Mouse T-Activator CD3/CD28) at a cell : bead ratio of 1 : 1 in T cell medium supplemented with IL-2 (1000 U/ml) for 72 h (37 °C, 5 % CO_2).

After 72 h supernatants were harvested by centrifugation of cell suspensions at 200x g for 10 min, followed by determination of cytokine concentrations of IL-4, IL-17 and IFN-γ with the mouse TH1/TH2 10-plex Kit (eBioscience) according to the manufacturer's protocol. Samples were analyzed by flow cytometry using a BD FACS Aria III with the parameters FSC, SSC and PerCP-Cy5.5 to discriminate bead populations as well as PE to assess cytokine concentration. Evaluation of the assay was performed with FCAP Array v2.0.1 software.

3 Results

3.1 The role of SATB1 in CD4$^+$ effector T cells

3.1.1 Generation of a mouse model for spatiotemporal deletion of SATB1

3.1.1.1 Development of a targeting strategy to conditionally knock-out *Satb1* with simultaneous reporter gene induction

To generate a conditional knock-out model for *Satb1*, we decided to target exon 2 of the murine *Satb1* locus, which is the first coding exon containing the start codon, to prevent the translation of C-terminally truncated SATB1 transcripts after Cre-mediated recombination of the conditional allele, which might still retain some residual function.

As every gene targeting approach involves insertion of new elements, such as lox sites and coding sequences of reporter proteins, into the genomic locus, the site of integration of these elements has to be carefully chosen to prevent destruction of regulatory elements, such as transcription factor binding regions or splice sites.

Therefore, we chose two regions (Chr17:51809396-51809365 and Chr17: 51808635-51808515), approx. 100 bp upstream and approx. 400 bp downstream of exon 2, as integration sites. These sites were chosen, as they showed low conservation to seven closely related species, under the assumption that a higher degree of conservation would correspond to a higher functional relevance of the respective genomic region (data not shown).

Using these regions for integrating the lox sites (Figure 3.1a), a targeting construct was designed and generated (Figure 3.1a) containing appropriate homologous regions to insert the construct via homologous recombination at the desired position around exon 2 of the *Satb1* locus (Figure 3.1b).

In addition to the conditional removal of *Satb1*, the final conditional allele should also allow tracing of cells, which underwent Cre-mediated recombination by switching on a GFP reporter. Therefore, the targeting construct was based on the Flex system (see paragraph 1.2.1.3), which allows the exchange of gene segments. *Satb1* exon 2 and an inversely orientated artificial exon 2 encoding the splice acceptor, the endogenous 5´ untranslated region (UTR), the start codon fused to the coding sequence of eGFP, and the 3´ UTR of the *Satb1* gene were cloned consecutively in between these Flex sites (Figure 3.1a).

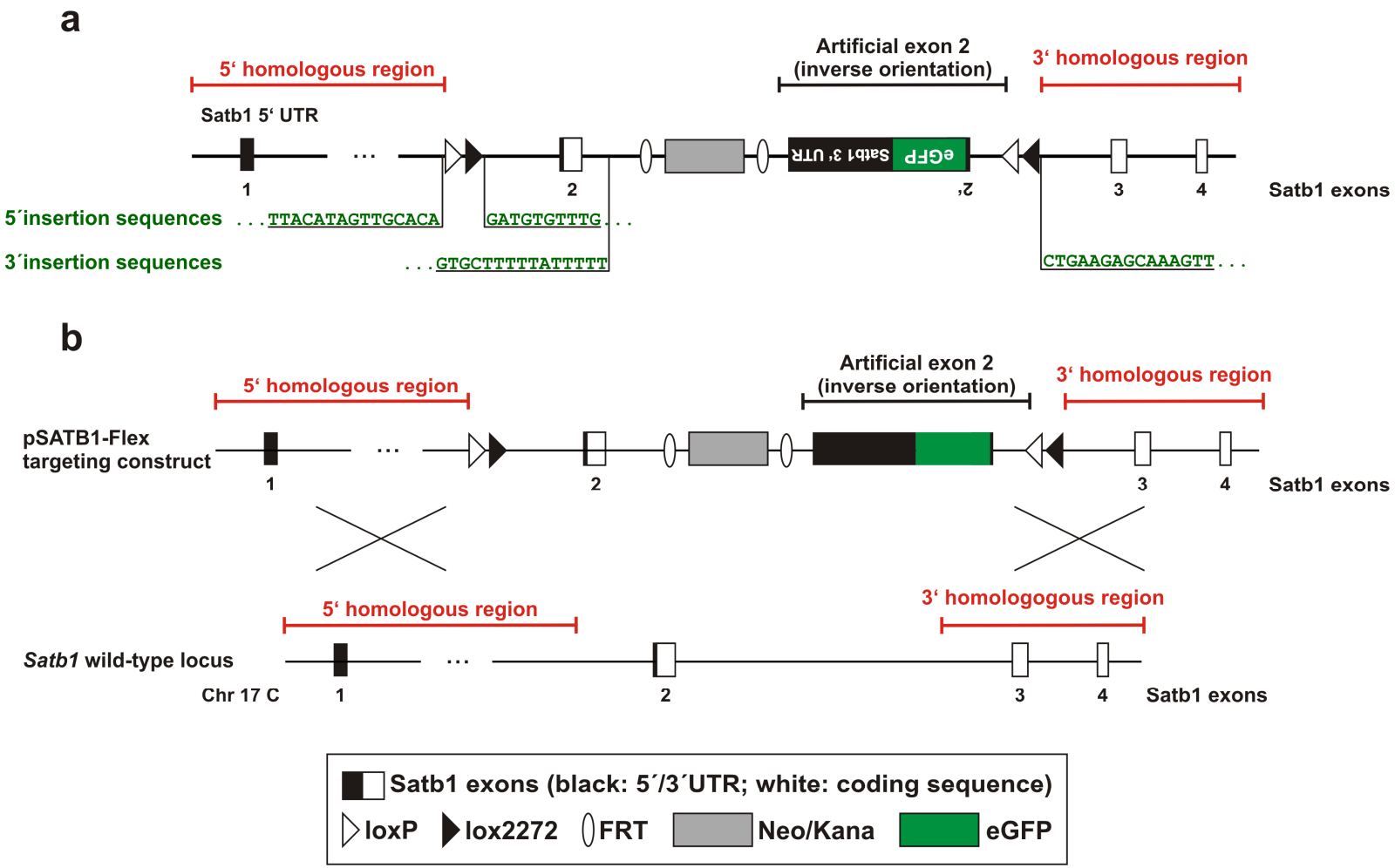

Figure 3.1 Integration of the pSATB1-Flex targeting construct into the murine *Satb1* locus
(a) Scheme of the targeting construct and the sites of the *Satb1* locus disrupted upon integration of the construct (5´and 3´insertion sequences); (b) Integration of the targeting construct into the *Satb1* locus by homologous recombination.

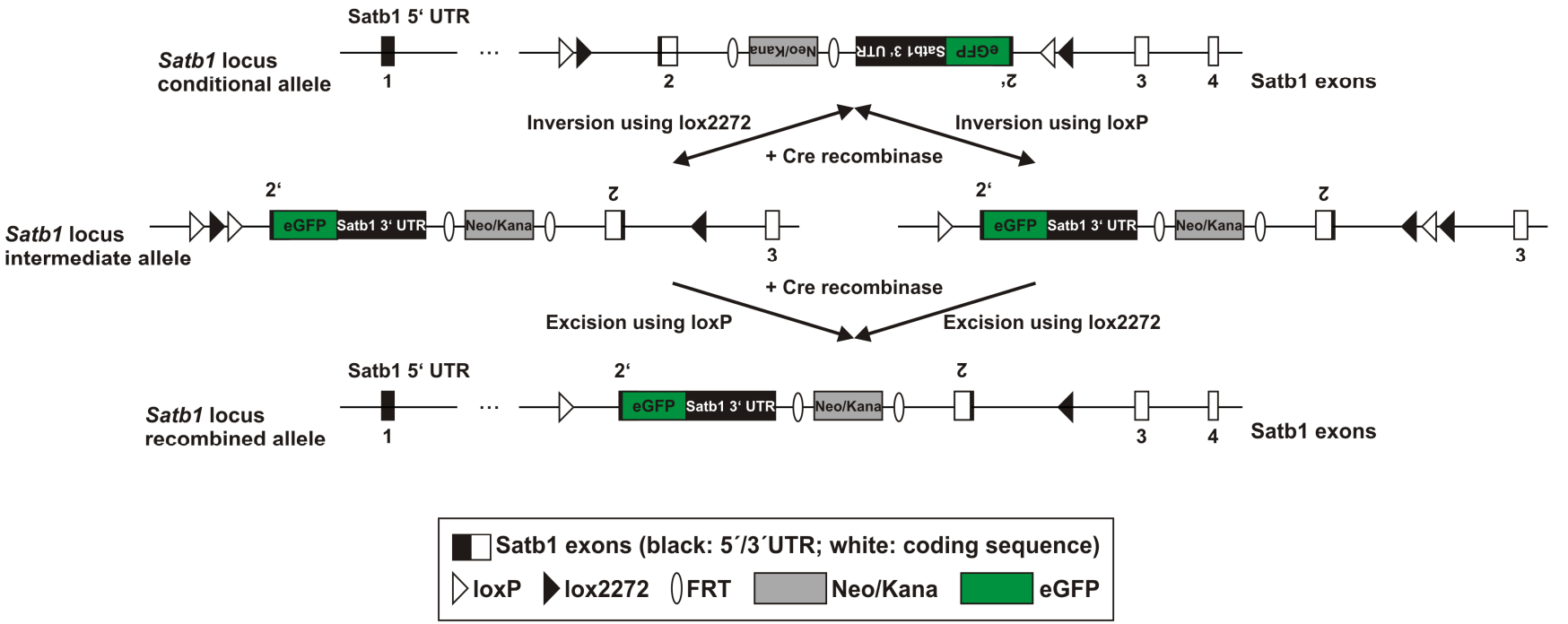

Figure 3.2 Conditional knock-out of *Satb1* with the SATB1-Flex conditional knock-out allele
Scheme illustrating the Cre-mediated irreversible exchange of *Satb1* exon 2 against the artificial exon 2 within the SATB1-Flex conditional knock-out allele, which results in the destruction of the SATB1 coding sequence and the concurrent induction of the GFP reporter.

Due to the Flex-switch both exons will be irreversibly inverted upon Cre-mediated recombination in a two-step process, whereby the endogenous exon 2 is replaced by the artificial exon, which in consequence will lead to destruction of the *Satb1* open reading frame as well as induction of the GFP reporter (Figure 3.2).

3.1.1.2 Full functionality of the Flex-switch in the pSATB1-Flex targeting construct

After generating the targeting construct (pSATB1-Flex) described in 3.1.1.1, the functionality of the Flex-switching approach was tested *in vitro* together with Tristan Wirtz during his Master thesis [115].

In an initial approach, the Cre-mediated recombination was successfully tested by PCR screening of Cre recombinase expressing bacterial clones transformed with pSATB1-Flex, which showed 100 % recombination efficiency (data not shown) and demonstrated that the targeting construct generally allowed for Cre-mediated switching of the Flex cassette.

In addition, we assessed, whether the eGFP reporter was functional after Cre-mediated recombination. Therefore, the Flex cassette of the pSATB1-Flex plasmid was cloned into the eukaryotic expression vector pTriEx4 (Figure 3.3a) and co-transfected with a Cre-encoding vector (pCre-Pac) into HEK293T cells. Cloning into the eukaryotic expression vector was necessary, as the targeting construct did not contain a eukaryotic or the endogenous promoter of the *Satb1* gene and thus was not able to induce transcription of the eGFP expression cassette.

Flow cytometric analysis of co-transfected cells and control cells transfected with pSATB1-Flex only revealed strong induction of eGFP in 25% of the double-transfected cells, while control cells did not show GFP expression (Figure 3.3b and c). These findings indicate that the eGFP encoded by pSATB1-Flex is functional after Cre-mediated recombination and that its induction is strictly dependent on the recombination status of the targeting construct, as eGFP expression was only detectable in cells expressing Cre, but not in the control cells lacking Cre expression.

Since switching of the FLEX cassette as well as eGFP induction could be shown in these *in vitro* systems, the pSATB1-Flex targeting construct was used for gene targeting in the mouse genome.

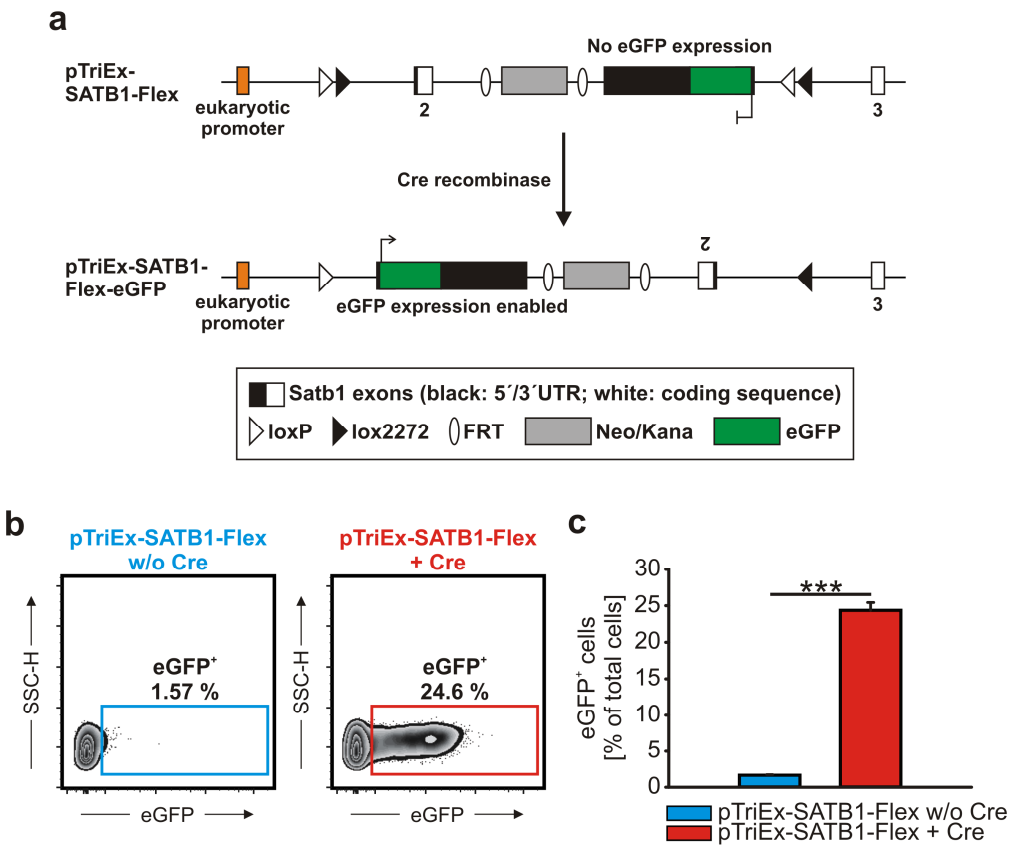

Figure 3.3 Assessment of Cre-mediated eGFP induction in the pSATB1-Flex construct in eukaryotic cells
(a) Scheme of Cre-mediated switching of the Flex cassette and induction of eGFP expression in the pTriExSATB1-Flex vector. (b) Representative dot plots of the flow cytomeric analysis of eGFP induction in HEK293T cells transfected either with pTriEx-SATB1-Flex alone or co-transfected with pCre-Pac vector encoding Cre-recombinase. (c) Quantification of the eGFP expression (n = 3; Mean and s.e.m; * P < 0.05, Student's t-test)

3.1.1.3 Generation of TALENs to target the murine *Satb1* locus

Recently, TALENs have been discovered and described as a valuable tool to enhance gene targeting efficiency (see paragraph 1.2.2).

Based on these findings we hypothesized that induction of a site-specific DNA DSB by specific TALENs should favor the integration of the pSATB1-Flex targeting construct into the murine *Satb1* locus.

A first step in designing appropriate TALENs is the selection of a proper targeting site in the locus of interest to which the TALENs can bind. As we intended to prevent alterations in the *Satb1* coding sequence, which might have fatal consequences for the cell, we restricted our search to intronic regions.

Furthermore, due to a lack of sufficient data at that time on the position of the TALEN targeting site relative to the intended integration site of the targeting construct, we hypothesized that TALEN-mediated DNA double-strand break formation should occur

in the intronic region between the 5´ and the 3´homology regions of the *Satb1* locus (Figure 3.4a). DNA double strand break formation in this region would generate DNA ends compatible to the homologies of the targeting construct, thus favoring homologous recombination via both homologies (Figure 3.4b). Generation of DSBs in one of the homologies, however, would probably lead to HR via the respective homology region and consequently to omitting the integration of the remaining targeting construct (Figure 3.4c and d).

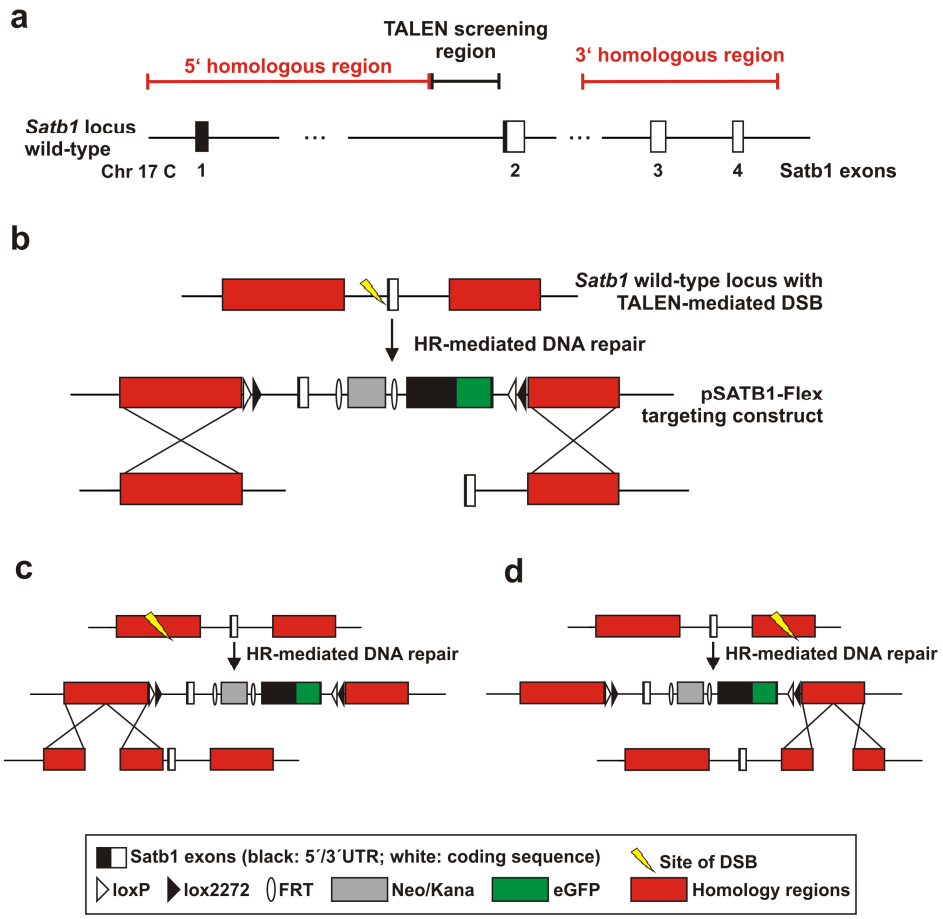

Figure 3.4 Selection of an appropriate region for TALEN-mediated induction of a DNA double-strand break at the *Satb1* locus
(a) Region of the *Satb1* locus selected for TALEN-mediated DNA DSB formation to allow HR-mediated integration of the pSATB1-Flex targeting construct; (b-d) Hypothetical outcomes of HR-mediated integration of the targeting construct after DSB formation in different regions of the *Satb1* locus: (b) DSB between the 5´ and 3´ homologies; (c) DSB in the 5´ homology; (d) DSB in the 3´ homology

To predict optimal sites for TALEN binding and activity in this region, we used the online-tool TAL Effector Nucleotide Targeter 2.0 [114]. This *in silico* prediction identified three TALEN binding sites in forward and two in reverse orientation (Table 3.1), which could be combined to four different TALEN pairs (Table 3.2).

As an additional criterion for selection of the optimal TALEN pair, the TAL Effector Nucleotide Targeter 2.0 was used to predict the number of potential off-targets of these four TALEN pairs in the murine promoterome, which at that time (January 2012) was the only murine reference provided by the tool which, could be used to predict potential off-target sites (Table 3.2 right column). As the combination of TAL1.3 and TAL2.2 showed the lowest number of predicted off-targets, this pair of TALENs was chosen for synthesis and subsequent functional evaluation. Reanalysis of off-targets of this TALEN pair with an advanced version of the TAL Effector Nucleotide Targeter 2.0 allowing for prediction of off-targets in the complete mouse genome revealed even less off-targets than the initial approach (data not shown), further indicating that the TALEN pair had high potential to induce a site-specific DNA DSB without inducing substantial DSBs at off-target sites.

Table 3.1 *Satb1*-locus specific TALEN motifs identified with the TAL Effector Nucleotide Targeter 2.0

	Orientation	RVD sequence	TAL length [bp]
TAL 1.1	forward	HD HD NI HD HD HD NI HD NG NN NI NG NI NI HD NN NG HD NG	19
TAL 1.2	forward	NI NG NI NN NI HD HD NG HD HD NI HD HD HD NI HD NG NN NI	19
TAL 1.3	forward	NI NN NI HD HD NG HD HD NI HD HD HD NI HD NG NN NI NG NI	19
TAL 2.1	reverse	NN NG HD NG NG NI HD NI NN NI NG HD NI HD HD NG NN HD HD	19
TAL 2.2	reverse	NI HD NI NN NI NG HD NI HD HD NG NN HD HD NI NN NI NI HD	19

Table 3.2 *Satb1*-locus specific TALEN pairs and the corresponding numbers of off-targets identified with the TAL Effector Nucleotide Targeter 2.0

TAL Pair	Targeted Locus	Targeting sequence			Spacer length [bp]	# of off-targets (TAL1/TAL2)
		TAL1	Spacer	TAL2		
TAL1.1/ TAL2.1	Chr17:51809317-51809264	CCACCCACTGATAACGTCT	TCTTTTCCAGTTCT	GGCAGGTGATCTGTAAGAC	14	14/119
TAL1.2/ TAL2.2	Chr17:51809325-51809269	ATAGACCTCCACCCACTGA	TAACGTCTTCTTTTCCA	GTTCTGGCAGGTGATCTGT	17	14/36
TAL1.3/ TAL2.1	Chr17:51809323-51809264	AGACCTCCACCCACTGATA	ACGTCTTCTTTTCCAGTTCT	GGCAGGTGATCTGTAAGAC	20	11/119
TAL1.3/ TAL2.2	Chr17:51809323-51809269	AGACCTCCACCCACTGATA	ACGTCTTCTTTTCCA	GTTCTGGCAGGTGATCTGT	15	11/36

#: number

3.1.1.4 Assessment of *in vitro* and *in vivo* functionality of the generated TALENs

After successful generation of the TALEN pair TAL1.3 (TALEN 1) and TAL2.2 (TALEN 2), the activity of these molecules to induce double-strand breaks was assessed.

For this purpose, an *in vitro* assay was applied, in which TALEN proteins are generated *in vitro* from TALEN-encoding plasmids using an *in vitro* transcription/translation system (TnT assay). After generation of TALEN proteins, a PCR product corresponding to the genomic region encompassing the TALEN targeting site is added to the TALEN proteins, which will be cleaved at the designated site by functional TALENs. The presence or absence of the cleavage fragments, which serves as marker for TALEN activity, is then assessed by agarose gel electrophoresis. To assess the *in vitro* activity of the TALENs directed against the *Satb1* locus, a 3 kb PCR product was added to the TnT assay, which should in case of functional TALENs be cleaved into 1.2 kb and 1.8 kb fragments (Figure 3.5).

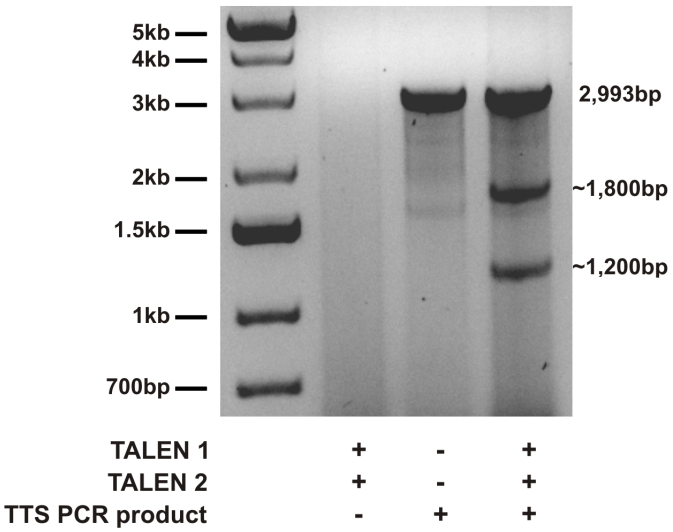

Figure 3.5 Evaluation of SATB1-TALEN activity *in vitro*
Agarose gel electrophoresis of TALEN-targeting-site-encoding PCR products subjected to the TnT assay.

Agarose gel electrophoresis of the TALEN-targeting site containing PCR product incubated in presence of the TALEN proteins yielded the 3 kb band representing the initial PCR product, as well as two 1.2 kb and 1.8 kb bands with sizes of the expected cleavage fragments, indicating successful TALEN-mediated DSB formation.

These bands were not present in the control reactions performed in the absence of TALEN-encoding plasmids or the PCR product, respectively, which shows that they did not result from a self-degraded PCR product or from the TnT system itself. Thus,

the TALENs generated to target the murine *Satb1* locus are able to recognize and cleave the TALEN targeting site *in vitro*.

In addition to the *in vitro* assay, the induction of mutations at the *Satb1* locus in NIH3T3 cells expressing the SATB1-TALENs was assessed using the T7 Endonuclease I assay [87, 117] to determine the potential of the SATB1-TALENs to induce DSBs at the *Satb1* locus in a cellular environment. Therefore, the murine fibroblast cell line NIH3T3 was transfected with a combination of the two plasmids encoding the TALENs directed against the murine *Satb1* locus, followed by isolation of genomic DNA from these cells 24 h, 48 h and 72 h after transfection. From this genomic DNA, a 606 bp PCR product spanning the designated TALEN targeting site was amplified, denatured, re-annealed and subsequently subjected to T7 endonuclease I cleavage (Figure 3.6a). Afterwards, the PCR product was separated by agarose gel electrophoresis to detect potential cleavage fragments of this T7 assay, which should result in bands of 400 bp and 200 bp in case of successful TALEN-induced mutations at this site (Figure 3.6a). In addition to cells transfected with both TALEN plasmids, the T7 assay was also performed with NIH3T3 cells transfected with one of the individual TALEN plasmids or a control plasmid not encoding TALENs. These cells served as negative controls as induction of mutations at the *Satb1* locus should not occur under these conditions.

Both the 400 bp and 200 bp cleavage fragments were present in the samples derived from the cells transfected with the combination of the two TALEN plasmids, but not in the samples derived from the control cells (Figure 3.6b).

This indicates that only in cells transfected with both TALENs mutations at the *Satb1* locus were induced, supporting that this TALEN pair is able to recognize and induce double-strand breaks at the *Satb1* TALEN-targeting site also in its *in vivo* environment.

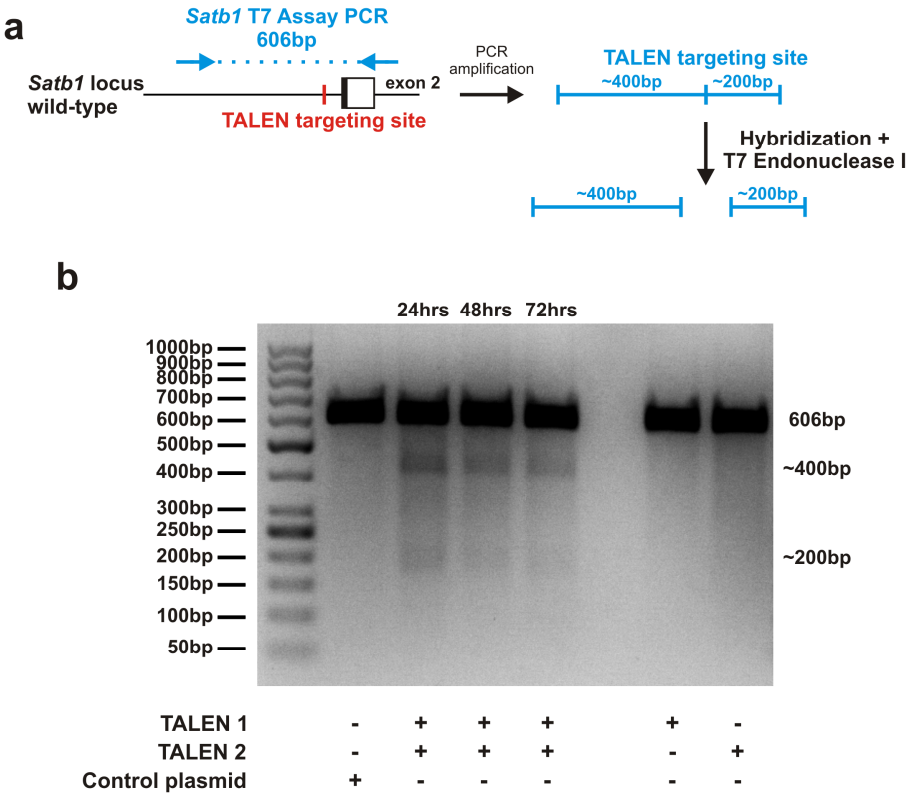

Figure 3.6 Evaluation of SATB1-TALEN activity *in vivo*
T7 Endonuclease I assay with genomic DNA isolated from NIH3T3 cells transfected with combinations of TALENs targeting the *Satb1* locus. (a) Principle of the T7 Endonuclease I assay. (b) Agarose gel electrophoresis of PCR products from transfected NIH3T3 after the T7 Endonuclease I assay.

3.1.1.5 Mutation of the TALEN-targeting site encoded in the pSATB1-Flex plasmid to prevent TALEN-mediated cleavage of the targeting construct

Since the TALEN-targeting site was not only present at the endogenous *Satb1* locus, but also in the pSATB1-Flex targeting construct, it was likely that the TALENs would also cleave the targeting construct, when used in combination. This would consequently lead to a mutation of the TALEN targeting site and thus to an undesired alteration of the pSATB1 targeting construct or the targeted allele. Thus, to prevent TALEN-mediated cleavage the TALEN-targeting site was mutated by introducing three point-mutations at each of the two TALEN-binding sites. To assess whether these point mutations were sufficient to prevent TALEN-mediated cleavage, a TnT assay was performed with the PCR-amplified TALEN-targeting site of the mutated pSATB1-Flex targeting construct (Figure 3.7). In addition, the assay was also performed with the TTS of the non-mutated construct, which served as positive control.

As expected, the non-mutated TTS showed the two cleavage fragments of 1.7 kb and 1.35 kb after TALEN-mediated cleavage. In contrast, these bands were absent in the TnT with the mutated TTS PCR product, indicating that the introduction of the six point-mutations prevented TALEN binding and subsequent cleavage.

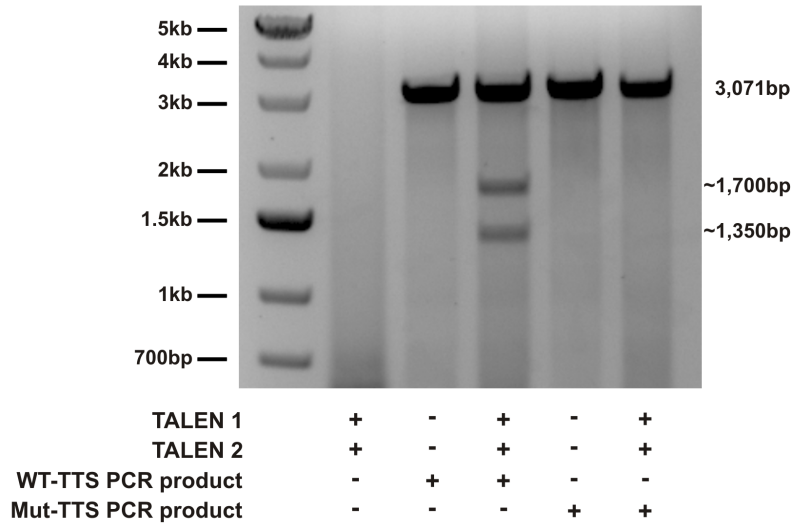

Figure 3.7 Mutation of the pSATB1-Flex targeting construct to prevent TALEN-mediated cleavage
Agarose gel electrophoresis after the TnT assay performed with the mutated (Mut-TTS PCR product) and non-mutated (WT-TTS PCR product) pSATB1-Flex targeting construct.

3.1.1.6 TALEN-assisted homologous recombination of the pSATB1-Flex plasmid in murine embryonic stem cells

After demonstrating that the TALENs targeting the *Satb1* locus were functional and did not cleave the mutated targeting construct, we tested, whether these TALENs enhanced site-directed integration of the pSATB1-Flex targeting construct *in vivo* by homologous recombination. Therefore, the pSATB1-Flex targeting construct was electroporated either alone or together with an equimolar amount of SATB1-TALEN plasmids into JM8A3 murine ES cells (Figure 3.8). Cells from both conditions were then cultured in the presence of G418 to select for clones with an integrated targeting construct, followed by expansion of single surviving clones and PCR-based screening to identify correctly targeted clones. This PCR-based screening consisted of a combination of three PCRs (Figure 3.9a) to confirm the integration of the pSATB1-Flex targeting construct (genotyping PCR) and to detect *Satb1*-locus specific integration at the 5´ (5´ homology PCR) and 3´ (3´ homology PCR) end, respectively.

Interestingly, ES cells transfected without TALEN plasmids showed a 2.4 times lower number of overall surviving clones than cells transfected with the combination of targeting construct and TALEN plasmids (see Table 3.3, 4th column). This already pointed towards a higher rate of locus-specific integration in the latter condition, as cells with randomly integrated parts of the construct should have a lower survival rate due to the presence of the DTA cassette in the targeting construct.

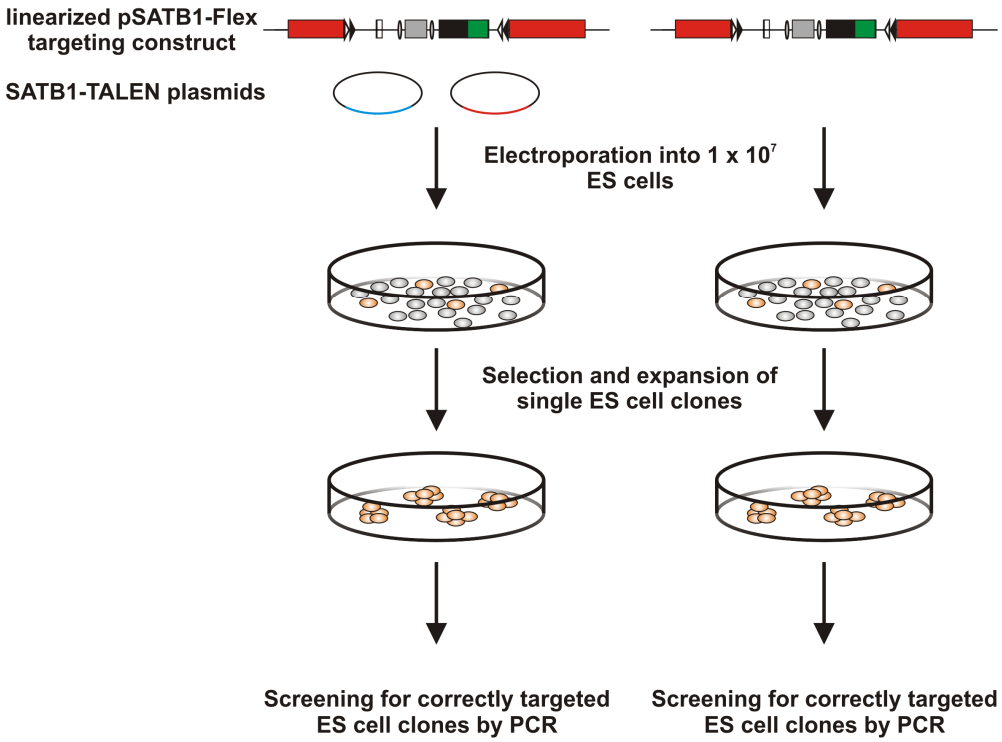

Figure 3.8 Experimental setup for the assessment of TALEN-assisted homologous recombination of the pSATB1-Flex construct in murine JM8A3 ES cells

Most of the surviving clones showed a 747 bp PCR product in the genotyping PCR (Appendix Figure 6.1), which confirmed that these clones contained the targeting construct within their genome. Furthermore, there was no difference in the percentage of clones positive in this PCR between cells treated with TALENs and those not transfected with TALENs (Table 3.3, 5th column). However, when these clones were assessed for correct 5´ integration of the pSATB1-Flex targeting vector at the *Satb1* locus using the 5´ homology PCR, 45.6 % of the clones treated with the SATB1-TALENs (n = 62) showed the 2106 bp PCR product indicating proper 5´ integration (Figure 3.9b and Table 3.3, 6th column). In contrast, there was not a single clone, which was positive in the 5´ homology PCR among those cells electroporated with the targeting construct alone (Figure 3.9c, left panel, and Table 3.3, 6th column).

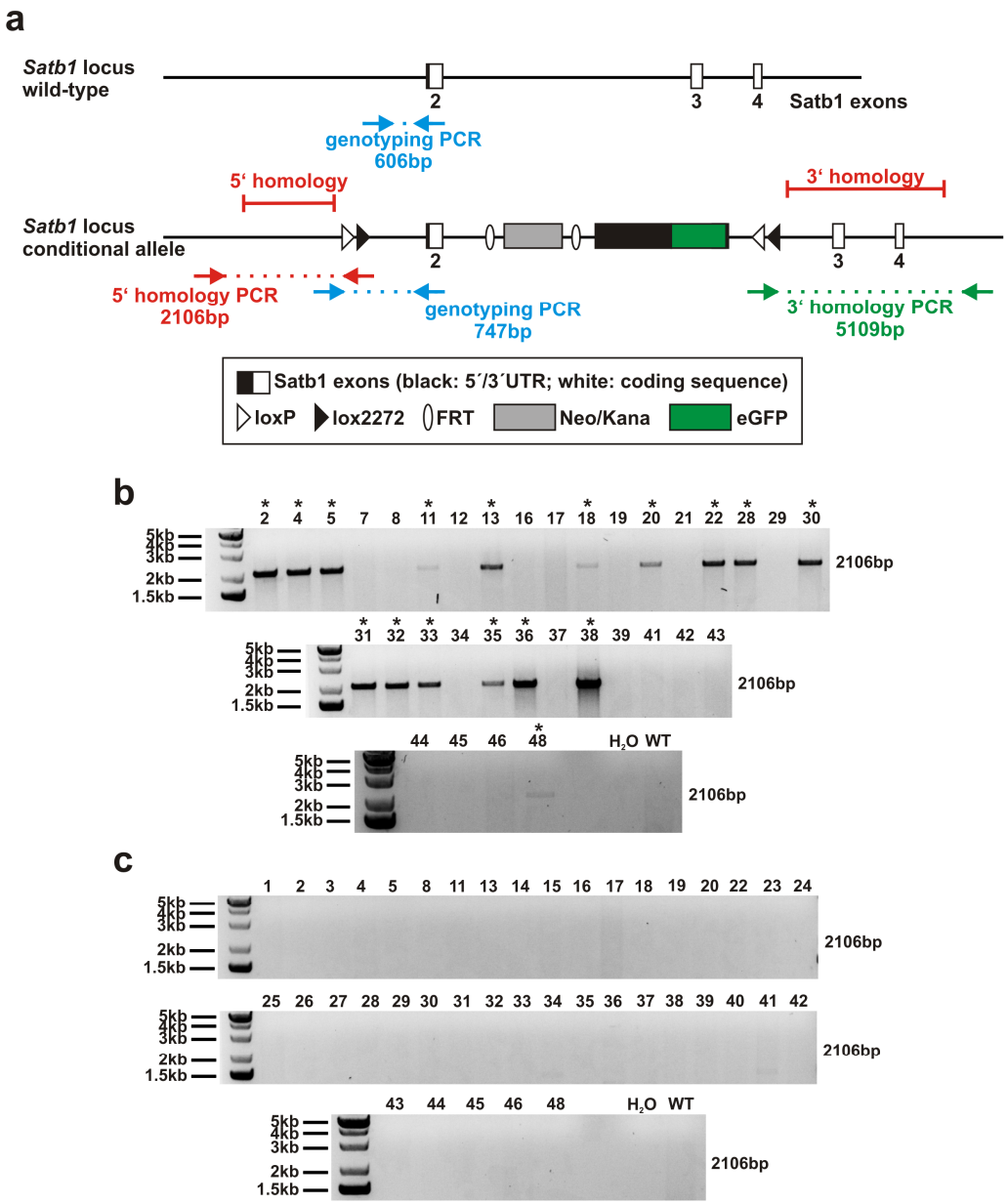

Figure 3.9 Analysis of TALEN-assisted homologous recombination of the pSATB1-Flex targeting construct in ES cells
(a) Scheme of the PCR-based approach to identify correctly targeted ES cell clones. (b) Agarose gel electrophoresis of the 5´ homology PCR performed on representative ES cell clones electroporated with TALENs and positive in the genotyping PCR (see Appendix Figure 6.1a). (c) Agarose gel electrophoresis of the 5´ homology PCR performed on representative ES cell clones electroporated without TALENs and positive in the genotyping PCR (Figure 6.1b). The asterisk (*) indicates clones positive in the respective PCR.

Of the 62 clones correctly targeted at the 5´ end, 41 clones showed the 5109 bp PCR product in the 3´ homology PCR, confirming that these clones were also correctly integrated at the 3´ end (Figure 3.10).

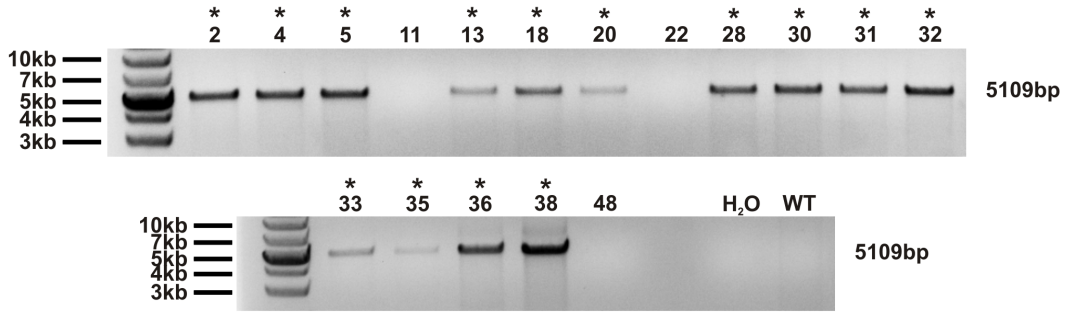

Figure 3.10 Analysis of correct 3´ homologous recombination of the pSATB1-Flex targeting construct in ES cells
Agarose gel electrophoresis of the 3´ homology PCR (Figure 3.9a) performed on ES cell clones positive in Figure 3.9b. The asterisk (*) indicates clones positive in the PCR.

This finally resulted in a percentage of 30.1 % of homologously recombined ES clones after transfection of an equimolar amount of targeting construct and TALENs compared to 0 % in cells transfected with the targeting construct alone (Table 3.3, 7th column).

Table 3.3 Summarized results of the TALEN-mediated *Satb1* gene targeting in JM8A3 ES cells

Dose of		Number (percentage) of				
Satb1-TALEN DNA [µg]	targeting vector DNA [µg]	transfected ES cells	clones surviving selection	clones with integrated targeting construct	clones with 5´-HR-mediated integration	clones with 3´-HR-mediated integration
-	40	1x 10^7	56	47 (83.9 %)	0 (0.0 %)	0 (0.0 %)
20 each	40	1x 10^7	136	114 (83.8 %)	62 (45.6 %)	41 (30.1 %)

Percentages were calculated using the number in each column as the numerator and the number of the surviving clones as the denominator.

In summary, these results show that the pSATB1-Flex targeting construct in combination with the SATB1-TALENs considerably increased the rate of correctly targeted ES cell clones as well as the number of surviving clones. In conjunction, this lead to a noticeable increase in the overall yield of correctly targeted clones compared to the classical methodology, which uses the targeting construct alone. Taken together, these results suggest that TALENs are a promising tool for simplifying the generation of cell lines with complex changes at defined sites in the genome.

3.1.1.7 Generation of a conditional *Satb1*-knock-out mouse by co-injection of TALENs and the targeting construct into mouse oocytes

With the substantial increase in locus-specific integration of the large and complex pSATB1-Flex targeting vector in ES cells, it was hypothesized that the TALEN-mediated increase in homologous recombination would be sufficient to perform gene-targeting directly in oocytes rather than in ES cells. As depicted in Figure 3.11, omitting the ES cell culture would shorten the time to obtain a potentially gene-targeted embryo for implantation from 1-2 months to a single day, thus making the process of mouse generation more efficient.

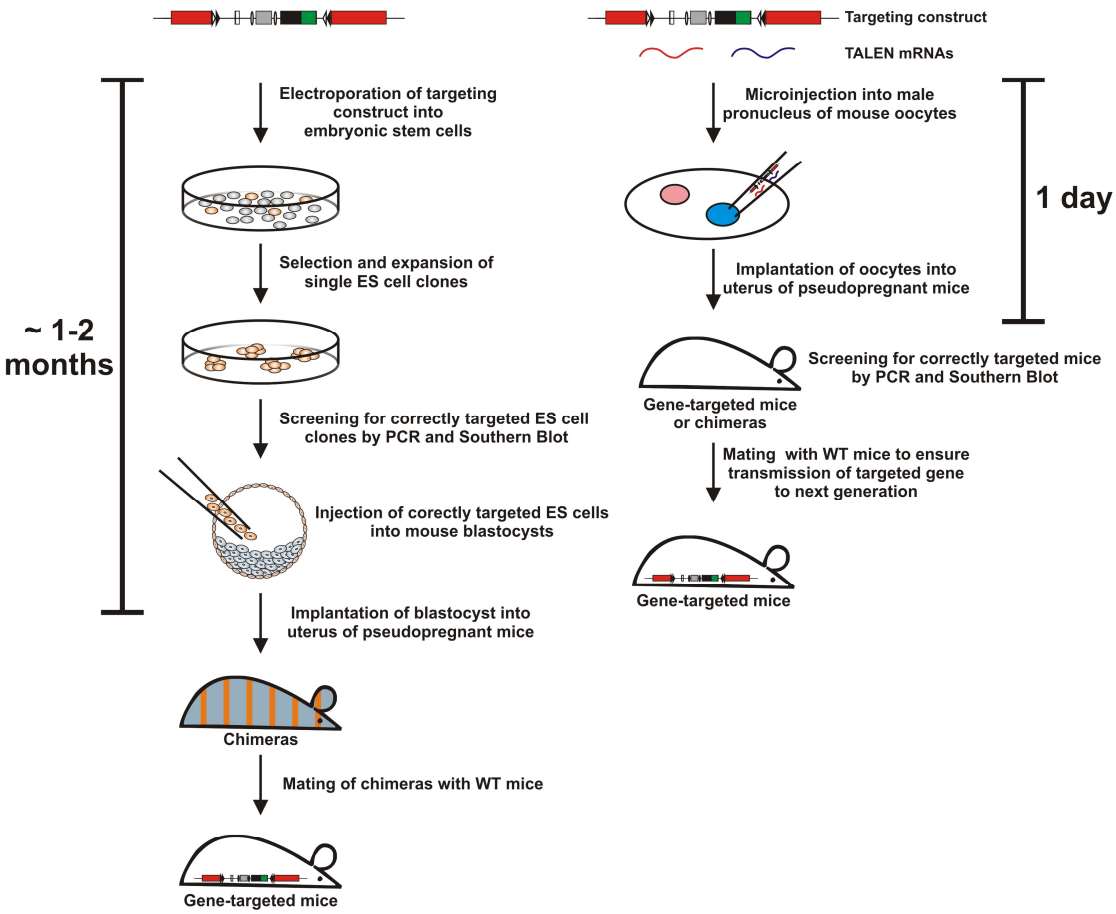

Figure 3.11 Comparison between the timelines of classical gene targeting in ES cells and TALEN-assisted gene targeting directly in oocytes

To test this hypothesis, the linearized pSATB1-Flex targeting construct was injected together with two different concentrations of *in vitro* transcribed SATB1-TALEN mRNAs (5 and 10 ng/µl) into mouse pro-nuclear stage oocytes from B6D2F1 mice, followed by implantation of surviving oocytes into pseudo-pregnant foster mice.

Finally, newborn mice derived from these oocytes were analyzed for mutations at the *Satb1* locus as well as locus-specific integration of the targeting construct.

As depicted in Table 3.4, microinjections with both TALEN mRNA concentrations resulted in viable mice. However, while there was no difference in the survival rates of oocytes directly after injection, the percentage of newborn mice derived from oocytes injected with the higher concentration of TALEN mRNAs was much lower than the percentage of mice derived from injections with the lower mRNA concentration. This relatively strong decrease in the overall survival rate suggests that the mRNA concentrations were already in a cytotoxic range, thus showing that the higher mRNA concentration at least in the combination with the pSATB1-Flex targeting vector was already at or above the upper concentration limit.

Table 3.4 Numbers and percentages of oocytes and newborn mice derived from oocyte microinjections with different SATB1-TALEN mRNA concentrations

Concentration of		Number (percentage) of			
Satb1-TALEN mRNA [ng/µl]	targeting vector DNA [ng/µl]	injected oocytes	surviving oocytes	implanted oocytes	newborn mice
10	5	364	297 (81.6 %)	297	11 (3.7 %)
5	5	533	426 (79.9 %)	426	56 (13.2 %)

Percentages were calculated using the number in each column as the numerator and the number in the column to its left as the denominator.

In addition to the survival rates, it was also analyzed whether the TALEN mRNA injections had led to mutations at the designated TALEN targeting site in the *Satb1* locus. For this purpose, DNA samples prepared from tail biopsies of all newborn mice were screened for mutations at the *Satb1*-TTS by Surveyor nuclease I assays. Positive samples were then confirmed by Sanger sequencing.

With this combinatorial approach 20 mice with mutations at the *Satb1*-TTS were identified in the Surveyor assay (Appendix Figure 6.2 and Figure 6.3), from which 16 could be confirmed by Sanger sequencing (Table 3.5).

Of these 16 mutated mice 11 originated from injections with the lower concentration of TALEN mRNAs, while injections with the higher concentration of TALEN mRNAs gave rise to only five mutated mice. However, considering the overall number of newborn mice generated with the respective TALEN mRNA concentration, the percentage of founder mice carrying a mutation was much higher in the injections with the higher TALEN concentration, which indicates that TALEN activity was dose-dependent. Most of the TALEN-induced mutations in the 16 founder mice were deletions ranging from one or two up to 11 base pairs. Four mice carried mutations

on both alleles (mice 701, 702, 714 and 715). One mouse was identified, which carried a wild-type allele and two differently mutated alleles, indicating a TALEN-mediated chimerism in this mouse.

Table 3.5 Sequencing of the *Satb1*-TTS in founder mice derived from oocyte injections

WT	AGACCTCCACCCACTGATAACGTCTTCTTTTCCAGTTCTGGCAGGTGATCTGT	Nucleotide sequence
719	AGACCTCCACCCACTGATAACGTC----------TTCTGGCAGGTGATCTGT	Δ11bp
	AGACCTCCACCCACTGATAACGTCTTCTTTTCCAGTTCTGGCAGGTGATCTGT	WT
724	AGACCTCCACCCACTGATAACGTC---TTTTCCAGTTCTGGCAGGTGATCTGT	Δ3bp
	AGACCTCCACCCACTGATAACGTCTTCTTTTCCAGTTCTGGCAGGTGATCTGT	WT
740	AGACCTCCACCCACTGATAACGTCTTCTTTTCCAGTTCTGGCAGGTGATCTGT	WT
	AGACCTCCACCCACTGATAACGTCTTCTTTTCCAGTTCTGGCAGGTGATCTGT	WT
	TGTCTTCCACCCACTGATAACGTCTTCTTTTCCAGTTCTGGCAGGTGCTTTTT	random integration
739	AGACCTCCACCCACTGATAACGTC--------CAGTTCTGGCAGGTGATCTGT	Δ8bp
	AGACCTCCACCCACTGATAACGTCTTCTTTTCCAGTTCTGGCAGGTGATCTGT	WT
	TGTCTTCCACCCACTGATAACGTCTTCTTTTCCAGTTCTGGCAGGTGCTTTTT	random integration
848	TGTCTTCCACCCACTGATAACGTCTTCTTTTCCAGTTCTGGCAGGTGCTTTTT	HDR
	AGACCTCCACCCACTGATAACGTCTTCTTTTCCAGTTCTGGCAGGTGATCTGT	WT
714	AGACCTCCACCCACTGATAACGTC---TTTTCCAGTTCTGGCAGGTGATCTGT	Δ3bp
	AGACCTCCACCCACTGATAACGTC---TTTTCCAGTTCTGGCAGGTGATCTGT	Δ3bp
716	AGACCTCCACCCACTGATAACGTCTTCTTTTCCAGTTCTGGCAGGTGATCTGT	WT
	AGACCTCCACCCACTGATAACGTCTTCTTTTCCAGTTCTGGCAGGTGATCTGT	WT
715	AGACCTCCACCCACTGATAACGTC--------CAGTTCTGGCAGGTGATCTGT	Δ8bp
	AGACCTCCACCCACTGATAACGTC---TTTTCCAGTTCTGGCAGGTGATCTGT	Δ3bp
701	AGACCTCCACCCACTGATAACGTC--C-TTTCCAGTTCTGGCAGGTGATCTGT	Δ1+2bp
	AGACCTCCACCCACTGATAACGTC----TTTCCAGTTCTGGCAGGTGATCTGT	Δ4bp
702	AGACCTCCACCCACTGATAACGTC----TTTCCAGTTCTGGCAGGTGATCTGT	Δ4bp
	AGACCTCCACCCACTGATAACGTC----TTTCCAGTTCTGGCAGGTGATCTGT	Δ4bp
747	AGACCTCCACCCACTGATAACGTC---TTTTCCAGTTCTGGCAGGTGATCTGT	Δ3bp
	AGACCTCCACCCACTGATAACGTCTTCTTTTCCAGTTCTGGCAGGTGATCTGT	WT
300	AGACCTCCACCCACTGATAACGTCTTC--TTCCAGTTCTGGCAGGTGATCTGT	Δ2bp
	AGACCTCCACCCACTGATAACGTCTTCTTTTCCAGTTCTGGCAGGTGATCTGT	WT
710	AGACCTCCACCCACTGATAACGTCTTCTTTTCCAGTTCTGGCAGGTGATCTGT	WT
	AGACCTCCACCCACTGATAACGTCTTCTTTTCCAGTTCTGGCAGGTGATCTGT	WT
753	AGACCTCCACCCACTGATAACGTCTTC--TTCCAGTTCTGGCAGGTGATCTGT	Δ2bp
	AGACCTCCACCCACTGATAACGTCTTCTTTTCCAGTTCTGGCAGGTGATCTGT	WT
754	AGACCTCCACCCACTGATAACGTC--------CAGTTCTGGCAGGTGATCTGT	Δ8bp
	AGACCTCCACCCACTGATAACGTCTTC-TTTCCAGTTCTGGCAGGTGATCTGT	Δ1bp
	AGACCTCCACCCACTGATAACGTCTTCTTTTCCAGTTCTGGCAGGTGATCTGT	WT
757	TGTCTTCCACCCACTGATAACGTCTTCTTTTCCAGTTCTGGCAGGTGCTTTTT	HDR
	AGACCTCCACCCACTGATAACGTCTTCTTTTCCAGTTCTGGCAGGTGATCTGT	WT
756	TGTCTTCCACCCACTGATAACGTCTTCTTTTCCAGTTCTGGCAGGTGATCTGT	partial HDR
	AGACCTCCACCCACTGATAACGTCTTCTTTTCCAGTTCTGGCAGGTGATCTGT	WT
729	AGACCTCCACCCACTGATAACGTC---TTTTCCAGTTCTGGCAGGTGATCTGT	Δ3bp
	AGACCTCCACCCACTGATAACGTCTTCTTTTCCAGTTCTGGCAGGTGATCTGT	WT
731	AGACCTCCACCCACTGATAACGTC---TTTTCCAGTTCTGGCAGGTGATCTGT	Δ3bp
	AGACCTCCACCCACTGATAACGTCTTCTTTTCCAGTTCTGGCAGGTGATCTGT	WT
737	AGACCTCCACCCACTGATAACGTC---TTTTCCAGTTCTGGCAGGTGATCTGT	Δ3bp
	AGACCTCCACCCACTGATAACGTCTTCTTTTCCAGTTCTGGCAGGTGATCTGT	WT

HDR: homology-directed repair; DNA sequences of the TALEN-targeting site at the Satb1 locus in founder mice; Sequences in red indicate the TALEN 1-binding site; sequences in blue indicate the TALEN 2-binding site; Black nucleotides within the TALEN-binding site sequences correspond to mutated nucleotides in the Satb1-targeting construct; Dashes indicate TALEN-induced base deletions.

Besides the mutations elicited by the erroneous repair of TALEN-induced double-strand breaks by non-homologous end-joining, the sequencing also revealed mice with an integrated pSATB1-Flex targeting construct (mice 739, 740, 756, 757 and 848), as here the mutations introduced into the TALEN-binding sites of the targeting vector were detected. Furthermore, the sequencing revealed that mice 740, 757 and 848 carried the wild-type allele next to the pSATB1-Flex targeting construct, suggesting that in these mice homology-directed integration of one *Satb1* allele, or random integration of the targeting construct had occurred. In contrast to this, the wild-type allele as well as an eight base-pair deletion in addition to the targeting construct were detected in mouse 739, either indicating random integration of the targeting construct or TALEN-induced chimerism. Unlike these four mice, in which the mutations were present in both TALEN-binding sites, mouse 756 harbored mutations only in the binding site of one of the TALENs. This suggests that here homologous recombination occurred via microhomologies around the TALEN-binding site, thus only integrating a small part of pSATB1-Flex into the murine *Satb1* locus.

To confirm the results of the targeting vector integration observed by the Sanger sequencing, the DNA samples of the 67 mice were additionally analyzed with the PCR-based approach used for screening of the ES cells (Figure 3.9a). To get a more detailed view about the targeting vector integration, this approach was expanded by an additional internal PCR (Figure 3.12a, genotyping PCR II) located downstream of the internal homology (exon 2). In combination with the internal PCR used for the screening of ES cells (Figure 3.12a, genotyping PCR I), this PCR was used to determine whether the whole targeting construct had been integrated, or if only parts were integrated by homologous recombination via the *Satb1* exon 2 as internal homology (Figure 3.13).

As depicted in Figure 3.12b, five mice of the 67 mice tested showed a positive band for integration of the pSATB1-Flex targeting construct in at least one of the genotyping PCRs. Among these, four mice (mice 739, 740, 757 and 848) were present, which had been regarded as carriers of the pSATB1-Flex targeting construct in the previous sequencing approach, confirming that these mice indeed contained at least parts of the targeting construct in their genome.

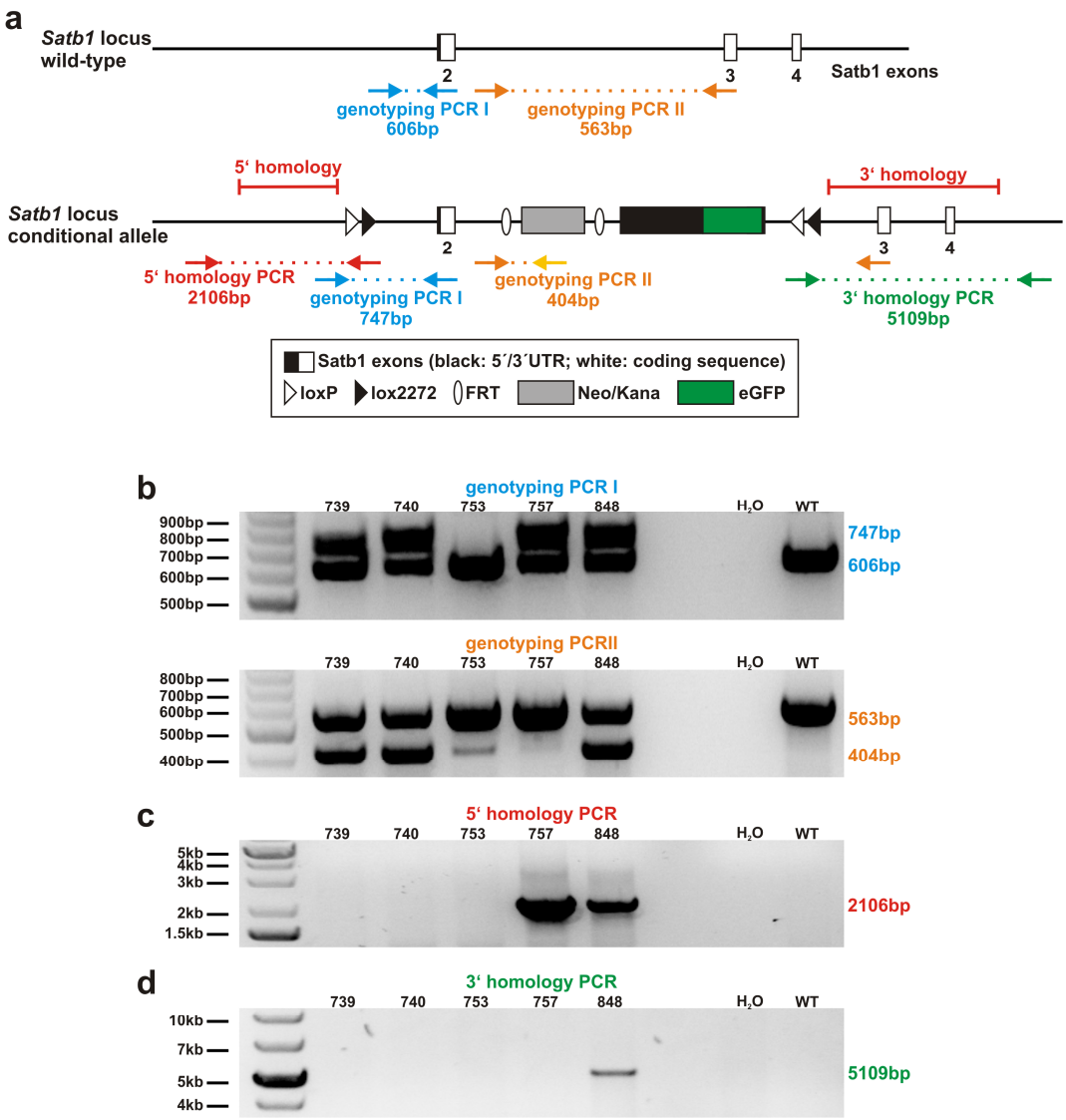

Figure 3.12 Analysis of TALEN-assisted homologous recombination of the pSATB1-Flex targeting construct in mice derived from oocyte injections
(a) Scheme of the PCR-based approach used to identify correctly targeted mice. (b) Agarose gel electrophoresis of the two genotyping PCRs performed on genomic DNA of mice derived from oocyte injections (the five mice positive in at least one of these two PCRs are shown). (c) Agarose gel electrophoresis of the 5´ homology PCRs performed on the mice in (b). (d) Agarose gel electrophoresis of the 3´ homology PCRs performed on the mice in (b).

Mice 739 and 740 showed the 747 bp and 404 bp PCR products in the genotyping PCRs I and II (Figure 3.12b), respectively, but were negative in the 5´ and 3´ homology PCRs (Figure 3.12c and d), which shows that the integration of the targeting construct had occurred at a random site in the genome, but not at the *Satb1* locus. Mouse 757 showed the 747 bp PCR product in genotyping PCR I, but was negative in the genotyping PCR II. Furthermore, this mouse was positive in the 5´ homology PCR (Figure 3.12c), but showed a negative result in the 3´ homology PCR (Figure 3.12d).

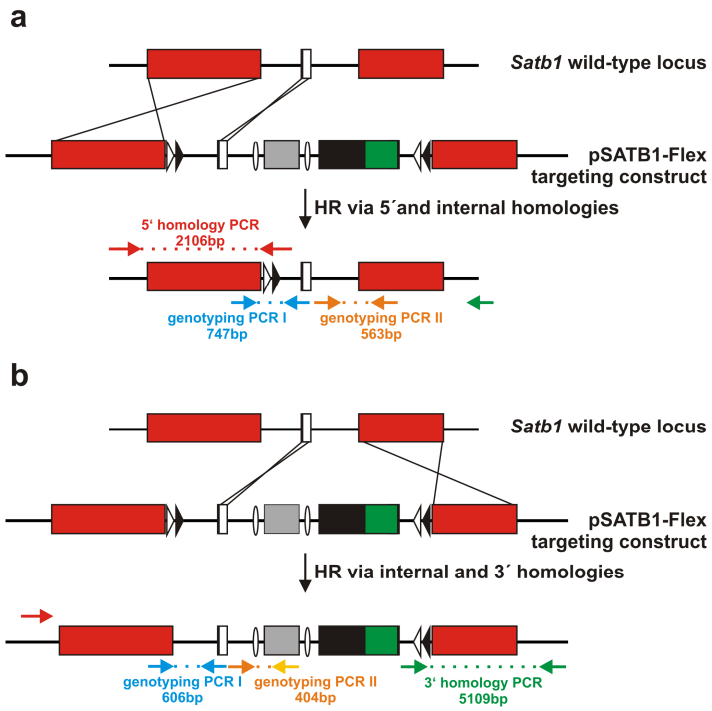

Figure 3.13 Alternative homologous recombinations of the pSATB1-Flex construct
Scheme illustrating the potential homologous recombination of the pSATB1-Flex targeting construct via the Satb1 exon2 as internal homology and the corresponding PCR pattern. (a) Homologous recombination via internal and 5´ external homologies. (b) Homologous recombination via internal and 3´ external homologies.

These results suggest that the pSATB1-Flex targeting construct in this case had been integrated partly by homologous recombination via the 5´ homology and the *Satb1* exon2 contained in the targeting construct serving as internal homology (Figure 3.13a).

Mouse 756, which had been positive for partial targeting vector integration in the sequencing, only showed the wild-type PCR products in the genotyping PCRs and was negative in the homology PCRs (data not shown), suggesting that homologous recombination via microhomologies occurred, which lead to the integration of only the mutated TALEN 1-binding site.

Besides those mice, in which integration of the targeting vector had been identified already in the sequencing, one mouse (mouse 753) not identified in the sequencing approach showed the 404 bp PCR product in genotyping PCR II, but only the wild-type band in genotyping PCR I. This indicates that in this mouse partial integration of the part downstream of exon 2 had taken place (Figure 3.13b), as otherwise the 747 bp band would have been present. Furthermore, this integration had not been site-specific, but at a random site in the genome, as both homology PCRs were negative for this mouse.

In contrast to the mice described so far, mouse 848 yielded the 747 bp and 404 bp PCR products in the respective genotyping PCRs (Figure 3.12b) and displayed a positive result in both homology PCRs (Figure 3.12c and d), showing that here the complete targeting construct had been correctly integrated at the *Satb1* locus in a heterozygous manner, as indicated by the presence of the additional wild-type bands in the genotyping PCRs.

Next, the offspring from mouse 848 was analyzed for the correct integration of the targeting construct with the PCR-based approach described above (Figure 3.12a) to confirm germline transmission of the targeted allele to the next generation (Figure 3.14).

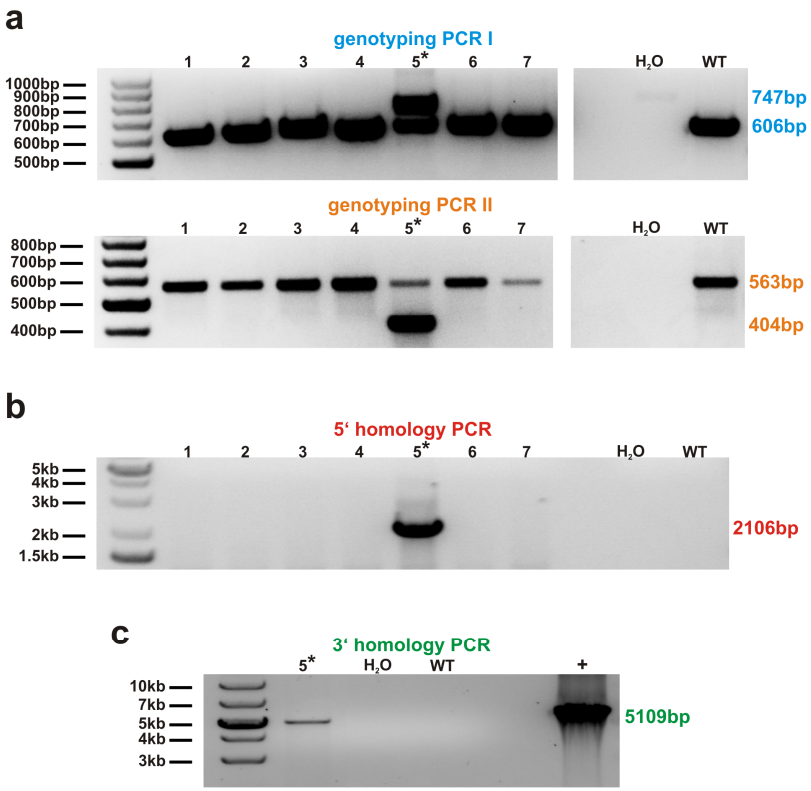

Figure 3.14 Assessment of germline transmission of the SATB1-Flex allele in founder mouse 848
PCR screening of one litter of mouse 848 to identify correctly targeted offspring. (a) Agarose gel electrophoresis of genotyping I and II PCR products. (b) Agarose gel electrophoresis of 5´ homology PCR products. (c) Agarose gel electrophoresis of 3´ homology PCR product derived from DNA of the mouse positive in (a) and (b). The asterisk (*) indicates mice positive in the respective PCR.

As depicted in Figure 3.14, PCR screening of one litter of mouse 848 revealed one mouse positive for the targeting construct in all four PCRs (mouse 5), while the others only showed the wild-type band in the genotyping PCRs and were negative in

the 5´ homology PCR, clearly indicating that mouse 5 harbored the targeted *Satb1* allele.

Thus, these results show that the correctly targeted founder mouse derived from the TALEN oocyte injections transmitted the targeted *Satb1* allele through the germline to the next generation.

After verifying the germline transmission of the targeted *Satb1* allele, a descendant of mouse 848 harboring the SATB1-Flex allele was sacrificed and DNA isolated from the liver was subjected to Southern blot analysis with 5´ and 3´ external probes as well as an internal probe to confirm the correct and single integration of the pSATB1-Flex targeting construct at the *Satb1* locus (Figure 3.15a).

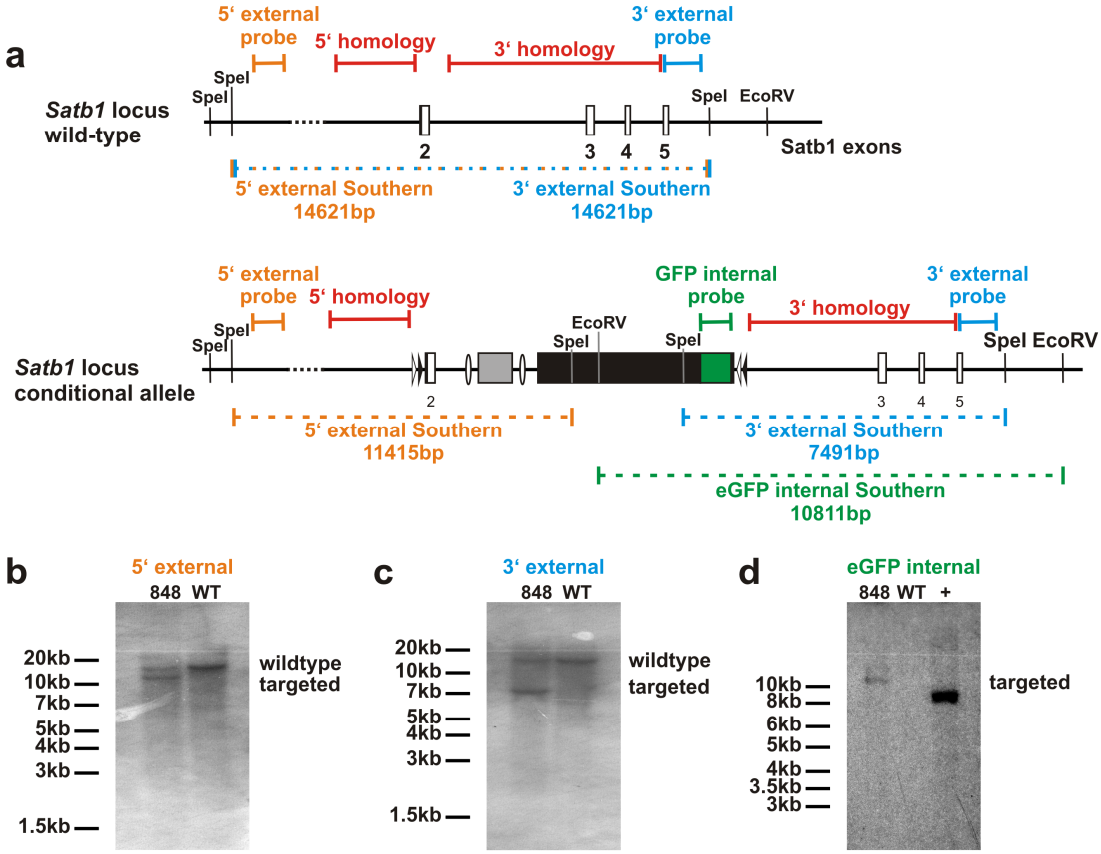

Figure 3.15 Confirmation of correct gene targeting in founder mouse 848 by Southern blot
Southern blot analyses were performed with DNA of a descendent of founder mouse 848 carrying the SATB1-Flex allele. (a) Scheme illustrating the Southern blot strategies for the wild-type and targeted *Satb1* alleles. (b-d) Results of the Southern blot analysis with 5´ external (b), 3´ external (c) and internal eGFP (d) probes.

Southern blot analysis with the 5´ and 3´ external probes revealed the presence of the 11.415 kb and 7.491 kb bands, respectively, corresponding to the targeted *Satb1* allele next to the 14.621 kb wild-type allele (Figure 3.15a, b and c), thus verifying the

correct heterozygous integration of the pSATB1-Flex targeting construct at the *Satb1* locus by homologous recombination.

Furthermore, a single band of 10.811 kb was detected with the internal eGFP probe, while there was no band present in the wild-type DNA sample, indicating the specific detection of the targeting construct with this probe. Since the detected 10.811 kb band matched the size of the band expected in case of correct gene targeting (Figure 3.15a) and since no additional bands were detected with the internal probe, this result further confirmed the correct targeting of the *Satb1* locus as well as the absence of integration of the pSATB1-Flex construct at random sites in the genome.

In summary, these results (Table 3.6) show that the combined injection of appropriate TALENs and a large and complex targeting construct lead to the generation of three mice with partial or complete homologous recombination of the targeting construct. One of these mice showed site-specific integration of the entire targeting construct, thereby generating an allele for the conditional knock-out of the murine *Satb1* gene, which could be passed on to the next generation.

Table 3.6 Summarized results of the TALEN-mediated *Satb1* gene targeting in newborn mice derived from oocyte microinjections with different SATB1-TALEN mRNA concentrations

Concentration of		Number (percentage) of			
Satb1-TALEN mRNA [ng μl^{-1}]	targeting vector DNA [ng μl^{-1}]	mice with TALEN-induced mutations	mice with positive genotyping	mice with homology-directed repair	founder mice
10	5	5 (45.5 %)	3	1	1
5	5	11 (21.4 %)	2	2	0

Percentages were calculated using the number in each column as the numerator and the number in column 6 of Table 3.4 as the denominator.

Thus, these results provide evidence that the combinatorial injection of TALENs and a targeting construct into oocytes in principle enables the establishment of gene targeted mouse lines, even when complex site-specific changes in the genome are intended. Thereby this method provides a fast and easy alternative to the laborious and time-consuming classical gene targeting approaches using ES cell culture.

3.1.2 Full functionality of the generated conditional SATB1-Flex knock-out mouse line

3.1.2.1 The conditional SATB1-Flex knock-out allele maintains SATB1 expression and function in the non-recombined state

Next**,** we assessed whether the integrated targeting construct was functional *in vivo*. To rule out that our manipulations in the genome disturbed *Satb1* gene function, we first evaluated, if the targeted, non-recombined SATB1-Flex allele maintained its function by monitoring of mice homozygous for the SATB1-Flex allele ($SATB1^{fl/fl}$). According to Alvarez *et al.* [98], mice deficient in *Satb1* do not survive weaning and die after three to four weeks of age from brain defects. Furthermore, these mice show a block of T-cell development at the DP stage and lack mature T cells in the periphery. In contrast, $SATB1^{fl/fl}$ mice survived weaning and did not die earlier than their WT littermates, which indicates that the conditional SATB1-Flex allele does not completely abrogate SATB1 expression. To assess the impact of the conditional SATB1-Flex allele in detail, we analyzed the development of T cell subsets in the thymus and the periphery by flow cytometry and determined their SATB1 protein expression (Figure 3.16).

As depicted in Figure 3.16a, $SATB1^{fl/fl}$ mice show normal thymic development of CD4 and CD8 single-positive T cells as well as distinct subsets of $CD4^+$ and $CD8^+$ T cells in peripheral lymphoid organs, such as the spleen, similar to WT littermate controls. Furthermore, there was no difference in SATB1 expression in $CD4^+$ T cells between $SATB1^{fl/fl}$ and WT littermates as shown in Figure 3.16c. This indicates that the conditional SATB1-Flex allele retains the function of the endogenous *Satb1* locus in the non-recombined state.

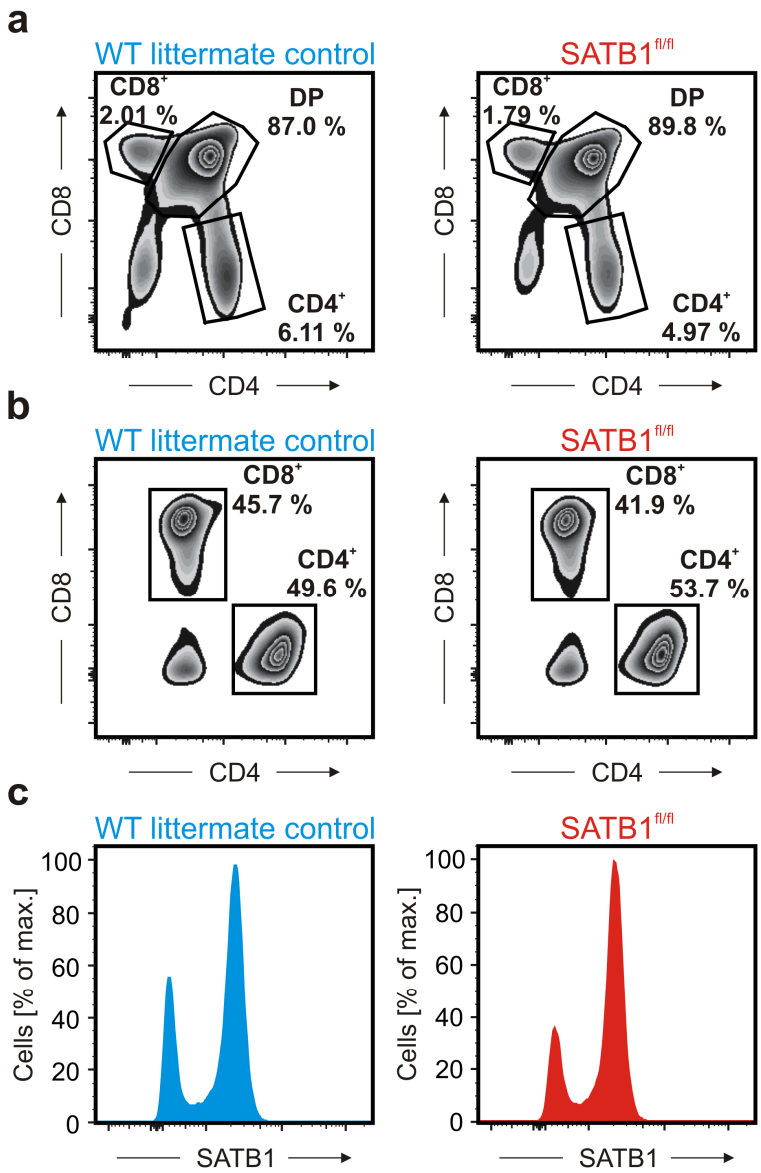

Figure 3.16 Preservation of SATB1 function in SATB1$^{fl/fl}$ mice
Assessment of thymocytes and T cells in thymus and spleen of SATB1$^{fl/fl}$ and wild-type mice by flow cytometry. (a and b) Representative dot plots of CD4 and CD8 expressing cells in thymus (a) and spleen (b); (c) SATB1 expression in splenic CD4$^+$ T cells from SATB1$^{fl/fl}$ and wild-type mice.

3.1.2.2 The SATB1-Flex GFP-reporter is efficiently induced upon recombination *in vivo* and serves as an appropriate surrogate marker for SATB1 expression

To determine the efficiency of Cre-mediated recombination of this allele *in vivo*, we crossed SATB1-Flex mice with mice expressing Cre-recombinase under control of the CD4 promoter (CD4-Cre) to generate mice heterozygously harboring both, Cre recombinase and the SATB1-Flex allele (SATB1$^{+/fl}$ x CD4$^{+/Cre}$). Due to the fact that CD4 is already expressed at the double-positive stage of thymic development, which is the common ancestor of mature CD4$^+$ and CD8$^+$ mature T cells, it was expected

that GFP expression in these mice should start in cells of the DP stage and should persist in both $CD4^+$ and $CD8^+$ mature T cells in the periphery. To test this hypothesis, thymus, spleen, and peripheral lymph nodes of $SATB1^{+/fl}$ x $CD4^{+/Cre}$ reporter mice were analyzed for GFP expression in the respective T cell subsets in comparison to WT littermates (Figure 3.17).

GFP expression was present at the DP stage and retained in the subsequent SP subsets, while no GFP expression was detectable in double-negative thymocytes, in which CD4 is not yet expressed (Figure 3.17a). This was confirmed for the majority of $CD4^+$ and $CD8^+$ T cells in spleen and peripheral lymph nodes (Figure 3.17b and c). However, in the periphery there was always a population negative for GFP. As GFP expression is coupled to the recombination status of the *Satb1-Flex* allele and to the expression of the *Satb1* gene (see paragraph 3.1.1.1), these negative populations could either correspond to cells, which did not undergo recombination of the allele, or which did not express SATB1 at the time-point of analysis. Thus, to examine whether the GFP^- cells did not express SATB1, we assessed SATB1 expression in splenic $CD4^+Foxp3^-$ conventional T cells from $SATB1^{+/fl}$ x $CD4^{+/Cre}$ reporter mice by intracellular flow cytometry (Figure 3.18). Furthermore, we measured the expression of the naive and memory T cell markers CD62L and CD44 in these cells, as memory $CD4^+$ T cells do not express SATB1 (see Appendix Figure 6.4).

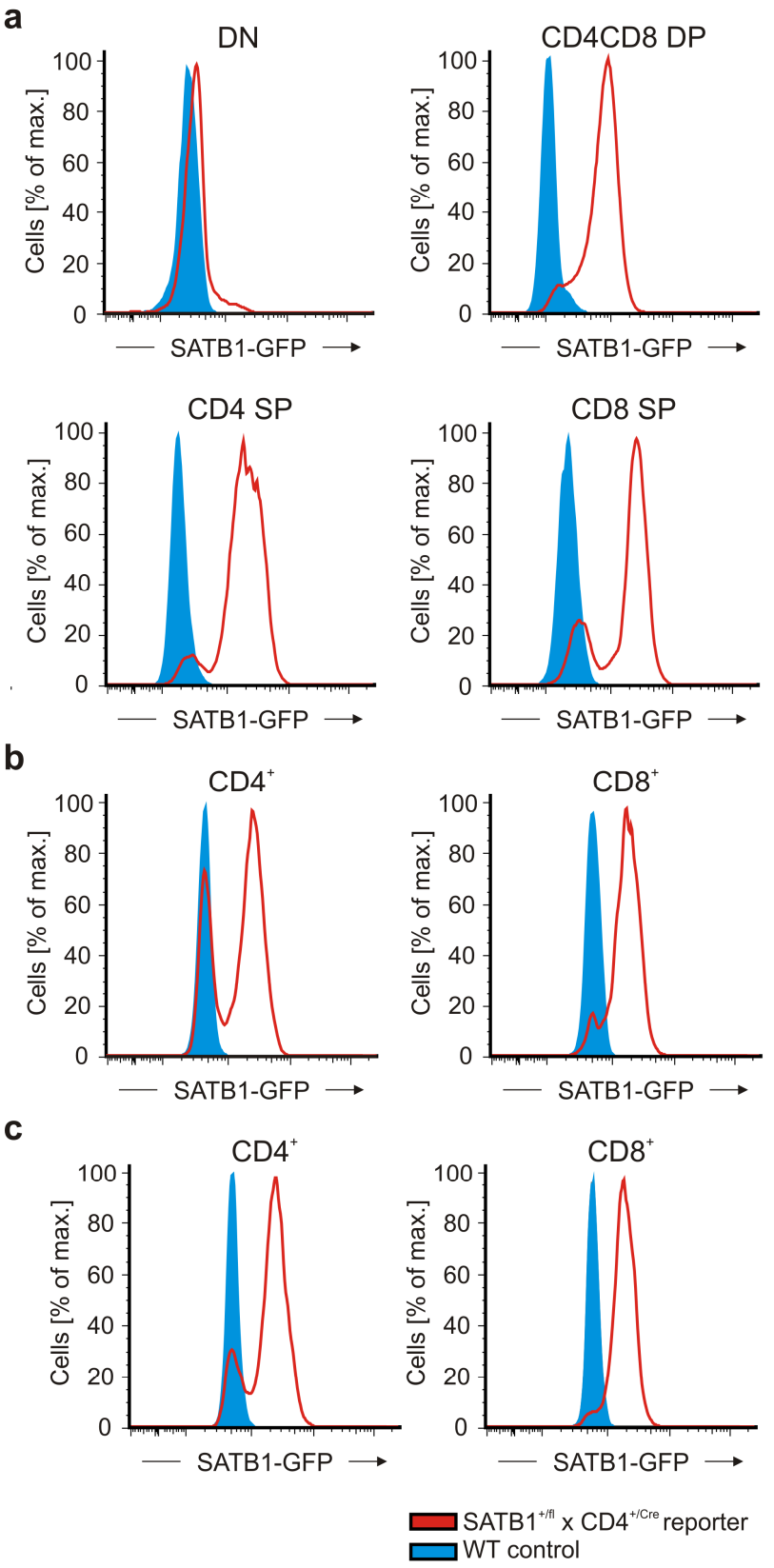

Figure 3.17 Evaluation of Cre-mediated recombination of the SATB1-Flex allele in the T cell compartment
Assessment of GFP expression as marker for Cre-mediated recombination of the SATB1-Flex allele in thymus (a), spleen (b) and pLN (c) of SATB1$^{+/fl}$ x CD4$^{+/Cre}$ and WT mice by flow cytometry.

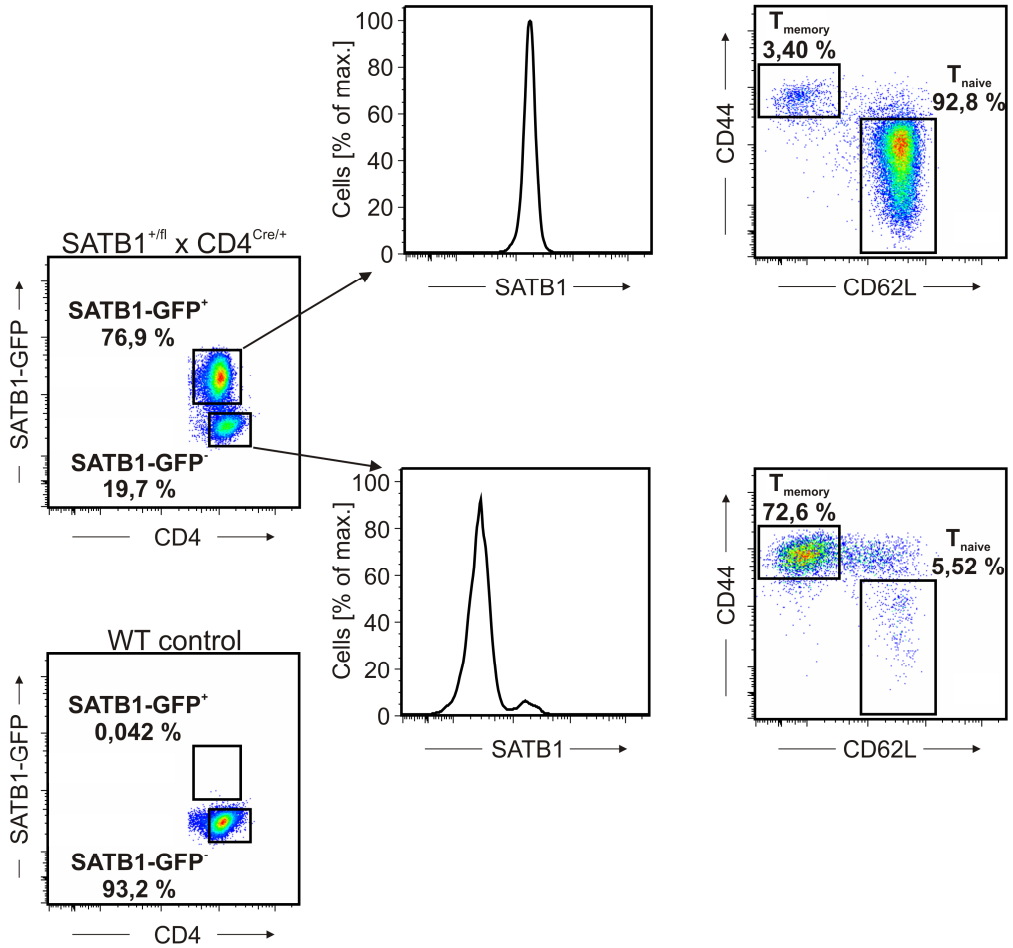

Figure 3.18 Correlation of SATB1-GFP expression with expression of SATB1 protein
Assessment of GFP and SATB1, as well as CD44 and CD62L expression in murine conventional $CD4^+$ T cells from $SATB1^{+/fl}$ x $CD4^{+/Cre}$ mice by flow cytometry. Representative dot plots illustrating GFP expression in $Foxp3^-$ $CD4^+$ T_{conv} cells from $SATB1^{+/fl}$ x $CD4^{+/Cre}$ and WT mice (left panel), as well as the expression of SATB1 (middle panel) and the naive and effector/memory T cell markers CD62L and CD44 (right panels) in the respective SATB1-GFP expressing cell subsets.

These experiments revealed that GFP^-CD4^+ T_{conv} cells indeed did not express SATB1 protein, while GFP^+ cells expressed high levels of SATB1. In concordance with the data obtained from wild-type mice (see Appendix Figure 6.4) $SATB1^{high}$ T cells mainly had a naive phenotype, while $SATB1^{low}$ cells were of memory phenotype (Figure 3.18, right panel).

Furthermore, subsequent assessment of *Satb1* gene expression by quantitative real-time PCR in these two populations of cells confirmed the differences in *Satb1* expression between GFP^+ and GFP^- cells also on mRNA level, as GFP^+ cells had significantly higher *Satb1* mRNA levels than GFP^- cells (Figure 3.19).

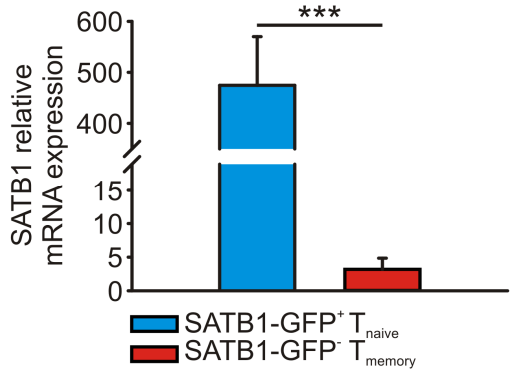

Figure 3.19 Correlation of SATB1-GFP expression with *Satb1* mRNA expression
Assessment of *Satb1* mRNA expression in SATB1-GFP$^+$ and SATB1-GFP$^-$ CD4$^+$ T cells sorted from splenocytes of SATB1$^{+/fl}$ x CD4$^{+/Cre}$ mice (n=3; mean and standard deviation; ***P<0.001, Student´s t-test).

Thus, taken together these data show that the SATB1-Flex reporter system is generally working *in vivo* and that GFP expression of the recombined allele can be used as surrogate marker for SATB1 expression. Furthermore, the absence of GFP expression in memory T cells suggests that these cells express very low levels of SATB1 protein.

3.1.2.3 Efficient SATB1 deletion after Cre-mediated recombination of the SATB1-Flex allele in T cells

Since we wanted to use the SATB1-Flex system for the conditional abrogation of SATB1, we next assessed whether Cre-mediated recombination of the SATB1-Flex allele also lead to the disruption of SATB1 expression. Therefore, SATB1 expression in CD4$^+$ T cells from SATB1$^{fl/fl}$ x CD4$^{+/Cre}$ and SATB1$^{+/fl}$ x CD4$^{+/Cre}$ mice, which served as SATB1-expressing control, were analyzed by flow cytometry (Figure 3.20).

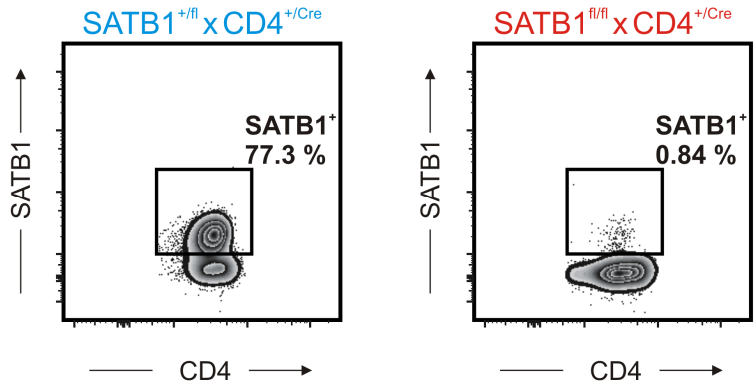

Figure 3.20 SATB1 expression in CD4$^+$ T cells isolated from spleens of SATB1$^{+/fl}$ x CD4$^{+/Cre}$ and SATB1$^{fl/fl}$ x CD4$^{+/Cre}$ mice

Almost all CD4$^+$ T cells from SATB1$^{fl/fl}$ x CD4$^{+/Cre}$ showed no SATB1 expression, indicating that the Cre-mediated recombination of the SATB1-Flex allele indeed leads to a termination of SATB1 expression. Interestingly, SATB1 expression of CD4$^+$ T cells from SATB1$^{fl/fl}$ x CD4$^{+/Cre}$ mice was equal to the SATB1 expression level of the SATB1 negative cell population in the heterozygous control mice (SATB1$^{+/fl}$ x CD4$^{+/Cre}$), which previously could be identified as memory T cell subset (Figure 3.18). Thus, these results also corroborate the findings that memory T cells do not express SATB1 or at least only at a level not detectable by flow cytometry.

Besides the loss of SATB1 expression in these mice, we also identified changes in T cell development, when examining the composition of the thymic T cell compartment by flow cytometry (Figure 3.21).

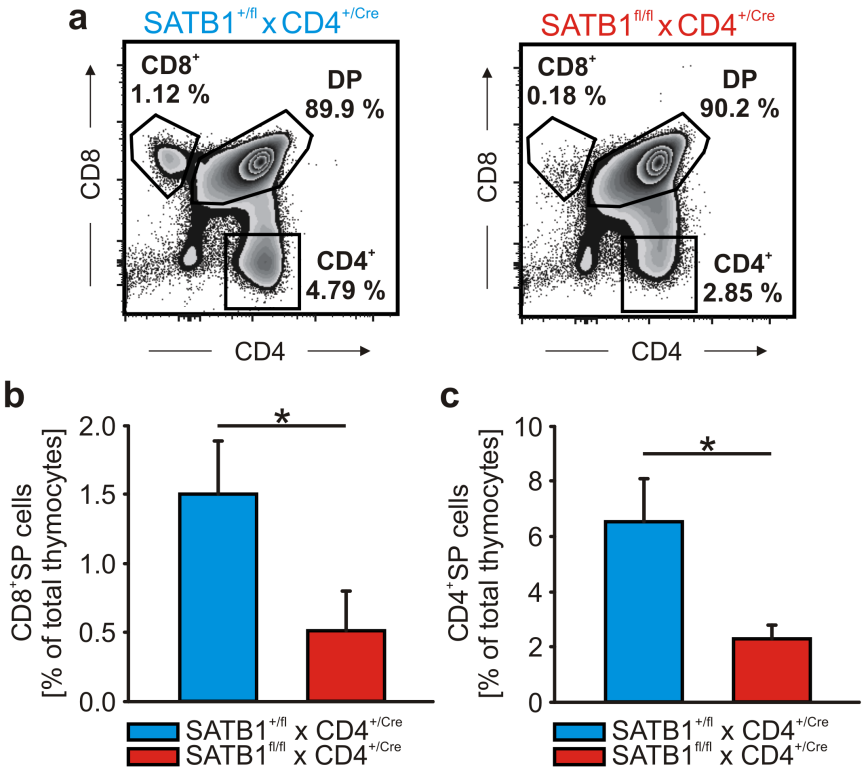

Figure 3.21 Changes in T cell development after SATB1 deletion in thymocytes
Flow cytometric analysis of T cells in thymi of SATB1$^{+/fl}$ x CD4$^{+/Cre}$ and SATB1$^{fl/fl}$ x CD4$^{+/Cre}$ mice. (a) Representative dot plots illustrating CD4 and CD8 expressing cell subsets among thymocytes of SATB1-sufficient (left panel) and -deficient mice (right panel). (b) Quantification of the fraction of CD8$^+$ (left panel) and CD4$^+$ SP thymocytes (right panel) shown in (a). (n=3; mean and standard deviation; *P<0.05; ***P<0.001, Student´s t-test).

SATB1$^{fl/fl}$ x CD4$^{+/Cre}$ mice had a significant decrease in CD4 and CD8 SP thymocyte subsets compared to SATB1-sufficient heterozygous control mice, similar to the complete SATB1 knock-out described by Alvarez *et al.* [98], which substantiates the loss of SATB1 in these mice on a functional level.

In summary, the absence of SATB1 expression as well as the changes in T cell development in SATB1$^{fl/fl}$ x CD4$^{+/Cre}$ mice confirm that we succeeded in generating a fully functional conditional SATB1 knock-out mouse.

3.1.2.4 Deletion of *Satb1* specifically in mature CD4$^+$ T cells using the CD4-CreERT2 system

Due to the observed changes in T cell development, the SATB1$^{fl/fl}$ x CD4$^{+/Cre}$ mouse model was not suitable for our aim to delete SATB1 specifically in mature CD4$^+$ T cells. We therefore assessed whether the CD4-CreERT2 system was appropriate for our approach, as it allows for the induction of Cre-mediated recombination in adult mice possessing an established peripheral T cell compartment.

For this purpose, SATB1$^{fl/fl}$ mice were crossed to the CD4-CreERT2 mouse line (SATB1$^{fl/fl}$ x CD4$^{+/CreERT2}$) and adult SATB1$^{fl/fl}$ x CD4$^{+/CreERT2}$ mice were treated with tamoxifen to induce Cre recombination (SATB1-Flex KO mice), followed by flow cytometric assessment of GFP expression in splenic CD4$^+$ and CD8$^+$ T cells. SATB1$^{fl/fl}$ x CD4$^{+/CreERT2}$ mice treated with olive oil (SATB1-Flex WT mice) served as vehicle control (Figure 3.22).

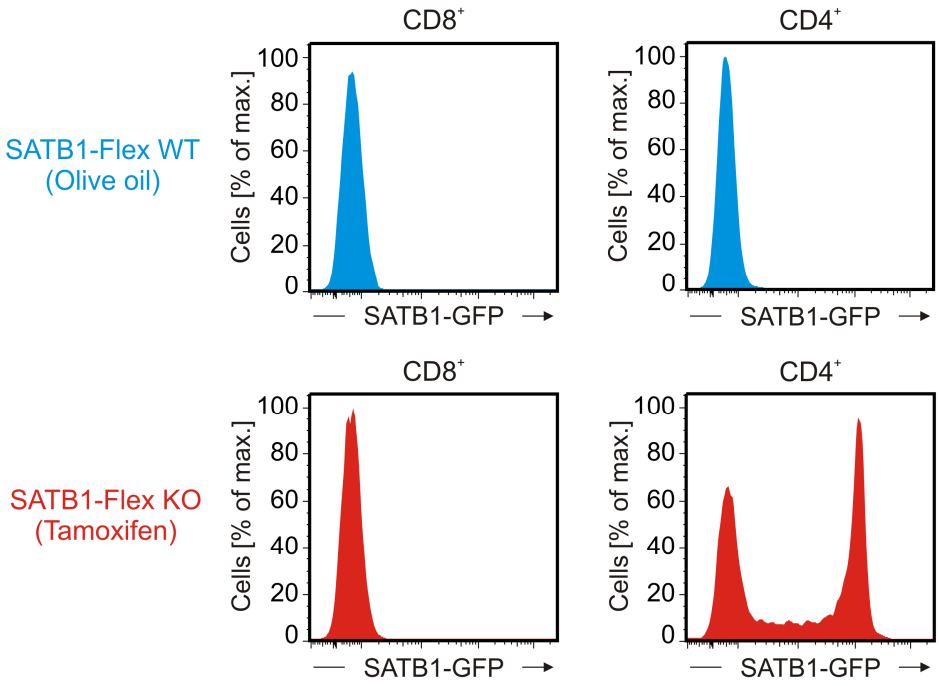

Figure 3.22 Evaluation of Cre-mediated recombination of the SATB1-Flex allele specifically in peripheral CD4$^+$ T cells
Assessment of SATB1-GFP expression in CD4$^+$ and CD8$^+$ T cells from spleens of SATB1$^{fl/fl}$ x CD4$^{+/CreERT2}$ mice seven days after the oral application of tamoxifen (lower panels) or olive oil as vehicle control (upper panels).

As depicted in Figure 3.22, GFP expression was only present in $CD4^+$ T cells from mice treated with tamoxifen, while no GFP expression was detectable in $CD4^+$ T cells from control mice, indicating that SATB1 could be specifically deleted using the CD4-CreERT2 system.

Furthermore, in contrast to the $SATB1^{fl/fl}$ x $CD4^{+/Cre}$ mouse model (see paragraph 3.1.2.2) no GFP expression was detectable in $CD8^+$ T cells. Since mature $CD8^+$ T cells do not express CD4, GFP^+CD8^+ T cells in this setting could have only originated from cells, which had been at the DP stage of thymocyte development at the time of tamoxifen treatment. Thus, the absence of SATB1-GFP^+ $CD8^+$ T cells indicates that the majority of SATB1-GFP^+ cells in the spleens of SATB1-Flex KO mice underwent Cre recombination as mature cells in the spleen and not during their development in the thymus.

However, due to the fact that GFP is not expressed in cells expressing low levels of SATB1, such as memory $CD4^+$ T cells, GFP assessment in $CD4^+$ T cells did not reveal the efficiency of Cre recombination after tamoxifen treatment, as GFP negative cells could either derive from non-recombined cells or cells with low SATB1 expression. Thus, to determine the efficiency of tamoxifen induction, GFP expression was determined solely in naive $CD4^+$ T cells (Figure 3.23), since these were shown to express high levels of SATB1 (Figure 3.18).

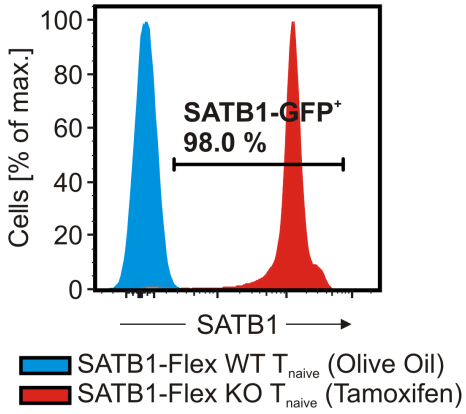

Figure 3.23 Efficiency of tamoxifen-induced Cre-mediated recombination in naive T cells
Assessment of SATB1-GFP expression in splenic T_{naive} cells from $SATB1^{fl/fl}$ x $CD4^{+/CreERT2}$ mice seven days after the oral application of tamoxifen or olive oil as vehicle control.

As depicted in Figure 3.23, 98 % of T_{naive} cells from tamoxifen treated mice showed expression of GFP, demonstrating that the tamoxifen application used in this setting efficiently induced Cre recombination of the SATB1-Flex allele.

In summary, these results show that the SATB1-Flex model in combination with the CD4-CreERT2 system is appropriate to disrupt SATB1 protein expression in mature

CD4$^+$ T cells and hence constitutes a promising model to study the function of SATB1 in these cells.

3.1.3 Analysis of SATB1$^{fl/fl}$ x CD4$^{+/CreERT2}$ mice indicates impaired development of pathogenic TH17 cells after SATB1 deletion

3.1.3.1 SATB1-deficient CD4$^+$ naive T cells are unable to induce colitis in an *in vivo* model of adoptive colitis

To analyze the functional consequences of SATB1 abrogation in mature CD4$^+$ T cells, a model for chronic colitis was applied. In this model, naive CD4$^+$ T cells are transferred into syngeneic lymphopenic hosts, such as RAG2$^{-/-}$ mice, resulting in the development of a pancolitis, which manifests in a wasting syndrome marked by loose stools, reduced physical activity and loss of body weight [118, 119]. This pancolitis develops as a result of activation of naive T cells by enteric antigens and their concomitant polarization into disease-promoting TH1 and TH17 effector cells [119], thus making this procedure an easy method to study CD4$^+$ T cell function an *in vivo* environment. To perform this model, GFP$^+$ and GFP$^-$ T$_{naive}$ cells were isolated from SATB1-Flex KO and SATB1-Flex WT mice and transferred into RAG2$^{-/-}$ mice by intravenous injection. Mice were then monitored for the development of wasting syndrome by assessment of general health conditions and body weight (Figure 3.24a).

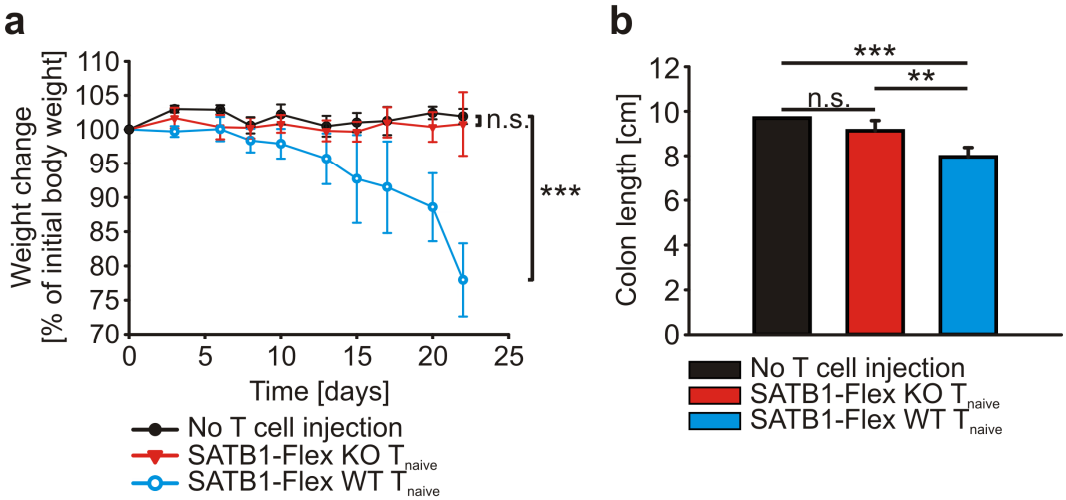

Figure 3.24 Assessment of colitis development in RAG2$^{-/-}$ mice receiving SATB1-deficient, SATB1-sufficient or no T$_{naive}$ cells
(a) Weight change over time after transfer of T$_{naive}$ cells; (b) Colon length 21 days after transfer of T$_{naive}$ cells (n=3-5 per cohort; mean and standard deviation; ***P<0.001, **P<0.01, n.s.: not significant, Student´s t-test).

RAG2$^{-/-}$ mice injected with SATB1-Flex WT T_{naive} cells lost weight over time and reached the defined endpoint of the experiment (weight loss more than 20% of initial body weight) after 21 days, indicating the development of colitis. In contrast, RAG2$^{-/-}$ mice injected with SATB1-Flex KO T_{naive} cells showed no reduction of body weight, similar to those mice, which had not received any naive T cells, indicating that SATB1-deficient T_{naive} cells were not able to induce colitis.

Besides weight loss, colon length was assessed as additional parameter of colitis development (Figure 3.24b), since colon inflammation is associated with a significant shortening of the colon in comparison to healthy, non-inflamed tissue [119].

In line with the analysis of body weight, the colon length of mice injected with SATB1-Flex WT T_{naive} cells was significantly shorter compared to mice (Figure 3.24b), which had received no T cells or SATB1-KO T_{naive} cells, showing a clear colitis establishment in mice receiving WT T_{naive} cells. Mice receiving the SATB1-Flex KO T_{naive} cells did not show a difference to the non-T-cell control, indicating the absence of colitis in these mice.

In summary, these results suggest that mature CD4$^+$ T_{naive} cells deficient in SATB1 are not able to induce colitis after transfer into lymphopenic recipient mice, which indicates a loss of CD4$^+$ effector T cell function after SATB1 ablation.

3.1.3.2 SATB1-deficient T_{naive} cells show a normal proliferative capacity *in vivo*

To identify the cause for the reduced development of colitis *in vivo*, we next assessed the proliferative capacity of transferred T cells by flow cytometric analysis of cell numbers of CD4$^+$ T cells in mesenteric lymph nodes and expression of the proliferation marker Ki-67 (Figure 3.25).

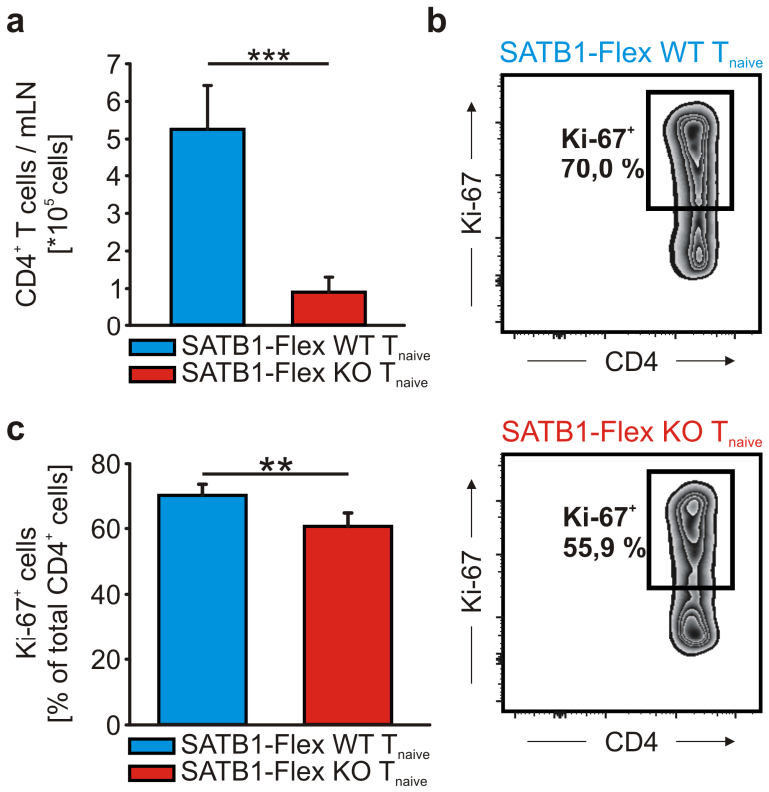

Figure 3.25 Proliferative competence of SATB1-Flex KO T_{naive} cells in mLNs of RAG2$^{-/-}$ mice
Cell numbers and Ki-67 expression of CD4$^+$ T cells in mLN of RAG2$^{-/-}$ mice receiving SATB1-deficient and -sufficient CD4$^+$ T cells determined by flow cytometry. (a) Quantification of CD4$^+$ T cell numbers in mLN; (b) Representative dot plots for Ki-67 expression in SATB1-Flex KO and SATB1-Flex WT T_{naive} cells; (c) Quantification of Ki-67-expressing cells in the T cell subsets shown in (b); (n=4 per cohort; mean and standard deviation; **P<0.01, ***P<0.001, Student´s t-test).

RAG2$^{-/-}$ mice injected with SATB1-Flex WT T_{naive} displayed significantly higher numbers of CD4$^+$ T cells infiltrating mLNs than mice receiving SATB1-Flex KO T_{naive}. This difference in cell numbers was accompanied by a significantly lower percentage of Ki-67 expressing cells among the SATB1-deficient CD4$^+$ T cells, indicating that the SATB1-deficient T_{naive} cells in mLNs proliferated at a lower rate *in vivo*.

However, as the gastrointestinal tract and the associated lymphatic system are the primary sites of inflammation in this model, the difference in T cell proliferation might also be a result of the inflammation itself rather than being the actual cause of the inflammation.

We therefore also determined the same parameters in the spleen (Figure 3.26), a site, which should be less affected by inflammation and thus should give a better insight into the cell intrinsic proliferative capacity of the transferred CD4$^+$ T cells.

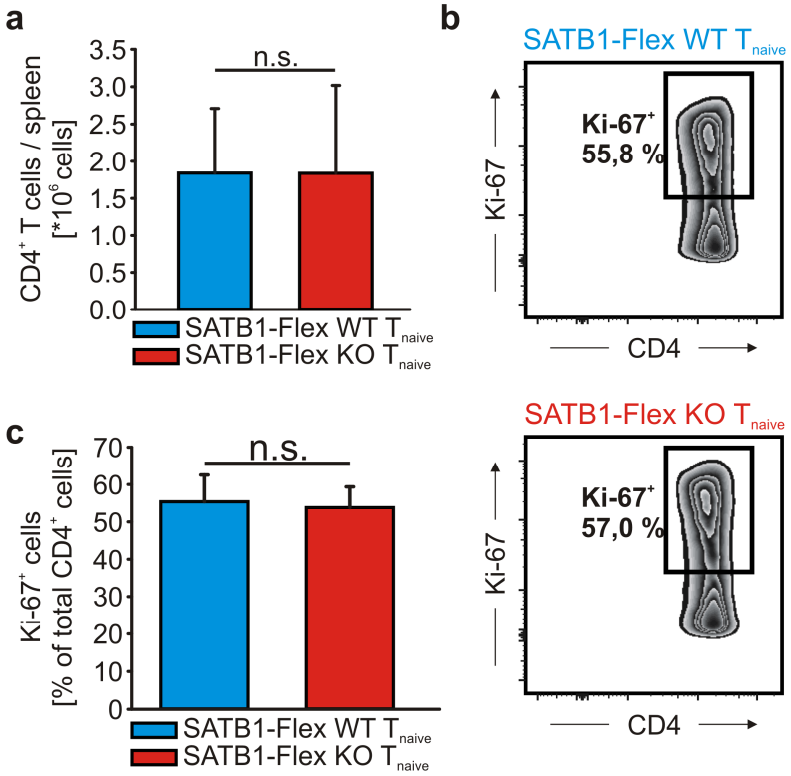

Figure 3.26 Proliferative competence of SATB1-Flex KO T_{naive} cells in the spleen of RAG2$^{-/-}$ mice
Cell numbers and Ki-67 expression of CD4$^+$ T cells in the spleen of RAG2$^{-/-}$ mice receiving SATB1-deficient and -sufficient CD4$^+$ T cells determined by flow cytometry. (a) Quantification of CD4$^+$ T cell numbers in spleen**;** (b) Representative dot plots for Ki-67 expression in SATB1-Flex KO and SATB1-Flex WT T_{naive} cells; (c) Quantification of Ki-67-expressing cells in the T cell subsets shown in (b); (n=4 per cohort; mean and standard deviation; n.s.: not significant, Student´s t-test).

CD4$^+$ T cell numbers and percentages of Ki-67-expressing cells in the spleen were indeed different from those obtained from mLNs, as no significant differences could be observed in the spleen. This indicates that the differences in proliferation observed in the mLNs is probably the result of the local reaction towards inflammation.

Furthermore, we directly assessed the proliferation of SATB1-Flex KO CD4$^+$ T cells using an *in vitro* proliferation assay to exclude an impaired proliferative capacity of these cells. Therefore, isolated SATB1 KO and WT CD4$^+$ T_{naive} cells were stained with the membrane intercalating dye eFluor450 and stimulated afterwards using soluble CD28 and plate-bound CD3 antibodies.

After two days of *in vitro* stimulation proliferation was measured by flow cytometry (Figure 3.27).

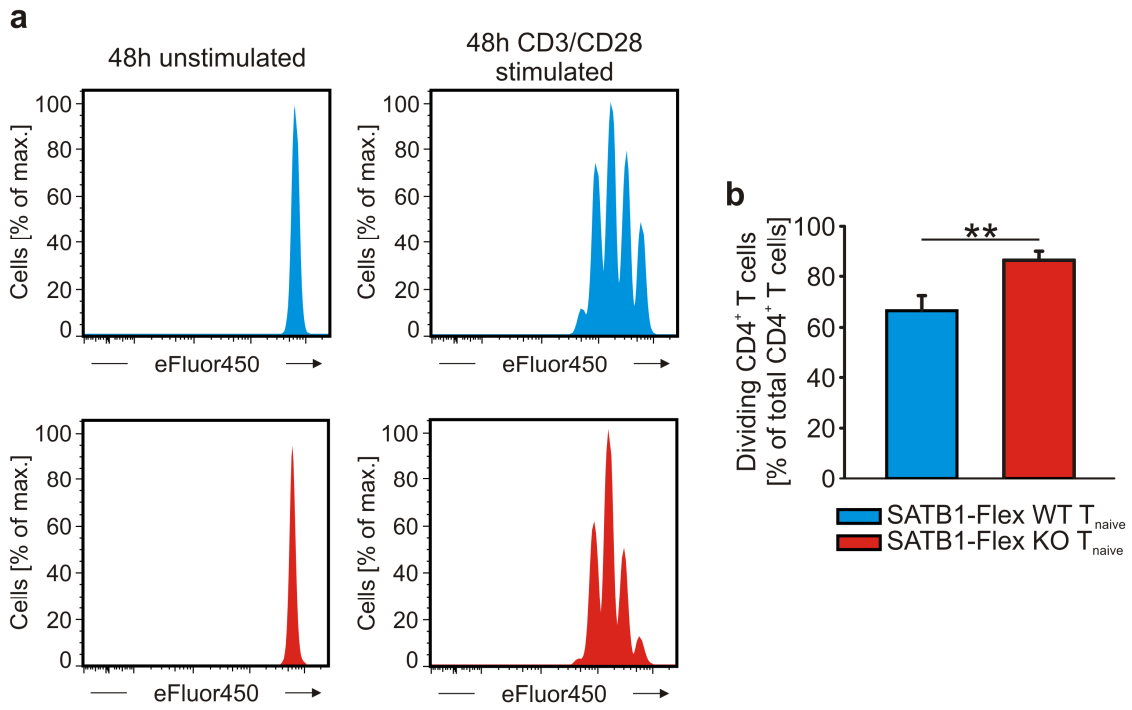

Figure 3.27 Proliferative competence of SATB1-Flex KO T_{naive} cells *in vitro*
Assessment of proliferation by flow cytometric measurement of eFlour450 dye dilution in SATB1-Flex KO and SATB1-Flex WT T_{naive} cells 48 h after stimulation via soluble CD28 and plate-bound CD3 antibodies. (a) Representative histograms illustrating eFluor450 dilution. (b) Quantification of the percentage of dividing cells (n=3; mean and standard deviation; **P<0.01, Student´s t-test).

The proliferation of SATB1-deficient cells was even stronger than that of SATB1-sufficient naive T cells stimulated under identical conditions (Figure 3.27), indicating that SATB1 is not required for activation-induced proliferation of $CD4^+$ T cells.

Taken together, the results show that the general proliferative capacity of $CD4^+$ T cells *in vivo* is not affected by the removal of SATB1 protein. This suggests that the impaired induction of colitis in mice transplanted with SATB1 KO T_{naive} cells is probably due to other reasons than compromised proliferation.

3.1.3.3 Impaired differentiation of SATB1-deficient T_{naive} into TH17 T cells leads to diminished colitis development

After excluding a decreased proliferative capacity of SATB1-deficient $CD4^+$ T cells as causative for the absence of colitis development, it was assessed whether an impaired differentiation of the SATB1-Flex KO T cells into the TH1 or TH17 effector subsets was the cause for the failed induction of colitis, as these cell types were shown to be the associated with the development of colitis in the adoptive colitis model [119].

Therefore, we determined the absolute number of IFN-γ and IL-17 producing $CD4^+$ T cells in mLNs from mice receiving SATB1-Flex KO or SATB1-Flex WT T_{naive} by

intracellular cytokine staining (Figure 3.28a), which served as surrogate markers for TH1 and TH17 differentiation, respectively.

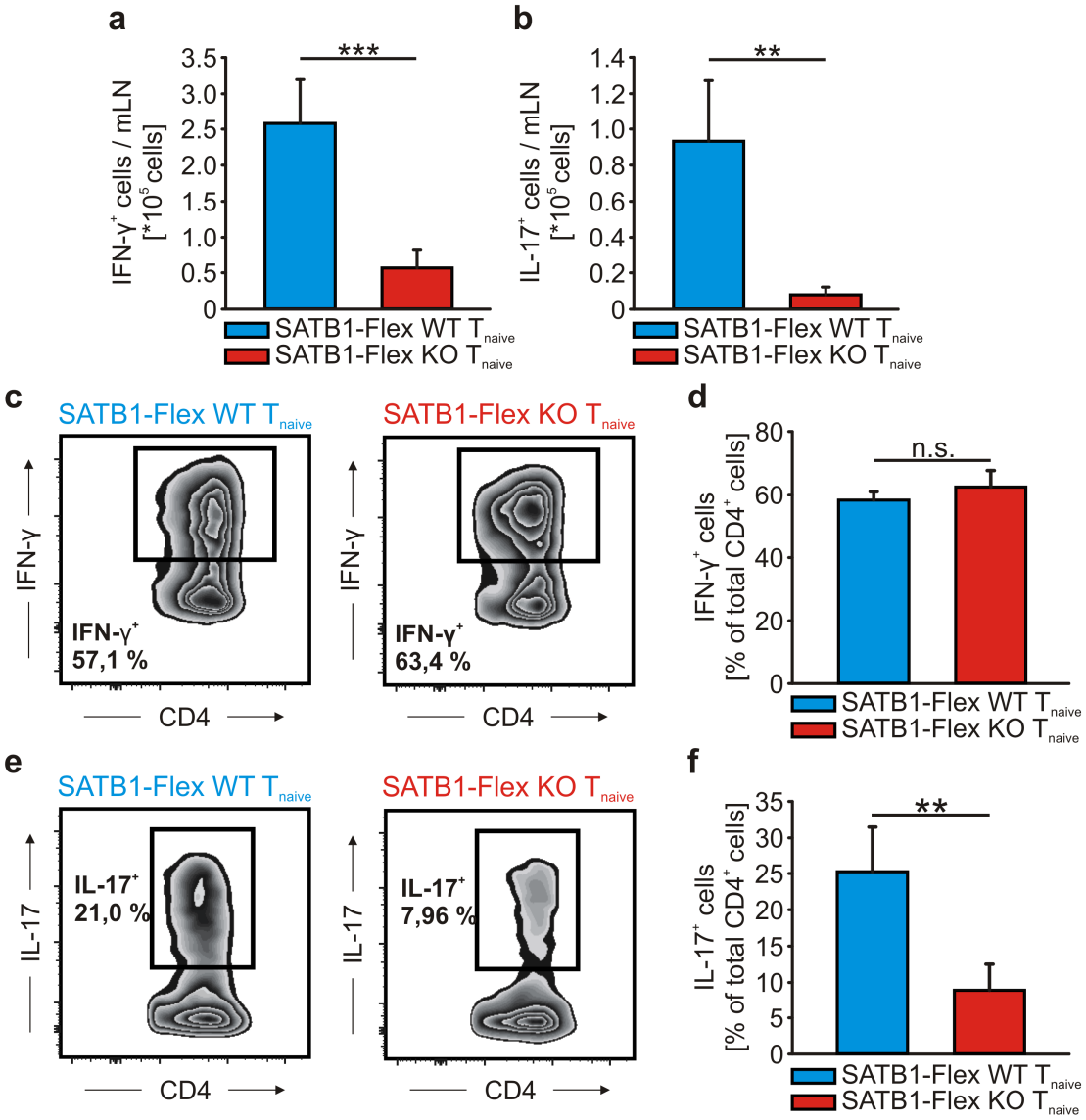

Figure 3.28 TH1 and TH17 cell development of SATB1-Flex KO T_{naive} cells *in vivo*
Assessment of IL-17- and IFN-γ-secreting CD4⁺ T cells in mLN of RAG2$^{-/-}$ mice after transfer of SATB1-Flex KO or SATB1-Flex WT T_{naive} cells. (a and b) Quantification of absolute numbers of IFN-γ- (a) and IL-17-secreting (b) SATB1-Flex KO and SATB1-Flex WT T cells. (c) Representative dot plots showing IFN-γ-secreting SATB1-Flex KO and SATB1-Flex WT T cells; (d) Quantification of IFN-γ-secreting T cells shown in (c); (e) Representative dot plots showing IL-17-secreting SATB1-Flex KO and SATB1-Flex WT T cells; (f) Quantification of IL17-secreting T cells shown in (d) (n=4 per cohort; mean and standard deviation; **P<0.01, ***P<0.001, n.s.: not significant, Student´s t-test).

As depicted in Figure Figure 3.28a, SATB1-Flex KO recipients had significantly lower numbers of TH1 and TH17 cells, indicating a disturbed differentiation of SATB1-deficient T cells into these subsets.

However, as the reduced number in effector T cells could also be due to the overall reduced number in CD4⁺ T cells in SATB1-Flex KO recipients, which could mask an

otherwise functional differentiation of a T cell subset, we additionally analyzed the composition of the T cell compartment in STAB1-Flex KO and SATB1-Flex WT recipients by determining the percentages of TH1 and TH17 cells in mLNs of these mice.

Interestingly, there was no significant difference in the percentage of IFN-γ producing cells between SATB1-deficient and -sufficient cells (Figure 3.28c and d), suggesting that the reduced number of TH1 cells was probably a result of the overall diminished number of $CD4^+$ T cells, rather than a lack of TH1 differentiation. This further indicated that the absence of SATB1 does not interfere with the differentiation into TH1 effector cells in this model.

In contrast, $RAG2^{-/-}$ mice administered with SATB1-Flex KO T_{naive} had significantly less IL-17 producing $CD4^+$ T cells in mLNs compared to animals that had received T_{naive} from WT control animals (Figure 3.28e and f). This, together with the reduced absolute number of TH17 cells, suggests that the absence of SATB1 indeed leads to an impaired differentiation of T_{naive} into TH17 effector cells, which subsequently causes the reduced development of colitis in mice receiving SATB1-KO T cells.

To confirm that this impaired differentiation of TH17 cells was a direct effect of SATB1 depletion, rather than an indirect effect, such as the production of other factors impairing a TH17-stimulating environment, we additionally cultured SATB1-deficient and -sufficient naive T cells under TH17 promoting conditions *in vitro* and assessed TH17 formation by intracellular cytokine staining (Figure 3.29a).

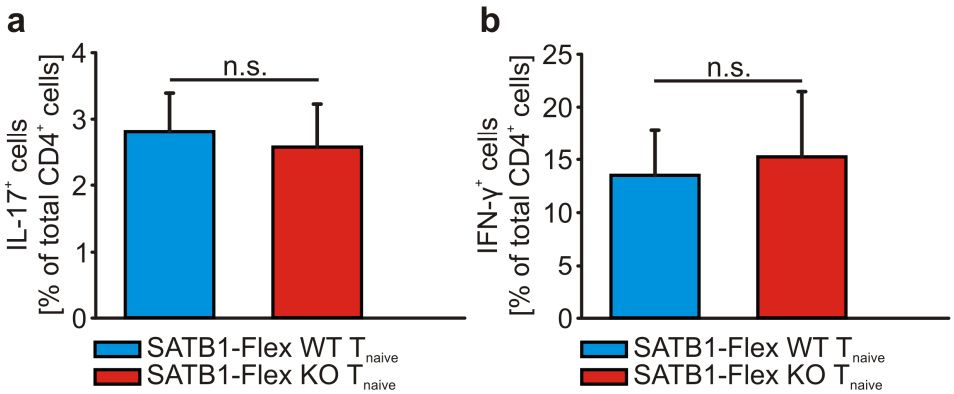

Figure 3.29 TH17 and TH1 cell development of SATB1-Flex KO T_{naive} cells *in vitro*
Quantification of the fractions of IL-17^+ (a) and IFN-γ^+ (b) cells as marker for the TH17 and TH1 cells after *in vitro* differentiation of SATB1-Flex KO and SATB1-Flex WT T_{naive} cells (n=3; mean and standard deviation; n.s.: not significant, Student´s t-test).

Interestingly, the *in vitro* differentiation into TH17 cells revealed results contrasting to the adoptive colitis model, as there was no difference in the formation of TH17 cells

between SATB1-Flex KO and WT control cells, indicating that SATB1 deficiency does not directly impair TH17 differentiation. However, it should be considered that due to the relatively low efficiency of TH17 generation (about 2-3 %), the TH17 differentiation could be suboptimal under the chosen differentiation conditions, which could explain this lack of difference between SATB1 competent and deficient T_{naive} cells.

Besides TH17 differentiation, we also performed *in vitro* differentiation under TH1 promoting conditions (Figure 3.29b) to confirm the apparently undisturbed TH1 differentiation *in vivo*, as these results disagreed with the conclusions from previous observations in human $CD4^+$ T cells by our group ([112] and Yasser Thabet, unpublished data) and others [108, 120], which suggested an active role of SATB1 during T helper cell differentiation.

In vitro differentiation into TH1 cells was not impaired by the loss of SATB1, which confirmed the observations in the colitis model, thus further corroborating that the absence of SATB1 does not interfere with TH1 differentiation in general.

3.1.3.4 Impaired differentiation of SATB1-deficient T_{naive} into pathogenic TH17 T cells after transfer into lymphopenic hosts

It has been shown that TH17 cells can differentiate into non-pathogenic and pathogenic TH17 cells, serving either homeostatic or effector function. The pathogenic TH17 cell subset co-expressing IFN-γ and IL-17 ($IL17^+IFN\text{-}\gamma^+$ TH17 cells) was shown to be associated with colitis development in the adoptive colitis model [121]. As these cells differentiate in the presence of IL-23, which was not used for the *in vitro* differentiation in this thesis (see paragraph 2.2.4.5), an alternative explanation for the discrepancy between our *in vitro* and *in vivo* results could be an impaired formation of the pathogenic $IL17^+IFN\text{-}\gamma^+$ TH17 subset.

To address this question, we determined the percentage of pathogenic and non-pathogenic TH17 cells by intracellular cytokine staining in mLNs of $RAG2^{-/-}$ mice after transfer of either SATB1-Flex KO T_{naive} or SATB1-Flex WT T_{naive} (Figure 3.30).

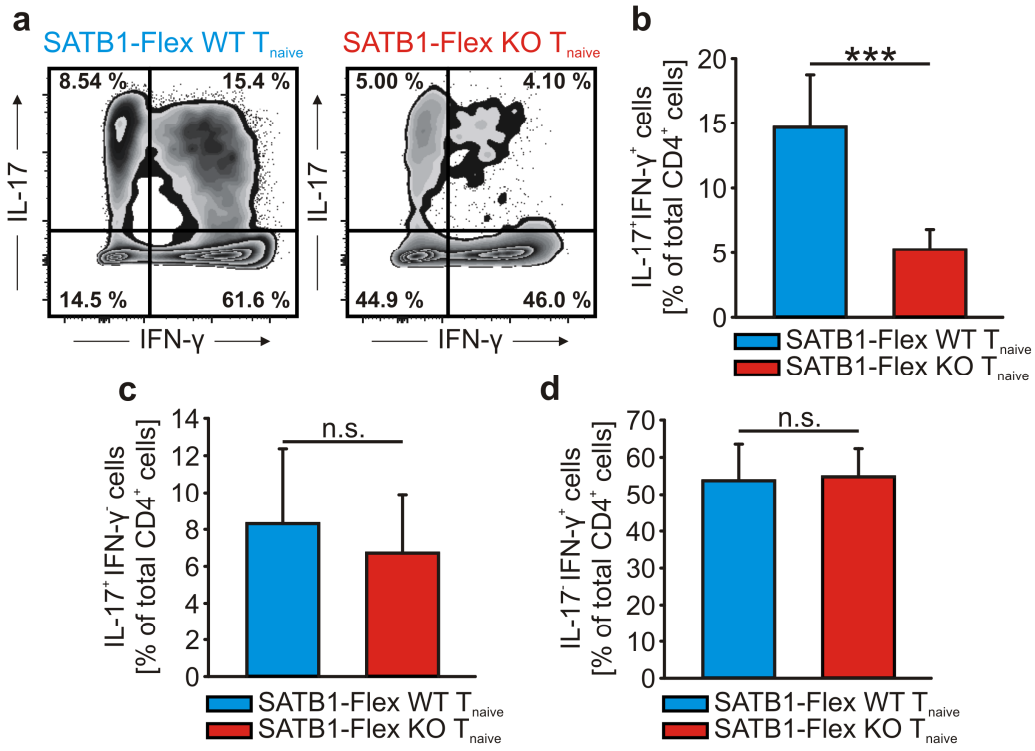

Figure 3.30 Pathogenic TH17 cell development of SATB1-Flex KO T_{naive} cells *in vivo*
Assessment of the fractions of IL-17$^+$IFN-γ$^+$, IL-17$^+$IFN-γ$^-$ and IL-17$^-$IFN-γ$^+$ cells amongst all CD4$^+$ T cells in mLNs of RAG2$^{-/-}$ mice after transfer of SATB1-Flex KO or SATB1-Flex WT T_{naive} cells by flow cytometry. (a) Representative dot plots showing IL-17 and IFN-γ producing cell subsets. (b-d) Quantification of IL-17$^+$IFN-γ$^+$ (b), IL-17$^+$IFN-γ$^-$ (c) and IL-17$^-$IFN-γ$^+$ (d) cells in the conditions shown in (a) (data from two independent experiments; n=5-8 per cohort; mean and standard deviation; ***P<0.001, n.s.: not significant, Student´s t-test).

As depicted in Figure 3.30, SATB1-deficient CD4$^+$ T cells showed decreased percentages of IL-17$^+$IFN-γ$^+$ T cells compared to SATB1-sufficient cells, while the percentages of IL-17$^+$IFN-γ$^-$ T cells were not significantly altered. Thus, these data indeed point towards an impaired generation of pathogenic TH17 cells in the absence of SATB1, while non-pathogenic TH17 are not affected.

3.1.3.5 Increased TH2 cell differentiation *in vitro* after depletion of SATB1

Due to the unexpected finding of an apparently undisturbed development of SATB1-deficient T_{naive} cells into TH1 cells, we also investigated the potential of SATB1-deficient cells to develop into TH2 cells, as previous studies have demonstrated that SATB1 was required for the expression of TH2 cytokines [108, 111]. Since the adoptive colitis model does not induce TH2 responses, we performed *in vitro* TH2 differentiation by culturing SATB1-deficient and -sufficient cells in the presence of TH2-promoting cytokines and assessed TH2 formation by intracellular cytokine staining (Figure 3.31).

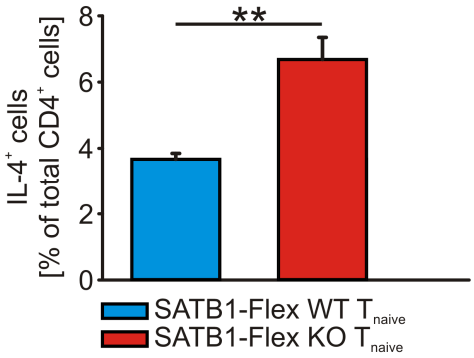

Figure 3.31 TH2 cell development of SATB1-Flex KO T_{naive} cells *in vitro*
Quantification of the fractions of IL-4$^+$ cells as marker for TH2 cells after *in vitro* differentiation of SATB1-Flex KO and SATB1-Flex WT T_{naive} cells (n=3; mean and standard deviation; **P<0.01, Student´s t-test).

This *in vitro* differentiation revealed that SATB1-deficient CD4$^+$ T cells were able to differentiate into TH2 cells. This result, in combination with the results of the TH1 differentiation, suggests that the absence of SATB1 does not prevent differentiation in TH1 or TH2 cells as previously reported for human CD4$^+$ T cells. Interestingly, the percentage of IL-4$^+$ T cells was even higher in SATB1-depleted CD4$^+$ T cells, indicating that SATB1 might also have an inhibitory effect on the development of TH2 cells.

Taken together, the results of the adoptive colitis model and the *in vitro* differentiation suggest an important role of SATB1 for the development of pathogenic TH17 cells, whereas it seems to be dispensable for the differentiation into TH1, TH2 and non-pathogenic TH17 cells. As this latter conclusion is in clear contrast to previous studies, which propose an active role of SATB1 in the differentiation of these T helper cell subsets, further experiments (see paragraphs 4.3.1 and 4.3.2) will be necessary to clarify the reasons for these observations.

3.2 The role of SATB1 in Foxp3$^+$ T_{reg} cells

3.2.1 Generation of a mouse model to conditionally overexpress SATB1 to study the role of SATB1 in T_{reg} cells

Our preceding studies had shown that SATB1 expression was repressed in T_{reg} cells by Foxp3 and that this repression was mandatory to maintain T_{reg} cell phenotype and function [113]. Since most of these studies had been conducted in human cells, or with murine *in vivo* models based on *in vitro* manipulation of T_{reg} cells, we decided to generate a genetically modified mouse model to be able to overexpress SATB1 *in*

vivo without prior manipulation of cells. Therefore, a mouse model for spatiotemporal overexpression should be generated to allow for SATB1 expression in T_{reg} cells independent of the Foxp3-mediated repression of the endogenous *Satb1* locus.

3.2.1.1 Targeting strategy to conditionally overexpress SATB1

To generate a mouse for the conditional overexpression of SATB1, it was decided to integrate a construct containing the *Satb1* open reading frame into the *Rosa26* locus (see paragraph 1.2.1.3).

For the generation of the targeting construct, the murine SATB1 coding sequence was cloned by Yasser Thabet into a vector containing regions homologous to the *Rosa26* locus, a chicken actin promoter, as well as a floxed transcriptional stop cassette and a downstream IRES-eGFP element serving as reporter for transgene expression (Figure 3.32).

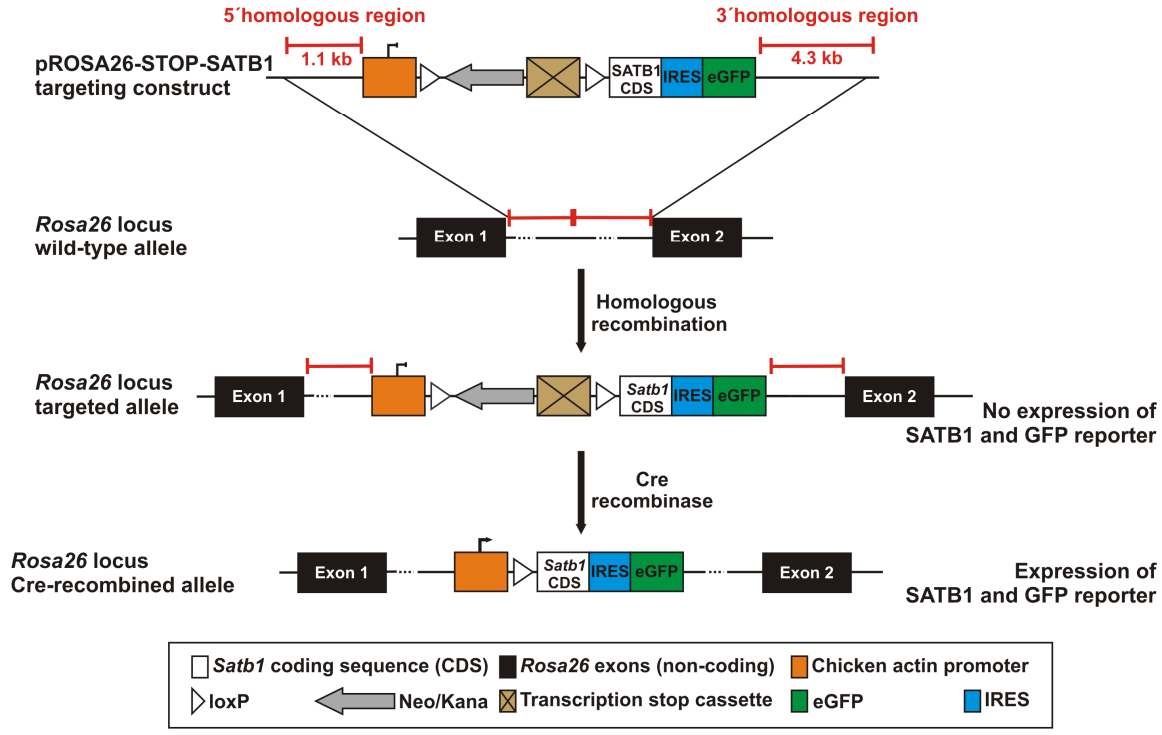

Figure 3.32 Targeting strategy for the conditional overexpression of SATB1
Scheme showing the pROSA26-STOP-SATB1 targeting construct used for homologous recombination at the *Rosa26* locus to generate the targeted allele, which can be used for Cre-mediated overexpression of SATB1.

After successful integration of this targeting construct into the *Rosa26* locus via homology directed repair the targeted allele would harbor the SATB1-IRES-eGFP coding sequence (CDS) under the control of a strong promoter (Figure 3.32), but due to the loxP-flanked transcription stop cassette located between the promoter and the

CDS, expression of the *Satb1* transgene and the reporter would be prevented. Upon Cre-mediated recombination this stop cassette would be removed, thus releasing the transcriptional blockade and enabling expression of the *Satb1* transgene and the reporter. Hence, by crossing this mouse to a mouse expressing Cre-recombinase under a tissue/cell-type-specific promoter, SATB1 can be overexpressed in a tissue or cell-type specific manner.

3.2.1.2 Generation of the ROSA26-STOP-SATB1 mouse by classical gene targeting in ES cells

To generate the mouse line to conditionally overexpress SATB1 as described above, the successfully assembled pROSA26-STOP-SATB1 targeting construct was site-specifically integrated into the genome by classical gene targeting in ES cells, followed by injection of correctly targeted clones into blastocysts and chimera generation, from which a mouse line could then be established (Figure 3.8, left panel). Since this project had already been started before the description of TALENs as efficient tool to enhance gene targeting, gene targeting in this case was not performed using TALEN technology.

After electroporation of ES cells with the targeting plasmid and subsequent antibiotic selection of targeted ES cell clones, the expanded single ES cell clones were assessed by PCR analysis for correct integration of the targeting construct.

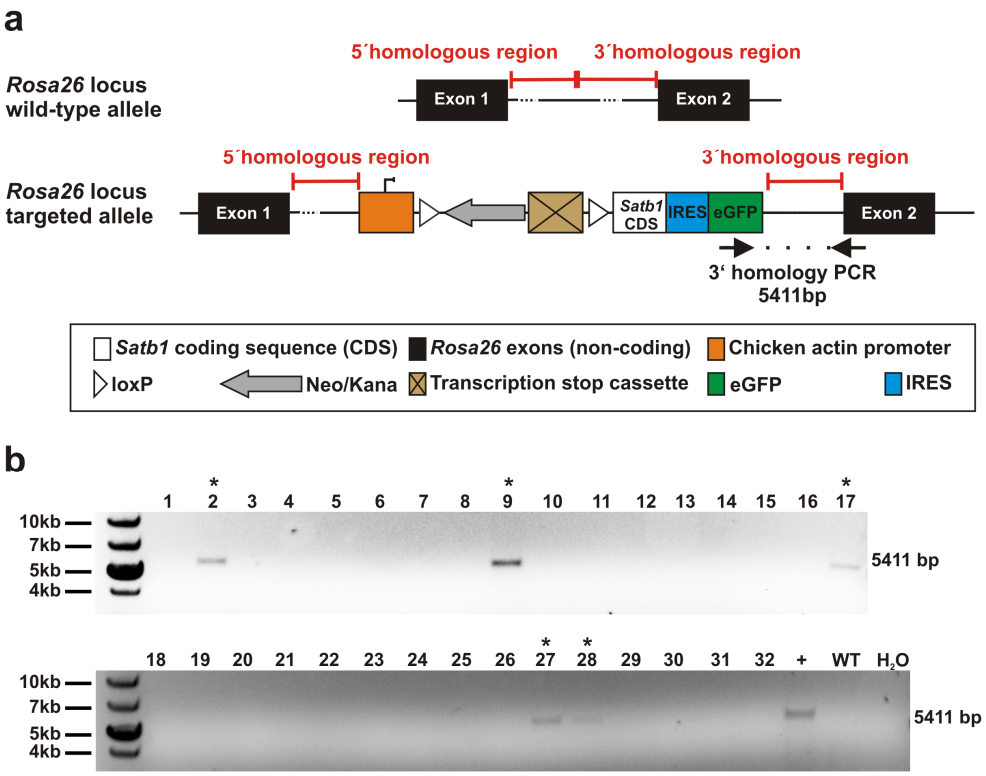

Figure 3.33 Homologous recombination of the pROSA26-STOP-SATB1 targeting construct in JM8A3 ES cells
(a) Scheme of the PCR used to identify correctly targeted ES cell clones. (b) Agarose gel electrophoresis of the 3´ homology PCRs performed on 32 representative clones out of 192. Clones marked with an asterisk depict clones with correct 3' integration of the targeting construct.

Therefore, a PCR spanning the 3´ homology region of the targeting construct was used, which in case of correct 3´ homologous recombination would result in a 5411 bp PCR product, while no PCR product would be generated, if locus-specific recombination had not taken place (Figure 3.33a).

This analysis revealed that from the 192 clones analyzed, 32 clones showed amplification of a 5411 bp PCR product, indicating correct integration of the pROSA26-STOP-SATB1 targeting construct at the 3´end (Figure 3.33b and data not shown).

To confirm the correct integration of the targeting vector, clones positive in the PCR analysis were further expanded and integration was assessed by Southern blot analysis. Southern blot analysis was performed with a 5´ probe to identify correct targeting via the 5´ homologous region as well as an internal GFP probe, which was used to confirm integration at a single site in the genome and to exclude additional randomly integrated copies of the targeting construct (Figure 3.34a).

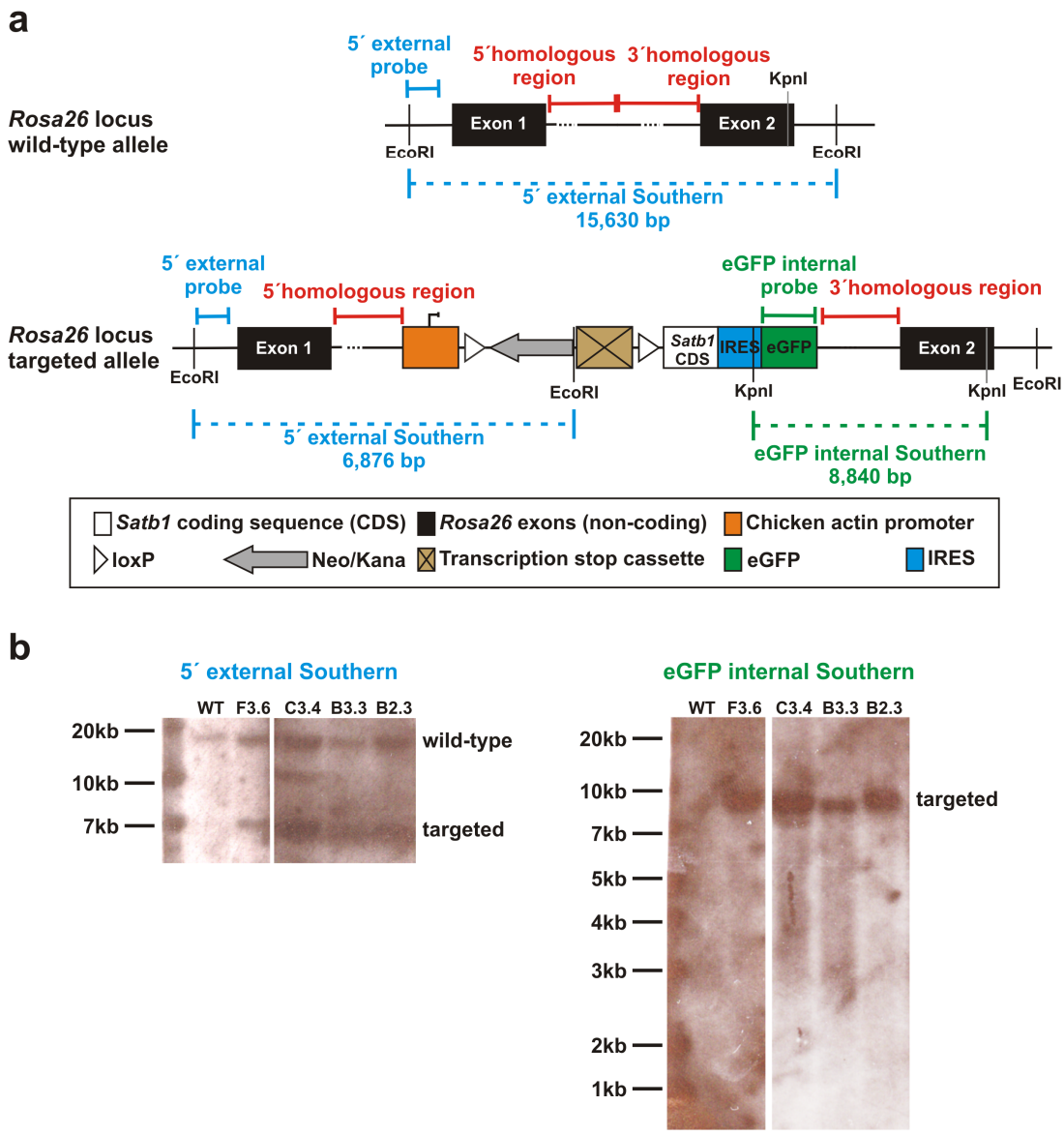

Figure 3.34 Confirmation of correct pROSA26-STOP-SATB1 integration at the Rosa26 locus by Southern blot analysis
Southern blot analysis was performed with 12 ES cell clones out of 32 clones positive in the 3´homology PCR. (a) Scheme illustrating the Southern blot strategies for the wild-type and the targeted *Rosa26* alleles. (b) Results of the Southern blot analysis with 5´external (left) and eGFP internal (right) probes of 4 representative clones out of 12 ES cell clones analyzed.

Since not all clones positive in the PCR analysis survived expansion or yielded sufficient amounts of DNA for Southern blot analysis, only twelve clones were subjected to Southern blot analysis. From these twelve clones six showed the targeted 6,876 bp band and the 15.63 kb wild-type band (Figure 3.34b, left panel and data not shown), indicating heterozygous homologous recombination via the 5´ homology. In addition, these clones showed a single band of 8.84 kb in the internal Southern (Figure 3.34b, right panel and data not shown) and thus confirmed correct homologous recombination of the targeting construct at the *Rosa26* locus.

Furthermore, the absence of additional bands confirmed the lack of random integration of additional copies of the targeting vector in the genome.

In summary, the combination of PCR and Southern blot analyses identified six clones with correct integration of the pROSA26-STOP-SATB1 targeting construct.

In the next step, two of these clones (clones B2.3 and B3.3) were used for blastocyst injections to yield chimeras, which could be used to establish a mouse line for the conditional overexpression of SATB1.

These injections resulted in four chimeras, from which one showed germline transmission of the targeted allele. Litters of this chimera consisted of descendants with white and black coat color (Figure 3.35a), respectively, indicating that parts of the germline of this chimera originated from the injected ES cells, as these encoded for black coat color, while the endogenous cells of the blastocyst encoded for white coat color.

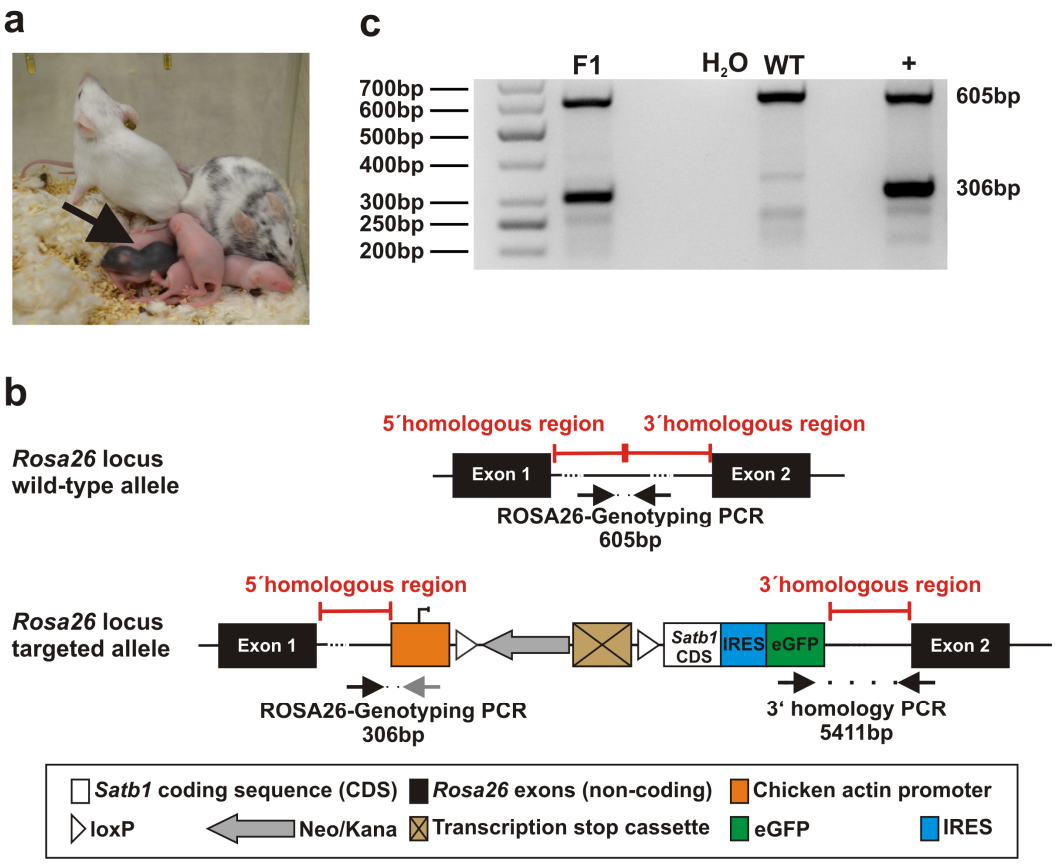

Figure 3.35 Germline transmission of the ROSA26-STOP-SATB1 conditional allele
(a) Picture of one representative litter of the fertile chimera derived from blastocyst injections with one black F1 animal (see black arrow) originating from the injected ES cell clone. (b) Scheme of the PCR used to genotype the black F1 animal shown in (a). (c) Agarose gel electrophoresis of PCR products derived from the DNA of the black F1 animal shown in (a).

To identify whether the targeted allele could be transmitted to the next generation, the black offspring of this chimera was genotyped by PCR to determine the presence of the targeted allele (Figure 3.35b). As depicted in Figure 3.35c for one exemplary animal, this PCR resulted in amplification of 306 bp and 605 bp products corresponding to the targeted and the wild-type allele, respectively. Taken together, this PCR analysis confirmed that the animal analyzed harbored the targeted allele, verified germline transmission of this allele and confirmed successful generation of the ROSA26-STOP-SATB1 mouse line for the conditional overexpression of SATB1.

3.2.1.3 Successful recombination of the ROSA26-STOP-SATB1 allele

After successfully establishing a mouse line for the conditional overexpression of SATB1, the allele was further tested for its functionality.

First, it was assessed whether the conditional allele impedes the expression of the *Satb1* transgene in the absence of Cre-recombinase. Therefore, expression of the GFP reporter was assessed in $CD4^+$ T cells in mice harboring the conditional ROSA-STOP-SATB1 allele ($ROSA26^{SATB1\text{-}GFP/+}$), but lacking an allele encoding Cre-recombinase in comparison to WT mice ($ROSA26^{+/+}$) (Figure 3.36a).

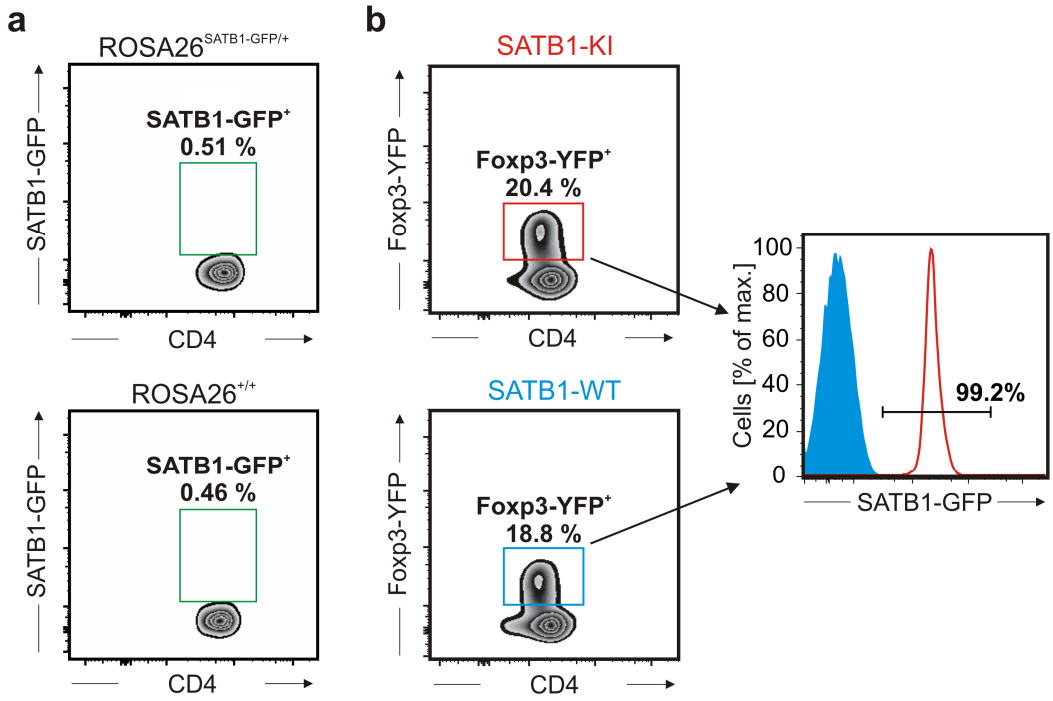

Figure 3.36 Cre-mediated induction of the ROSA26-SATB1 transgene
Assessment of GFP expression in $CD4^+$ T cells from different mice by flow cytometry to demonstrate inducibility of the transgene by Cre-mediated recombination. (a) Representative dot plots showing SATB1-GFP expression in $CD4^+$ T cells from $ROSA26^{SATB1\text{-}GFP/+}$ and $ROSA26^{+/+}$ mice. (b) Representative dot plots showing SATB1-GFP expression in $CD4^+Foxp3\text{-}YFP^+$ T_{reg} cells from SATB1-KI and SATB1-WT mice.

$CD4^+$ T cells from $ROSA26^{SATB1\text{-}GFP/+}$ mice, just like $CD4^+$ T cells derived from the $ROSA26^{+/+}$ mice, lacked GFP expressing cells, confirming that the conditional ROSA-STOP-SATB1 allele indeed inhibits expression of the transgene when Cre-recombinase is not present.

Next, we assessed, if the *Satb1* transgene and GFP reporter were expressed in the presence of Cre-recombinase. Therefore, the ROSA26-STOP-SATB1 mouse was crossed to the Foxp3-YFP-Cre mouse, which expresses Cre-recombinase under the control of the Foxp3-promoter. The Foxp3-YFP-Cre mouse allows easy identification of cells expressing the Cre-recombinase due to the co-expression of the YFP reporter. Since Foxp3 is encoded on the X-chromosome and is therefore affected by random X-chromosome inactivation, heterozygous presence of the Foxp3-YFP-Cre allele could lead to inconsistent results, as not all cells expressing Foxp3 would also express Cre-recombinase. Therefore, the analysis was restricted to male mice expressing the Foxp3-YFP-Cre allele in a hemizygous manner ($Foxp3^{YFP\text{-}Cre/Y}$), which are not affected by random X-chromosome inactivation. Male mice harboring a hemizygous Foxp3-YFP-Cre and a heterozygous ROSA-STOP-SATB1 allele ($Foxp3^{YFP\text{-}Cre/Y}$ x $ROSA26^{SATB1\text{-}GFP/+}$ mice, further referred to as SATB1-KI mice) were used for the analysis of transgene induction and subsequent analysis of the effects of SATB1 overexpression on T_{reg} cell biology.

As shown in Figure 3.36b, more than 99 % of YFP^+CD4^+ T_{reg} cells showed expression of the GFP reporter, indicating efficient Cre-mediated excision of the STOP cassette preventing transcription of the *Satb1* transgene.

To assess whether the expression of the transgene was sufficient to result in an overexpression of SATB1 protein, we also directly measured SATB1 expression by intracellular immunostaining followed by flow cytometry in SATB1-KI T_{reg} and T_{conv} cells compared to the corresponding cell subsets derived from $Foxp3^{YFP\text{-}Cre/Y}$ x $ROSA26^{+/+}$ control mice (SATB1-WT) (Figure 3.37).

Analysis of SATB1 expression in T_{reg} cells from SATB1-WT control mice, revealed two populations of cells with different SATB1 levels ($SATB1^{low}$ and $SATB1^{high}$), whereas YFP^+ T_{reg} cells derived from SATB1-KI mice showed relatively uniform SATB1 expression with a higher mean fluorescence intensity (MFI) than the $SATB1^{high}$ population in the WT control, indicating that transgenic expression of SATB1 overall resulted in an overexpression of SATB1 in T_{reg} cells (Figure 3.37a). However, overexpression of SATB1 did not reach the SATB1 expression in T_{conv}

cells, which showed higher SATB1 expression in the SATB1^{high} population (Figure 3.37b).

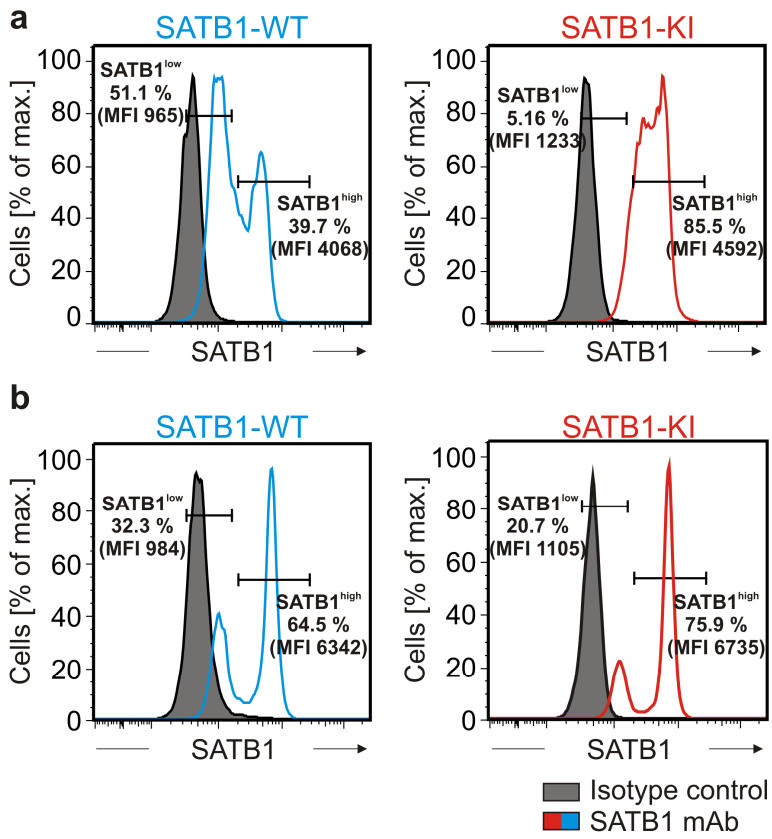

Figure 3.37 Overexpression of SATB1 in T_{reg} cells with induced ROSA26-SATB1 transgene
Assessment of SATB1 expression in T_{reg} and T_{conv} cells from SATB1-KI and SATB1-WT mice by intracellular immunostaining of SATB1 and flow cytometry. (a) Representative histograms showing SATB1 expression in T_{reg} cells from SATB1-KI and SATB1-WT mice. (b) Representative histograms showing SATB1 expression in T_{conv} cells from those mice shown in (a).

Taken together these results demonstrate that the ROSA26-STOP-SATB1 mouse indeed allows for the conditional overexpression of SATB1 in T_{reg} cells.

3.2.2 Identification of Foxp3^{-}GFP^{+} cells in SATB1-KI mice

To investigate whether the overexpression of SATB1 in T_{reg} cells resulted in changes of the T_{reg} cell compartment, SATB1-KI mice were analyzed in more detail. Therefore, Foxp3-YFP and SATB1-transgene expression were assessed in CD4^{+} T cells from spleens of SATB1-KI mice to evaluate whether SATB1 overexpression led to an alteration of Foxp3 expression in T_{reg} cells (Figure 3.38).

CD4^{+} T cells from SATB1-KI mice contained a Foxp3-YFP^{+} T_{reg} cell compartment of similar size as SATB1-WT mice, since in both mouse lines ~ 20 % of CD4^{+} T cells expressed Foxp3. However, in addition to cells expressing both YFP as reporter for Foxp3 and GFP as fate-mapper for previous Foxp3 expression, we also identified a

subset of cells in SATB1-KI mice, which expressed GFP but no YFP (Figure 3.38a, left panel). These results were further confirmed by flow cytometric isolation of these two populations followed by intracellular Foxp3 staining to assess Foxp3 protein expression directly (Figure 3.38a, right panel, and b).

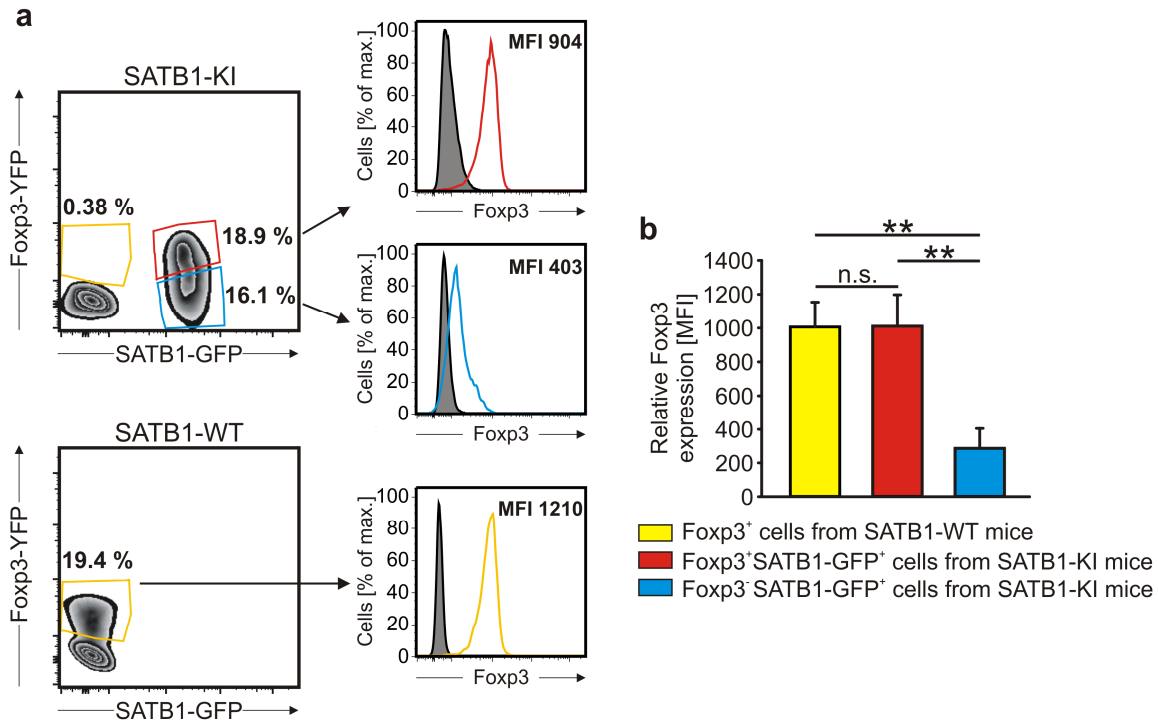

Figure 3.38 exFopx3 T cells in SATB1-KI mice
Assessment of Foxp3 and SATB1-GFP transgene expression in $CD3^+CD4^+$ T cells from SATB1-KI mice and WT controls. (a) Flow cytometric analysis of Foxp3-YFP and SATB1-GFP expressing cell subsets among $CD4^+$ T cells in SATB1-KI and SATB1-WT mice (left panels) and assessment of Foxp3 expression by intracellular staining and flow cytometry (right panels) after flow cytometric isolation of the respective populations shown in the left panels; (b) Quantification of Foxp3 expression assessed by intracellular staining of populations shown in (a) (n=3-4; mean and standard deviation; **P<0.01, n.s.: not significant, Student´s t-test).

Besides the spleen, these $Foxp3^-SATB1^-GFP^+$ were also present in other lymphoid organs, such as lymph nodes and Peyer´s patches (Figure 3.39) with varying Foxp3-YFP^+ : Foxp3-YFP^- cell ratios among the SATB1-GFP^+ cells ranging from 2:1 to 1:1.5. Since the previous results excluded an induction of the SATB1-GFP transgene without prior Cre-recombinase activity (Figure 3.36a), these $Foxp3^-$SATB1-GFP^+ cells could only derive from cells, which at a certain point of their life had expressed Foxp3 (and with it Cre-recombinase) and lost Foxp3 expression over time.

The existence of such exFoxp3 T_{reg} cells [33-36], which lose Foxp3 expression and their suppressive phenotype, has been controversially debated over the last years with very recent evidence suggesting that such cells hardly exist under homeostatic conditions with a maximal T_{reg}/exFoxp3-T_{reg} ratio of 10:1 to 10:2.

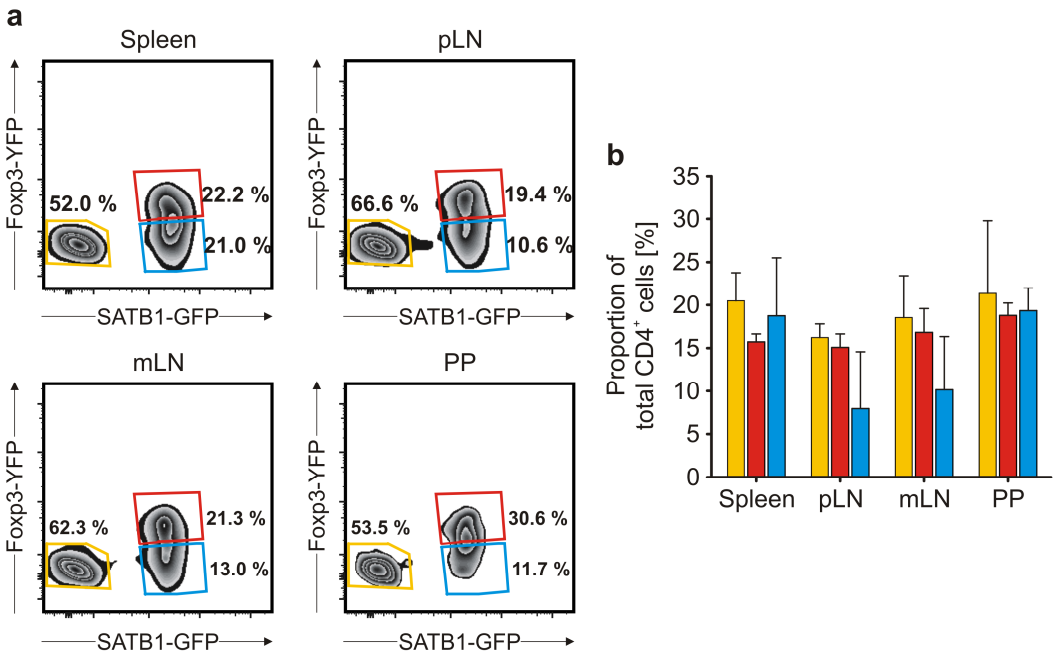

Figure 3.39 exFoxp3 T cells in different lymphoid organs
Flow cytometric analysis of Foxp3-YFP and SATB1-GFP transgene expression among $CD3^+CD4^+$ T cells in different lymphoid organs of SATB1-KI mice. (a) Representative dot plots of Foxp3-YFP and SATB1-GFP expressing $CD4^+$ T cell subsets in different lymphoid organs and (b) quantification of these results. (n=4-13; mean and standard deviation; pLN: peripheral lymph nodes; mLN: mesenteric lymph nodes; PP: Peyer´s patches).

Since the percentage of exFoxp3 cells in the SATB1-KI mice was markedly higher than in these reports (Figure 3.39b), we hypothesized that this increased ratio of exFoxp3 cells was due to a reprogramming of T_{reg} cells through overexpression of SATB1. Thus, these cells as well as those T_{reg} cells, which overexpressed SATB1 but still retained Foxp3 expression, were analyzed together with Maren Koehne during her Master thesis to further characterize these cells and identify the mechanisms underlying this apparent SATB1-mediated reprogramming of T_{reg} cells.

Therefore, we first assessed the suppressive function of the T_{reg} and exFoxp3 cell subsets in an *in vitro* suppression assay, as our previous study had demonstrated a change in this parameter after lentiviral overexpression of SATB1 in T_{reg} cells [113].

For the *in vitro* suppression assay, the respective exFoxp3 and T_{reg} cell subsets from SATB1-KI and SATB1-WT mice were co-cultured with eFluor670-labeled conventional $CD4^+$ T cells under stimulatory conditions (anti-CD3/anti-CD28-coated beads and IL-2). After 72 h of co-culture T_{conv} proliferation was assessed by flow cytometry as a marker for T_{reg}-mediated suppression by comparing T_{conv} proliferation of the respective co-cultures with proliferation of T_{conv} cultured alone (Figure 3.40).

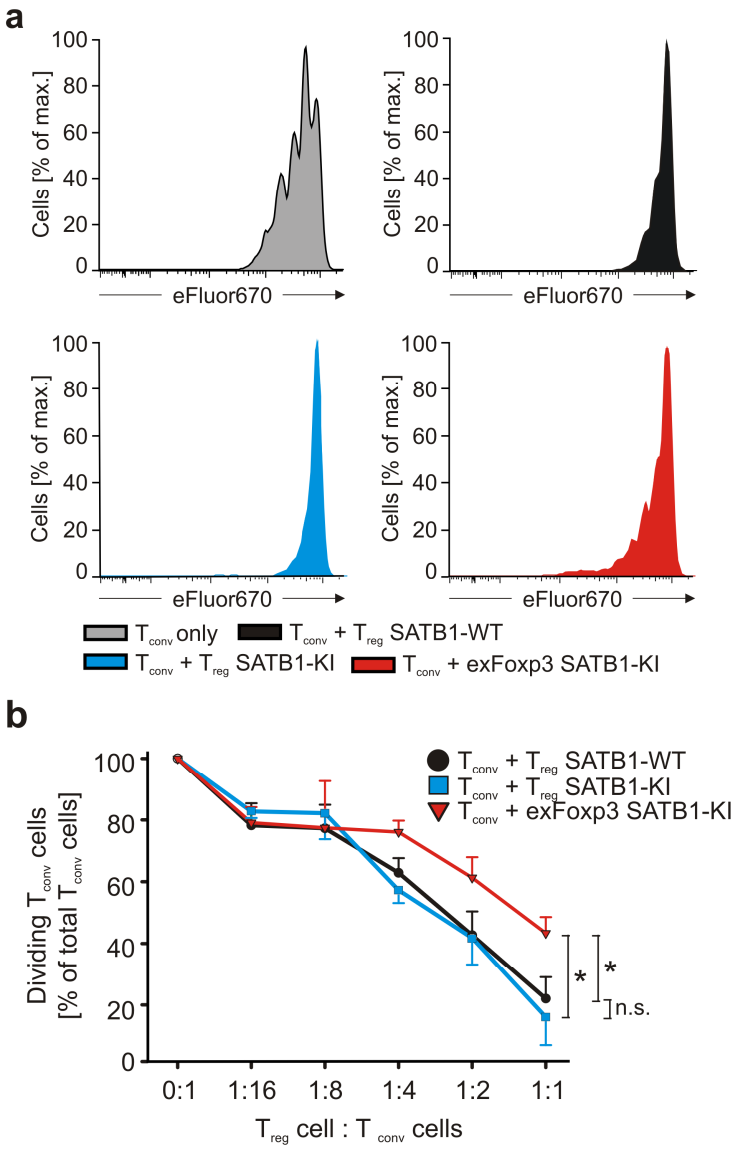

Figure 3.40 Suppressive capacity of T_{reg} and exFoxp3 T cell subsets *in vitro*
Assessment of proliferation of T_{conv} cells after co-culture with SATB1-WT T_{reg}, SATB1-KI T_{reg} and SATB1-KI exFoxp3 cells as a marker for suppressive activity of the respective cell subset. (a) Representative histograms illustrating the eFluor670 dilution of the T_{conv} cells co-cultured with the respective cell subset. (b) Quantification of T_{conv} suppression in the different co-cultures presented as percentage of dividing T_{conv} cells (n=3; mean and standard deviation; *P<0.05, n.s.: not significant, Student´s t-test).

WT T_{reg} cells as well as T_{reg} cells from SATB1-KI mice clearly inhibited T_{conv} cell proliferation in a dose-dependent manner with a maximum suppression in the 1:1 T_{reg}:T_{conv} condition with only 25 % proliferating T_{conv} cells (Figure 3.40b), which indicates that SATB1-KI T_{reg} cells are functionally similar to WT T_{reg} cells. In contrast, exFoxp3 cells showed substantially less suppression of T_{conv} proliferation, as the maximum suppression mediated by these cells allowed about 50 % of T_{conv} cells to proliferate, suggesting that exFoxp3 cells are functionally distinct from T_{reg} cells.

Besides assessment of suppressive activity, we also determined the production of effector T cell cytokines of exFoxp3 and T_{reg} cells *in vitro*, as lentiviral overexpression of SATB1 in T_{reg} cells had also demonstrated induction of these cytokines [113]. Therefore, exFoxp3 and T_{reg} cell subsets were cultured under stimulatory conditions (plate-bound CD3, soluble CD28 antibody and IL-2), followed by determination of cytokine concentrations in cell culture supernatants by cytokine bead arrays (Figure 3.41).

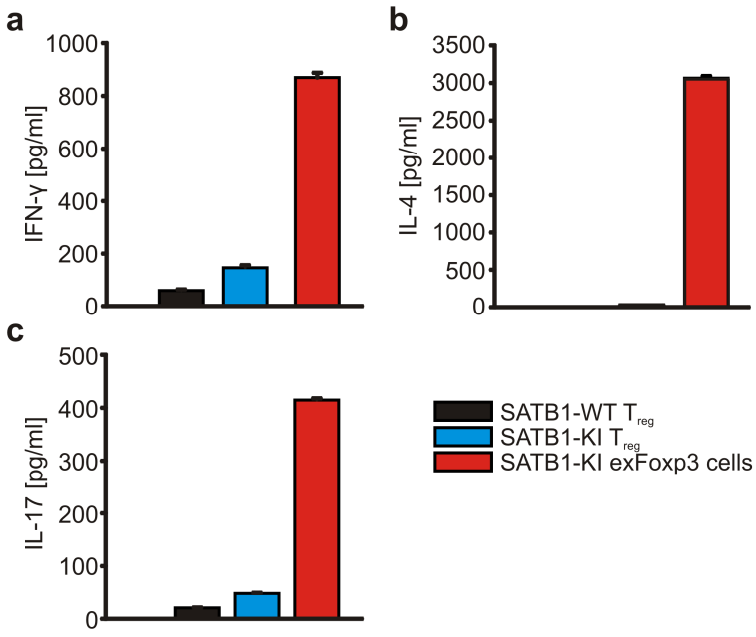

Figure 3.41 T_{eff} cytokine production by T_{reg} and exFoxp3 cells
Assessment of cytokine secretion of T_{reg} and exFoxp3 cells from SATB1-KI and SATB1-WT mice after *in vitro* culture under stimulation with CD3/CD28 and IL-2. Results of a representative cytokine bead array showing concentrations of IFN-γ (a), IL-4 (b) and IL-17 (c) in the supernatant of the respective cell subset (Mean and standard error of the mean (SEM)).

This analysis revealed that exFoxp3 cells produced high amounts of the inflammatory cytokines IFN-γ, IL-4 and IL-17, while T_{reg} cells from SATB1-KI and SATB1-WT mice produced substantially lower or not-detectable amounts of these cytokines, suggesting an effector T cell phenotype of exFoxp3 cells, while SATB1-KI T_{reg} cells resemble WT T_{reg} cells.

In addition to these functional evaluations, further studies, which were based on transcriptome analysis, T_{reg} marker protein assessment, as well as assessment of *in vivo* function, also revealed that exFoxp3 cells were different from WT T_{reg} cells, while SATB1-overexpressing T_{reg} cells were very similar to WT T_{reg} cells (data not shown). Thus, these results suggested that overexpression of SATB1 in T_{reg} cells could possibly reprogram T_{reg} cells towards an effector phenotype.

3.2.3 Detection of exFoxp3 cells in Foxp3$^{YFP\text{-}Cre/Y}$ x ROSA26 $^{LSL\text{-}tdTomato/+}$ mice challenges T_{reg} cell origin of exFoxp3 cells

The experiments described above were conducted with Foxp3-YFP-Cre mice as WT controls. Although this mouse line was suitable for comparing exFoxp3 and T_{reg} cell subsets from SATB1-KI mice with WT T_{reg} cells, it was not suitable to assess the existence of exFoxp3 cells in WT mice, as exFoxp3 cells in these mice would be indistinguishable from T_{conv} cells.

To rule out the possibility that these exFoxp3 T cells exist independent of SATB1 overexpression we crossed a true fate-mapper mouse strain (ROSA26-LSL-tdTomato) with the Foxp3-YFP-Cre mice (Foxp3$^{YFP\text{-}Cre/Y}$ x ROSA26$^{LSL\text{-}tdTomato/+}$, further referred to as tdTomato) and analyzed these mice for the presence of exFoxp3 cells. Therefore, the ratios of Foxp3$^+$ T_{regs} and exFoxp3 cells were assessed by flow cyotmetric analysis of Foxp3-YFP and tdTomato expression in CD4$^+$ T cells isolated from spleens of tdTomato mice and compared to the ratios of the respective cell subsets in age-matched SATB1-KI mice (Figure 3.42a and b).

As depicted in Figure 3.42a, tdTomato mice possessed a noticeable amount of exFoxp3 cells with a T_{reg}/exFoxp3 cell ratio similar to SATB1-KI mice (Figure 3.42b), indicating that the loss of Foxp3 in exFoxp3 cells was not necessarily driven by the SATB1 overexpression. To further characterize exFoxp3 cells in tdTomato mice, we additionally assessed the expression of naive and effector T-cell markers CD62L and CD44 by flow cytometry in T_{reg} and exFoxp3 cells of these mice and compared it to the expression of these markers in the respective cell populations of age-matched SATB1-KI mice (Figure 3.42c-h).

This analysis revealed that most of the exFoxp3 cells in the tdTomato mice had high expression of CD62L and low expression of CD44, indicating a naive phenotype of these cells, while the exFoxp3 cells in SATB1-KI mice had an opposite expression of these markers, thus showing an effector/memory T-cell phenotype (Figure 3.42c-e).

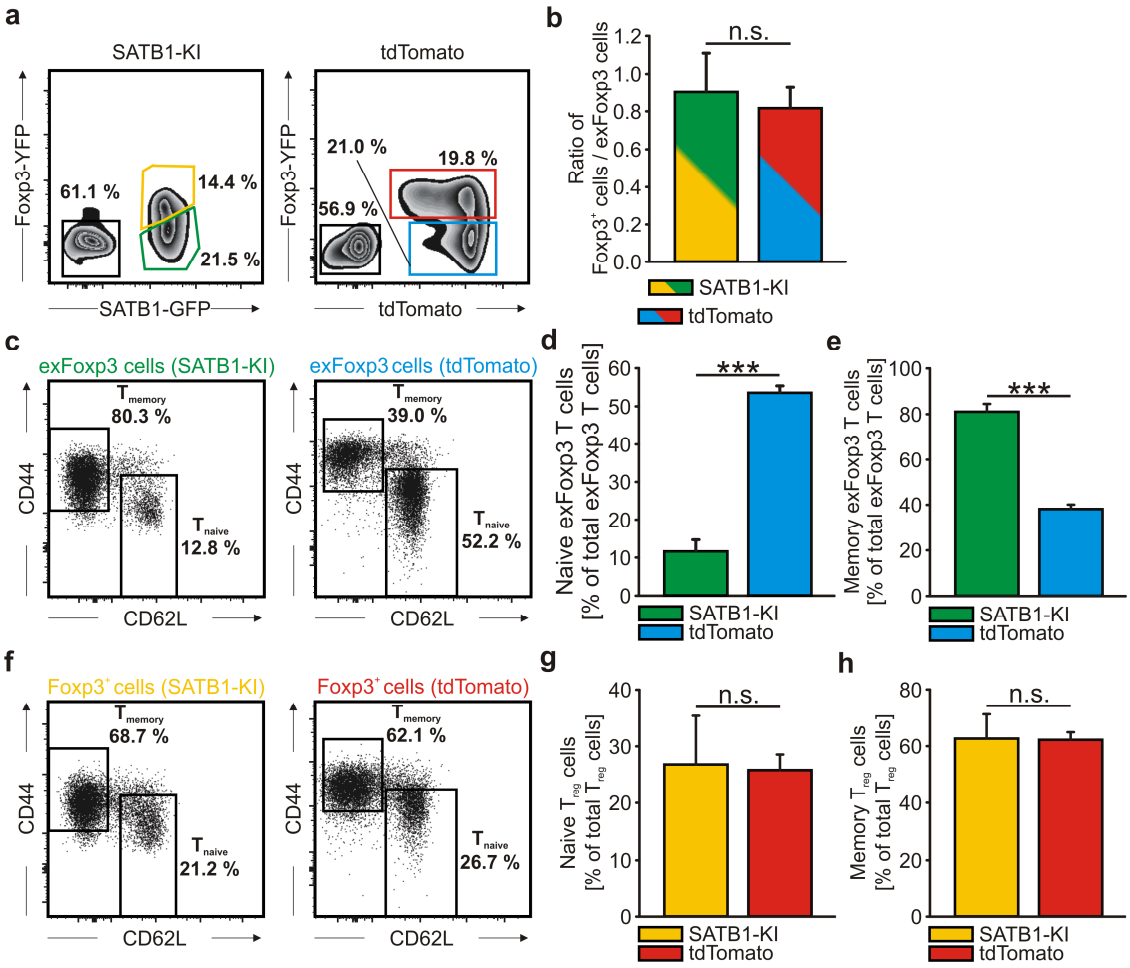

Figure 3.42 Characterisation of exFoxp3 cells in SATB1-KI and tdTomato mice
Flow cytometric analysis of Foxp3 and transgene expression in CD4⁺ T cell subsets of SATB1-KI and tdTomato mice. (a) Representative dot plots showing Foxp3 and transgene expressing CD4⁺ T cells in the analyzed mouse lines. (b) Quantification of the T_{reg}/exFoxp3 cell ratios in those mice shown in (a). (c) Representative dot plots showing CD62L and CD44 expression of exFoxp3 cells in SATB1-KI and tdTomato mice. (d) and (e) Quantification of the T cell populations shown in (c). (f) Representative dot plots showing CD62L and CD44 expression of Foxp3⁺ T_{reg} cells in SATB1-KI and tdTomato mice. (g) and (h) Quantification of the T cell populations shown in (f). (n=3 per mouse line; mean and standard deviation; n.s.: not significant, ***P<0.001Student´s t-test)

In contrast to this, there was no difference in the CD62L and CD44 expression pattern between the Foxp3⁺ T_{regs} from both mice (Figure 3.42f-h).

Thus, in summary these results indicate that the presence of exFoxp3 cells in the SATB1-KI mice is likely not a direct consequence of SATB1 overexpression, but that SATB1 overexpression still leads to a phenotypic change in these cells. Furthermore, since Foxp3⁺ T_{reg} cells are not phenotypically altered upon SATB1 overexpression (Figure 3.40, Figure 3.41 and data not shown), these results suggest that exFoxp3 cells might be derived from a unique subset among naive T cells susceptible to SATB1-mediated transcriptional and phenotypic changes.

4 Discussion

To investigate the *in vivo* role of the genome organizer SATB1 in peripheral $CD4^+$ T cells, which so far had been poorly understood, two mouse models were generated in this thesis, which allowed the spatiotemporal removal (SATB1-Flex knock-out mouse) and overexpression of SATB1 (ROSA26-STOP-SATB1 mouse).

Crossing the conditional SATB1-Flex knock-out mice with CD4-CreERT2 animals, allowed us to abrogate SATB1 expression specifically in mature $CD4^+$ T cells and thereby to circumvent the detrimental effects of SATB1 deficiency on T cell development [98], which so far had been the major obstacle in the assessment of the *in vivo* function of SATB1 in mature T cells.

The analysis of SATB1-deficient mature $CD4^+$ T cells revealed new insights into the biological function of SATB1 in $CD4^+$ T cell function, as SATB1-deficiency lead to a yet undescribed impairment of the differentiation into pathogenic TH17 cells, whereas differentiation into classical subsets, such as TH1, TH2 and non-pathogenic TH17, cells seemed to be uninhibited.

The second mouse model (ROSA26-STOP-SATB1), which was generated in this thesis, was used in combination with the Foxp3-YFP-Cre system to overexpress SATB1 in regulatory T cells, which under homeostatic conditions express only low levels of SATB1 [113]. However, instead of complementing the knock-out model, this overexpression model raised new questions about the function of SATB1, as phenotypic changes were detected in a subset of cells (exFoxp3 cells), which according to current knowledge should not be present under homeostatic conditions, while $Foxp3^+$ T cells remained phenotypically and functionally unaffected upon the overexpression of SATB1.

Besides the immunological analysis of the generated mouse models, this thesis also focused on the generation of gene-targeted mice using the novel genome engineering tool of TAL effector nucleases. We thereby showed for the first time that TALENs can enhance the site-directed integration of even large and complex targeting constructs even when directly injected into oocytes.

4.1 TALENs as appropriate tools for the fast and facile introduction of even complex changes into the murine genome

4.1.1 Performance of the TALEN-assisted homologous recombination of a complex targeting construct in oocytes

In the first part of this thesis a gene targeted mouse was successfully generated by gene editing directly in oocytes, rather than embryonic stem cells, using a combinatorial injection of TALEN mRNAs and a complex targeting construct into the male pronucleus of murine oocytes. With this approach, we showed for the first time that TALEN technology can facilitate homologous recombination so that even complex changes can be introduced site-specifically into the murine genome by simple microinjections without the need of laborious and time-consuming cell culture work.

Reports prior to our study had already shown that TALEN-assisted homology-directed integration of targeting constructs was generally possible in oocytes [92, 93, 122, 123]. However, in these reports only small changes, such as loxP sites or single base pair mutations, were introduced into the genome, while we used a 14.4 kb targeting construct to integrate a 7.6 kb fragment consisting of four lox sites, a reporter gene, internal homologous regions, as well as a 3.8 kb 3´ untranslated region. Despite the complexity of our targeting construct, three out of 67 animals carried an allele derived from homology-directed integration of the targeting construct, or at least parts of it, which results in a rate of homologous recombination slightly lower, but still in the range of the afore mentioned studies, as well as other studies using ZFN-assisted homologous recombination in murine oocytes [124, 125]. Given the complexity of the targeting construct, the rate of homologous recombination in our study is still in an acceptable range, particularly, when taking into account that the *Satb1* locus is not easy to target as shown by classical targeting of ES cells using our targeting construct, which did not yield a single clone with site-directed integration of the targeting construct in 10^7 electroporated cells.

4.1.2 Improvement of TALEN-assisted gene targeting in oocytes

Although the gene targeting efficiency in our TALEN-assisted oocyte injections was in the range of other studies and yielded a correctly targeted founder mouse, there is room for improvement of this approach to yield higher numbers of correctly targeted mice. Higher numbers of founder mice would be desirable, so that a sufficient

number of mice would be available for the establishment of a targeted mouse line, to compensate for the possibility of founders dropping out, e.g. due to premature death or infertility.

One of the first aspects to consider for improvement of TALEN-assisted gene targeting certainly is the efficiency of TALEN-mediated induction of DNA double-strand breaks. However, our SATB1 TALENs showed a frequency of 25.4 % mutated mice after oocyte injections, which was slightly lower, but still in the range of other studies [92, 123, 126], given the higher concentration of TALEN mRNAs used for injection in these studies. Furthermore, the strongly decreased survival rate of oocytes after implantation in the injections using the higher TALEN concentration indicates that we were already using maximal concentrations of TALEN mRNA and targeting construct. This indicates that the efficiency of the SATB1 TALENs was in the maximally achievable range and that the improvement of other factors would probably be more effective.

The targeting site in the *Satb1* locus might be an additional factor for improvement, as two of the three mice showing site-specific integration of the targeting construct, had only integrated parts of the targeting construct due to homologous recombination via the internal homology around *Satb1* exon 2 for (see Figure 3.12 and Figure 3.13). Similar findings have been demonstrated in another study [92] using TALENs for the integration of small oligodeoxynucleotides, in which all founders showed only partial integration of the ssODNs with a preferred integration of those ssODN parts located around the site of the TALEN-induced DSB. Thus, an approach using two TALEN pairs cutting downstream of the 5´ and upstream of the 3´ homology, which would remove the internal homology from the endogenous *Satb1* locus, while leaving the outer homologies intact, could prevent partial integration of the targeting construct thereby increasing targeting efficiency.

Besides technical improvements, however, the major obstacle, which has to be overcome to increase integration efficiency, originates from the cell itself, as the site-directed integration of the targeting construct even in TALEN-assisted gene targeting still depends on the cell intrinsic DNA repair mechanism of homologous recombination. DSBs are mostly repaired by NHEJ instead of homologous recombination, which leads to mutation of the locus, but not to integration of the targeting construct. Based on this, targeting approaches have been established, which enable site-directed integration of a targeting construct via the NHEJ pathway

[127-129]. This is due to the presence of a nuclease targeting site in the targeting construct, which allows nuclease-mediated cleavage of the construct and the subsequent generation of DNA ends compatible to the nuclease-mediated DSB at the targeting locus, which further leads to NHEJ-mediated ligation of these compatible ends. This approach has recently been extended by the addition of ssODNs. These ssODNs facilitated the ligation of the generated DNA ends in the genomic targeting site and the targeting construct after injection into rat and mouse oocytes, so that integration of even very large constructs, such as BACs, were possible with good recombination efficiency [130].

In addition to these approaches utilizing NHEJ for the integration of targeting constructs, Maruyama *et al.* and Ma *et al.* [131, 132] suggested an opposing approach for increasing integration efficiency, as they used a NHEJ inhibitor (SCR7) to block the NHEJ pathway and thus concomitantly increased the activity of the HR machinery. Testing this approach in cell lines and mouse oocytes together with CRISPR/Cas9-mediated induction of DSBs and small targeting constructs showed that the inhibition indeed increased HR rates and thus increased overall site-directed integration efficiencies. In line with this another approach confirmed the increased HR efficiency after SCR7 treatment in cell lines [133]. Furthermore, this study showed that NHEJ can also be blocked by other approaches, such as shRNA-mediated suppression of key molecules of the NHEJ pathway or the co-expression of adenovirus4 E1B55K and E4orf6 proteins, which force the degradation of DNA Ligase IV. While shRNA-mediated NHEJ suppression yielded similar HR rates as the SCR7 treatment, the co-expression of the adenovirus 4 proteins even increased HR efficiency over the rate achieved with SCR7, which indicates that these alternative NHEJ blocking approaches are valuable alternatives to the treatment with SCR7. Since the general mode of action of the CRISPR/Cas9 and the TALEN system are identical, it is likely that the NHEJ inhibition is also applicable in combination with TALEN-induced DSBs. However, it still needs to be determined whether it is also applicable for the integration of large targeting constructs, as used in this thesis.

In summary, these considerations show that the efficiency of TALEN-assisted site-directed integration in oocytes can certainly be further increased, which will further enlarge the advantages of this method over classical gene targeting in ES cells.

4.2 SATB1-Flex as an appropriate system for deletion of SATB1 and assessment of its functional properties in peripheral CD4$^+$ T cells

The deleterious effect of SATB1 removal for T cell development in the thymus reported by Alvarez *et al.* [98] has precluded in-depth *in vivo* studies of the function of SATB1 in fully mature peripheral T cells. An alternative approach, which deleted one allele of *Satb1* and further reduced SATB1 expression by expression of an anti-sense RNA specifically in T cells, was also not suitable for the assessment of SATB1 function in peripheral T cells as it still interfered with thymic development, although not as severe as the complete knock-out [134]. In addition, a classical conditional approach using a Cre-recombinase under control of a T-cell specific promoter, such as CD4, would also lead to a disturbance of T cell development, as CD4 is already expressed at the thymic double-positive stage, the development stage, in which SATB1 was shown to be required for proper T cell development [98]. In line with this, we could show that crossing the SATB1-Flex conditional mouse model with a CD4-Cre mouse (SATB1$^{fl/fl}$ x CD4$^{+/Cre}$) indeed affected thymocyte development (see paragraph 3.1.2.3).

Thus, to generate an appropriate model to study the function of SATB1 in peripheral CD4$^+$ T cells with minimal influence of the thymus, we decided to use a conditional SATB1 knock-out model in combination with the CD4-CreERT2 system. In this model the removal of SATB1 is induced by short pulses of tamoxifen administration in adult mice, which possess an established peripheral T cell compartment. Thus, the timely restricted tamoxifen administration should induce Cre-recombination all in peripheral CD4$^+$ T cells as well as all DP and SP thymocytes at the time point of tamoxifen administration. But due to the relatively low number of cells leaving the thymus [135, 136] compared to the number of peripheral T cells in the established T cell compartments during adolescence, the influence of thymic developmental defects should be relatively low. In line with this, Śledzińska *et al.* [137] used the CD4-CreERT2 system and a five-day period of tamoxifen administration in adult mice to remove the TGF-β receptor specifically in peripheral CD4$^+$ T cells. Thereby they observed a different phenotype to models using conventional tissue/cell-type specific Cre-lines abrogating the TGF-β receptor in developing thymocytes, which demonstrates that the CD4-CreERT2 system is indeed able to confine the removal of the gene of interest to peripheral CD4$^+$ T cells.

Our results confirmed these observations, as GFP expression was only detected in $CD4^+$ T cells, but not in $CD8^+$ T cells. This demonstrated minimal contribution of SATB1-deficient cells from the thymus to the pool of peripheral T cells, as otherwise GFP expression would have been observed in $CD8^+$ T cells due to the induction of Cre-mediated recombination at the thymic DP stage.

Furthermore, we observed an almost 100 % recombination efficiency (see Figure 3.23) in the $SATB1^{fl/fl}$ x $CD4^{+/CreERT2}$ mice with a lower total dose of tamoxifen (16 mg distributed over only two pulses at day 0 and day 3) than Śledzińska *et al.* [137]. This further reduced the potential influence of developmental defects of thymocytes contributing to the pool of peripheral T cells, as thymocytes were exposed to tamoxifen for shorter periods of time. Moreover, we initiated experiments with the tamoxifen treated mice already one week after the first tamoxifen application, which further reduced the time for SATB1-deficient thymocytes to leave the thymus compared to the protocol described by Śledzińska *et al.* [137]. Thus, in summary these results demonstrate that the SATB1-Flex/CD4-CreERT2 system is a suitable system to study the function of SATB1 specifically in peripheral $CD4^+$ T cells.

Besides the specific removal of SATB1, the SATB1-Flex system also enables easy traceability of cells, which underwent Cre-mediated loss of the target gene, as it combines the removal of a gene segment with the induction of a reporter gene [70, 138]. This traceability is not possible with a conventionally floxed allele, as the arrangement of the lox sites prevents insertion of a reporter gene. To allow for the traceability of Cre-recombined cells this can only be achieved with an additional Cre-inducible reporter allele, which requires additional breeding steps. Furthermore, removal of the targeted gene and induction of the reporter are achieved by different Cre-recombination steps, which can impede an extrapolation of Cre-mediated reporter gene recombination to the recombination of the knock-out allele due to varying recombination efficiencies between these alleles [139]. In contrast, reporter gene expression in the Flex system clearly reflects target gene removal, as both processes are exerted in the same Cre recombination step (see Figure 1.4 and Figure 3.2).

In addition to the reporter function, the Flex system, and especially the version of the system used here (SATB1-Flex), has another advantage over conventionally floxed alleles: most conventional strategies target exons downstream of the first coding exon to prevent the use of alternative start codons, which in consequence would

prevent depletion of the protein. The SATB1-Flex approach, however, allows targeting of the first coding exon without the risk of alternative start codon usage, as the transcriptional stop signal encoded by the 3´UTR will terminate transcription after the GFP-reporter-SATB1-3´UTR fusion construct in the recombined state. Thus, the exons downstream of the targeted exon are excluded from transcription, which in consequence precludes translation of alternative start codons due to the lack of the respective mRNA. Targeting of the first coding exon is of further advantage, as it prevents the translation of N-terminal protein fragments with functional domains and consequently potentially preserved protein function. In case of SATB1, the nuclear localization signal is encoded by the first exons [96] so that targeting of downstream exons could lead to the generation of an N-terminal SATB1 fragment with the potential to translocate into the nucleus with an unknown functional impact.

Auxiliary to its function as transcriptional terminator, the fusion of the SATB1 3´ UTR to the GFP reporter also enables the use of the GFP reporter as surrogate marker for SATB1 expression, as it had been previously shown that SATB1 expression is also regulated by miRNAs targeting the *Satb1* 3´ UTR [113, 140]. In accordance with these considerations, GFP expression nicely mirrored the different SATB1 expression levels in naive and memory $CD4^+$ T cells, which experimentally confirmed that the GFP reporter was indeed suitable as surrogate marker for SATB1 expression.

However, although GFP nicely reflected SATB1 expression in these cells under homeostatic conditions, it should be considered that the reporter in the SATB1-Flex allele can only mirror SATB1 expression until the posttranscriptional level. Posttranslational regulation of SATB1 expression cannot be phenocopied by the GFP reporter. Due to this limitation, SATB1 expression should be confirmed once by direct assessment in the respective experimental condition before using the SATB1-Flex GFP reporter as surrogate marker to prevent false results.

In summary, the mentioned advantages of the SATB1-Flex/CD4-CreERT2 system over classical gene targeting approaches demonstrate that this is a suitable system to study the function of SATB1 in peripheral $CD4^+$ T cells *in vivo*, as it helps to overcome technical obstacles, ranging from simple isolation of SATB1-deficient cells via facile assessment of SATB1 expression to, most importantly, the deletion of SATB1 in mature T cells, which had been difficult to achieve with conventional model systems.

4.3 SATB1 depletion in peripheral CD4$^+$ T cells proposes new aspects of SATB1 function in T helper cell differentiation

4.3.1 Loss of SATB1 expression in peripheral CD4$^+$ T cells affects transition of non-pathogenic to pathogenic TH17 cells

To analyze the function of SATB1 in peripheral CD4$^+$ T cells, we used T_{naive} cells from the SATB1-Flex/CD4-CreERT2 system in an adoptive model of colitis, a facile *in vivo* model to assess T cell function. The results of this adoptive colitis model indicate that the lack of colitis development in mice receiving SATB1-deficient cells is due to a reduction of TH17 cells expressing IL-17 and IFN-γ, which belong to a subset known as pathogenic TH17 cells (for review see [141]).

In a study performed by Ahern *et al.* [121] these IL-17$^+$IFN-γ$^+$ pathogenic TH17 cells were shown to require IL-23 signaling for their development and were additionally associated with the development of RAG adoptive colitis, as inhibition of IL-23 signaling lead to a reduction in these cells accompanied by a prevention of colitis. In line with this Krausgruber *et al.* [142] demonstrated this association in another model of chronic colitis and other reports related these cells to various autoimmune diseases in humans and mice, such as multiple sclerosis, diabetes and Crohn´s disease [30, 143, 144]. This suggests that the impaired colitis development after transfer of SATB1-deficient cells is also due to an impaired development of IL-17$^+$IFN-γ$^+$ pathogenic TH17.

In contrast to the pathogenic TH17 cell subset, the development of IL-17$^+$IFN-γ$^-$ TH17 cells was not affected by the deletion of SATB1 in the RAG adoptive colitis model, which suggests that the differentiation into this TH17 effector subset was not impaired by the loss of SATB1. In addition, it has been shown that *in vitro* generated TH17 cells converted into IFN-γ-producing cells after transfer into lymphopenic host [145, 146], which suggested that pathogenic TH17 cells derive from IL-17$^+$IFN-γ$^-$ TH17 effector cells. These findings were corroborated by fate mapping experiments, which revealed that pathogenic TH17 cells indeed originate from IL-17$^+$IFN-γ$^-$ TH17 effector cells under chronic inflammatory conditions [29] and thus derive from a phenotypic change of the cell in response to its environment rather than from a fixed developmental program via a separate differentiation pathway. Taking these data into account, the inability of SATB1-deficient cells to develop into pathogenic TH17 cells as well as the undisturbed formation of IL-17$^+$IFN-γ$^-$ TH17 cells in the adoptive colitis

model, which is also characterized by a chronically inflamed environment, points towards a functional implication of SATB1 in the phenotypic change from pathogenic to non-pathogenic TH17 cells rather than in the initial differentiation of TH17 cells in general.

The underlying mechanisms how SATB1 influences this transition to pathogenic TH17 cells, however, currently remain elusive. Transfer experiments demonstrated that IL-23 signaling is crucial for the phenotypic change of TH17 cells into the IL-17$^+$IFN-γ$^+$ pathogenic phenotype [29, 121]. Thus, it is conceivable that SATB1 is involved in this signaling pathway, either directly as downstream target to induce or repress TH17 related genes or indirectly by providing the appropriate chromosomal architecture for expression and repression of target genes in the IL-23 signaling pathway. Furthermore, it has been reported that IL-23 deprivation as well as blockade of IL-23 signaling lead to an increase in Foxp3$^+$ pT$_{reg}$ cells in the adoptive colitis model, suggesting an inhibition of Foxp3 by IL-23 in addition to the IL-23-mediated induction of the pathogenic TH17 cell program [121, 147]. In contrast to that, we did not observe lower percentages of Foxp3$^+$ pT$_{reg}$ among the SATB1-deficient cells in the RAG adoptive colitis model compared to those cells harboring SATB1 (see Appendix Figure 6.5). This indicates that IL-23 signaling is not completely blocked by a loss of SATB1, which in consequence suggests that SATB1 might act further downstream of IL-23, thus not directly influencing the IL-23-mediated inhibition of Foxp3.

Taken together, based on the results of the adoptive colitis model with SATB1-deficient CD4$^+$ T cells we propose a model, in which SATB1 plays a role (either directly or indirectly) in the downstream pathway of IL-23 signaling to promote the transition from non-pathogenic to pathogenic IL-17$^+$IFN-γ$^+$ TH17 cells, which subsequently are responsible for the development of colitis in this *in vivo* model.

However, one has to take into account that these conclusions are based on first observations and thus need to be confirmed by more detailed experiments. For instance, the results of the colitis model do not exclude an indirect effect of SATB1 deletion on the development of pathogenic TH17 cells, in which SATB1 could influence other extrinsic/environmental factors, which would consequently inhibit the development of pathogenic TH17 cells. To exclude such indirect effects, we are currently optimizing the TH17 *in vitro* differentiation to increase the efficiency of TH17 generation, as the low efficiency observed in this thesis might mask a lack of non-

pathogenic TH17 differentiation in SATB1-deficient $CD4^+$ T cells. Additionally we will establish *in vitro* models to induce TH17 transition from the non-pathogenic to the pathogenic state and to identify whether deletion of SATB1 will abrogate this transition *in vitro*. Such *in vitro* models have already been described [145] and showed that IFN-γ^+ expression could be induced in TH17 cells by several rounds of IL-23 or IL-12 treatment, which indicated transition into the pathogenic TH17 subset without extrinsic factors other than IL-23. The major obstacle of this approach, however, is that the generation of pathogenic IL-17^+IFN-γ^+ TH17 cells is inefficient and instable, whereas it generates IL-17^-IFN-γ^+ TH17 cells with much higher efficiency [145, 148]. These IL-17^-IFN-γ^+ TH17 cells also belong to the pathogenic subpopulation of TH17 cells and, like the IL-17^+IFN-γ^+ TH17 cells, have been associated with colitis development after transfer into $RAG^{-/-}$ and other T cell deficient mice [145, 149, 150]. Furthermore, these cells also derive from non-pathogenic IL-17^+IFN-γ^- TH17 cells as shown by fate-mapping experiments [29]. Nevertheless, these fate-mapping experiments do not unambiguously clarify whether IL-17^+IFN-γ^+ TH17 cells exist as a separate subtype or whether they are precursors of IL-17^-IFN-γ^+ TH17 cells, although the latter case is favored from the currently available data. Therefore, to use the *in vitro* model described by Lee *et al.* [145] for confirming the impaired TH17 transition of SATB1-deficient cells, it will be necessary to clarify, if there is an additional reduction of IL-17^-IFN-γ^+ TH17 cells in the RAG adoptive colitis model, which is not possible from the current data, as IL-17^-IFN-γ^+ TH17 cells cannot be distinguished from IFN-γ^+ TH1 cells. To discriminate these cell subsets, we will hence assess the expression of the aryl hydrocarbon receptor (AhR) and the interleukine-1 receptor (IL-1R) in the RAG adoptive colitis model, as both showed higher expression in TH17-derived IFN-γ^+ $CD4^+$ T cells compared to those of the TH1 subset in a model for EAE [29] and thus could also differ between these subsets in the adoptive colitis model.

Besides the *in vitro* model, we will also confirm the reduced transition to pathogenic TH17 cells in an additional *in vivo* model (EAE). As it has been shown that the change into pathogenic TH17 cells is required to establish the disease phenotype in this model [29], a lack of disease development in mice harboring SATB1-deficient $CD4^+$ T cells would thus confirm the results gained in the adoptive colitis model.

Moreover, we will perform molecular approaches, such as whole transcriptome analysis, analysis of chromatin accessibility and folding, as well as histone

modifications and SATB1-DNA interactions in SATB1-deficient TH17 cells to delineate the underlying molecular mechanisms leading to the observed functional changes, which will consequently shed light on the molecular mode of action of SATB1 in these cells.

4.3.2 Proposed function of SATB1 in peripheral CD4$^+$ T cells beyond TH17 cells

In addition to the observations in TH17 cells, we also assessed, if TH1 and TH2 effector T cell subsets were affected by the deletion of SATB1, as preceding experiments with a murine TH2 clone [108] and our own data gained from TH1 *in vitro* differentiation of human CD4$^+$ T cells after siRNA-mediated knock-down of SATB1 (Yasser Thabet, unpublished data) had shown that the reduction of SATB1 impaired secretion of IL-4 and IFN-γ, respectively, which suggested that SATB1 was required for the differentiation of naive T cells into these subsets.

Interestingly, the results of our adoptive colitis model revealed no difference in IFN-γ secretion between SATB1-sufficient and -deficient cells. This finding was also confirmed *in vitro*, which suggests that the removal of SATB1 in T_{naive} cells does not interfere with TH1 differentiation. Furthermore, our *in vitro* data for TH2 differentiation point into the same direction. Here, SATB1-deficient cells showed even better differentiation into TH2 cells indicated by higher percentages of IL-4 producing cells.

A possible explanation for the difference in TH1 differentiation might be species-specific differences between humans and mice. In line with this, we observed posttranslational cleavage of SATB1 upon stimulation of human CD4$^+$ T cells (Daniel Sommer, unpublished data), which cannot be observed in stimulated murine CD4$^+$ T cells. Although the functional impact of this stimulation-induced SATB1 cleavage is still elusive, it might be possible that this cleavage is part of a mechanism resulting in a gain-of-function, where the cleavage fragments would have novel functions important for T cell differentiation. According to this, a reduction of SATB1 expression before T cell differentiation, as done by Yasser Thabet, would lead to a reduction in the cleavage fragments and consequently to an impairment of T cell differentiation, which would explain the reduced IFN-γ production in human cells.

In contrast to the TH1 differentiation the diverging results of the TH2 studies cannot be explained by species-specific differences, as both studies were conducted in murine T cells. However, while we used freshly isolated naive T cells expressing high levels of SATB1, Cai *et al.* [108] performed their experiments in a TH2 cell clone with

low SATB1 expression. With this TH2 clone it was shown that upon T cell activation SATB1 folds the TH2 cytokine locus into chromatin loops thereby changing the chromatin into a transcriptionally active form, which is required for the expression of the TH2 cytokines IL-4, IL-5 and IL-13. However, it was not stated whether this chromatin loop structures need to be maintained during the whole differentiation process or whether the loop formation is only required before cytokine expression to reorganize the chromatin into an active state. Thereby, the latter case could explain the differences between our results and those obtained in the TH2 clone: since the naive T cells used in our study possess high levels of SATB1 before Cre-mediated knock-out of the *Satb1* gene, the TH2 locus would already be in the transcriptionally active state, thus allowing expression of IL-4 even despite the removal of SATB1 as observed in our *in vitro* differentiation. In contrast to that, the TH2 clone used by Cai *et al.* [108] harbors low SATB1 expression accompanied by an inactive chromatin state before the activation, which through the knock-down of SATB1 is not able to change into the active state, thereby impeding TH2 cytokine expression.

Thus, our results of the TH2 *in vitro* differentiation suggest that SATB1 does not play an active role during the differentiation process itself, but rather provides an appropriate genomic framework for the activation of TH2 cytokine expression upon encounter of the respective environmental activation signals.

Considering that SATB1 acts as a global chromatin organizer [107, 108, 110] and its wide range of regulated genes [98], it is furthermore likely that this mode of action of SATB1 is not only restricted to TH2 differentiation, but might also apply to the differentiation processes into other T helper subsets. This would explain the undisturbed differentiation of SATB1-deficient T_{naive} cells into TH1 and non-pathogenic TH17 cells as observed in our *in vitro* and *in vivo* models.

Furthermore, considering the proposed SATB1-mediated transition into pathogenic TH17 cells, SATB1 could also play a major role in providing the appropriate genomic framework for phenotypic changes observed in TH1 and TH2 cell subsets (see paragraph 1.1.3).

Thus, we propose a general model for the function of SATB1 in peripheral $CD4^+$ T cells (see Figure 4.1), in which SATB1 provides a chromatin structure, which initiates a transcriptionally active framework for the differentiation into the different T effector cell subsets. Once this active framework has been established, the chromatin structure is dispensable for the subsequent differentiation process, in which the

respective T effector cell subset develops in response to environmental stimuli. However, as the establishment of a certain T helper cell phenotype leads to an epigenetic silencing of several genes associated with the other T helper cell subsets, such as the signature cytokine genes [39], a further transition from an established T cell subset into another subset, e.g. due to an altered environment, will again require the SATB1-mediated chromatin looping to rebuild the active chromatin.

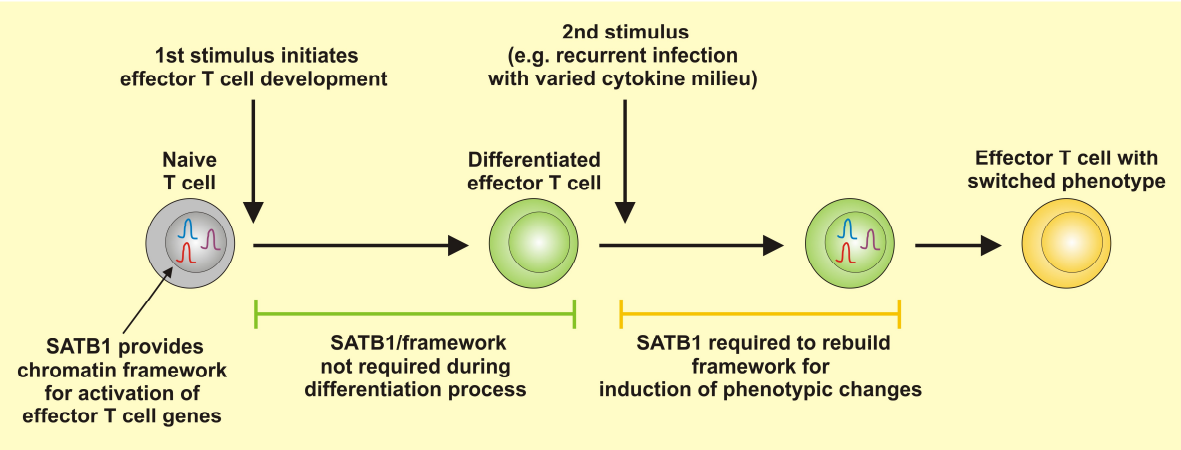

Figure 4.1 Model for the function of SATB1 during the differentiation of peripheral CD4⁺ T cells
Figure illustrating a model of the mode of action of SATB1 during the development of effector T cell subsets, which integrates the findings of previous studies and those obtained with the analyses of the SATB1-Flex KO model:
SATB1 provides a chromatin framework in naive T cells by formation of chromatin loops and epigenetic modifications, which allows differentiation into effector T cell subsets upon encountering of activation signals. SATB1 and the corresponding framework are not required during the subsequent differentiation process, but will be necessary for a phenotypic switch in the effector T cell phenotype, e.g. for the adaptation of the immune response to an altered cytokine environment.

This proposed model describing the mode of action of SATB1 in peripheral CD4⁺ T cells does not only integrate our observations, but is also in agreement with the previous findings of SATB1 repression in Foxp3⁺ T_{reg} cells [113]. Since T_{reg} cells are nowadays generally regarded as a stable T cell subset [34, 35], the repression of SATB1 in these cells according to our model would be required to repress the acquisition of other T effector cell subsets under changing environmental conditions, as shown in the study of Beyer *et al.* [113].

However, one has to be aware that this model only relies on first indications and that additional experiments are needed to confirm the observations and elucidate the underlying molecular mechanisms. Furthermore, there are still open questions, which cannot be answered by this model and require further investigation. For instance, while the proposed mode of action explains why SATB1 deficiency in T_{naive} cells still

enables TH2 differentiation despite the apparently opposing findings of Cai *et al.* [108], it does not elucidate the higher efficiency of TH2 generation in comparison to SATB1-sufficent T_{naive} cells. This higher efficiency indicates that SATB1 might exert inhibitory effects onto the TH2 differentiation, rather than providing a TH2-promoting environment, which would be entirely contrary to the currently available literature. To further investigate this question, we will therefore confirm the TH2 differentiation of SATB1-deficient cells in an appropriate *in vivo* model, such as the initiation of a TH2 response by the injection of peptide loaded dendritic cells pulsed with helminth antigen [151], which will elucidate whether the increased TH2 differentiation is generally detectable or due to the *in vitro* model used.

Moreover, analogous to TH17 cells, we will perform analyses of global changes in transcriptome, epigenome and chromatin structure after SATB1 ablation in TH1 and TH2 cells to assess the hypothesized mechanisms on the molecular level.

In addition to these studies, we will also investigate the effect of SATB1 depletion on $CD4^+$ memory T cells, as our results suggest that these cells only express very low levels of SATB1. Therefore, it will be interesting to see, whether memory T cells also rely on the SATB1-mediated chromatin structure for cytokine expression upon activation. For this purpose, we will use the model described by Krawczyk *et al.* [151], to induce TH1 and TH2 memory T cells *in vivo*, followed by tamoxifen-mediated depletion of SATB1, as well as the assessment of the response to a re-challenge with the corresponding antigen.

Furthermore, it was demonstrated with this model that memory T cells can also undergo transition to another T helper phenotype upon re-challenge with the same antigen under conditions favoring the other T cell subset. Thus, we will also apply this model to our SATB1-depleted cells to see whether SATB1 will also be responsible for phenotypic changes in memory T cells.

In summary, these experiments together with our current findings will provide a comprehensive picture to further delineate the functional role of SATB1 in peripheral $CD4^+$ T cells.

4.4 Foxp3-mediated overexpression of SATB1 causes changes in an unusual subset of exFoxp3 T cells

4.4.1 exFoxp3 T cells in SATB1-KI mice are presumably not derived from SATB1-mediated reprogramming of fully committed T_{reg} cells

Our initial findings with the SATB1-KI mouse model apparently confirmed our hypothesis that SATB1 repression is crucial for the maintenance of the T_{reg} cell phenotype and function [113], as we detected SATB1 overexpressing cells showing a loss of Foxp3 accompanied by an effector phenotype and lack of suppressive activity. This suggested that SATB1 overexpression in Foxp3 expressing cells resulted in a reprogramming of these cells from suppressor to effector cells. Previous data supported this hypothesis, as the presence of such exFoxp3 T_{reg} cells had been reported at a much lower ratio [33] or their existence under homeostatic conditions had even been challenged [34, 35].

However, the analysis of an additional control mouse (tdTomato) revealed that these exFoxp3 cells were probably not derived from T_{reg} cells reprogrammed by SATB1, as exFoxp3 cells were also detected to a similar extend in tdTomato mice, which do not overexpress SATB1.

Since the Foxp3-YFP-Cre line served as the Cre-driver line in both, the SATB1-KI and the tdTomato mice, it is conceivable that this Cre-driver line might be the reason for the presence of the exFoxp3 cells, e.g. due to a spurious, but unstable Cre expression in non-T_{reg} cells. In line with this, another study [152], which was published while this thesis was in preparation, reported similar findings. Here, Foxp3-YFP-Cre mice were used to conditionally remove CD28 from T_{reg} cells and a high percentage of $Foxp3^{-}CD4^{+}$ T cells also showed loss of CD28, which corroborates that this Foxp3-YFP-Cre model might be “leaky” and thus can lead to the appearance of exFoxp3 cells. Furthermore, in the initial description of this mouse model [64] spurious expression of Cre recombinase was reported for other cells types, such as B cells, $CD8^{+}$ T cells and myeloid cells. This further substantiates that the occurrence of exFoxp3 cells in the SATB1-KI mouse model resulted from an unspecific expression of Cre-recombinase rather than a reprogramming of T_{reg} cells upon SATB1 overexpression.

Moreover, the fact that we could not detect major differences in the phenotype, function and transcriptional profiles between SATB1-KI T_{reg} cells and WT T_{reg} cells

(Figure 3.40, Figure 3.41 and data not shown) indicates that the overexpression of SATB1 was not able to reprogram these cells into effector T cells, which makes it highly unlikely that the exFoxp3 cells in SATB1-KI mice resulted from a SATB1-mediated reprogramming of Foxp3$^+$ T_{reg} cells.

Thus, the exFoxp3 cells observed in SATB1-KI mice are probably not derived from SATB1-mediated reprogramming of T_{reg} cells into effector T cells, but rather result from a yet unknown and non-stable Foxp3 expression in otherwise Foxp3$^-$CD4$^+$ T cells.

4.4.2 exFoxp3 cells could be due to genomic changes in the Foxp3 allele

The detection of the high amount of exFoxp3 T cells in SATB1-KI and tdTomato mice raises the question what might be the reason of the non-stable Foxp3 expression in non-T_{reg} cells.

Rubtsov *et al.* (2008) and Franckaert *et al.* (2015) explained this phenomenon as a result of stochastic recombination events due to pervasive transcription of otherwise silent genes in developing cells and thus as a general mechanism in cell differentiation [64, 152]. This explanation, however, is arguable, as, given the extent of exFoxp3 cells in these mice, this pervasive transcription would have caused a similar phenomenon in other conditional mouse lines, especially those used for fate mapping experiments. Furthermore, if this was the case, the application of Cre recombinases under control of tissue-specific promotors in conditional gene targeting would be debatable in general, as specificity of Cre activity could not be granted. Though, as many of these Cre lines exist and as reports about unspecific activity of those lines are rare, it is doubtful whether this stochastic recombination due to pervasive transcription is applicable here as sole explanation.

Instead of this more general explanation, it is more likely that the leakiness of the Foxp3-YFP-Cre mouse, which leads to the high amount of exFoxp3 cells, is due to the changes introduced into the genome, when targeting the *Foxp3* locus, as this would explain why this leakiness is not observed in other Foxp3-Cre mice used for fate mapping [33, 35]. This becomes apparent when regarding the different strategies for the generation of these mice. These mouse models were generated with constructs, which do not alter the *Foxp3* regulatory elements in the respective transgene [33, 153] or endogenous *Foxp3* locus [35], as the Reporter-Cre fusion cassettes were either inserted upstream of the first *Foxp3* coding exon, or between the last coding exon and the 3´ UTR. Thereby the inserted cassettes did not contain

transcription stop signals and thus should not interfere with *Foxp3* mRNA transcription. The targeting approach for generation of the Foxp3-YFP-Cre mouse model, however, contains a transcriptional stop signal after the IRES-YFP-Cre cassette, which was inserted at the *Foxp3* locus between the last coding exon and the 3´ UTR [64]. This poly-A signal should consequently prevent transcription of the Foxp3 3´ UTR, which, at least in human cells, has been shown to be involved in suppression of Foxp3 expression in non-T_{reg} cells [154, 155]. Thus, it is conceivable that due to this artificially inserted poly-A signal the Foxp3-YFP-Cre mouse model might have a partially deregulated *Foxp3* gene allowing an easier induction of Foxp3 in non-T_{reg} cells due to the lack of one of the suppressive mechanisms, which, in combination with the pervasive transcription model given by Rubtsov *et al.* [64] could lead to Foxp3 expression in non-T_{reg} cells lasting long enough to allow Cre-mediated recombination of the reporter transgene and thus would explain the high abundance of exFoxp3 cells.

However, although this combination of *Foxp3* locus changes and pervasive transcription explains the higher abundance of exFoxp3 cells in Foxp3-YFP-Cre mice as spontaneous occurrence, it does not explain the changes in naive and effector/memory subset composition between exFoxp3 T cells of tdTomato mice and the SATB1 overexpressing exFoxp3 T cells of SATB1-KI mice. This rather suggests that exFoxp3 T cells derive from a certain subset of developing T cells susceptible to SATB1-mediated changes. This is further supported by the finding that the ROSA26-STOP-SATB1 mouse model only weakly overexpresses SATB1 (see Figure 3.37), which in consequence will only lead to changes in cells with low endogenous expression of SATB1. As most cells in the thymus, such as DP thymocytes and SP thymocytes developing into naive T cells, however, express high levels of SATB1, these exFoxp3 T cells must be derived from a defined small subset of developing thymocytes. Miyao *et al.* (2012) had shown that exFoxp3 T cells evolve from developing T_{reg} cells not yet fully committed to the stable T_{reg} lineage [35]. Given the fact that a major part of developing T_{reg} cells originates from $Foxp3^{+}CD25^{-}$ precursor cells [6], which due to their Foxp3 expression should exhibit low levels of SATB1 [113, 140], such uncommitted developing T_{reg} cells could be a possible source for an exFoxp3 cell type susceptible to SATB1 overexpression.

Taken together, we conclude that the exFoxp3 T cells in the SATB1-KI and tdTomato mice originate from a distinct subset of developing thymocytes, rather than solely

from a spontaneous short-lived expression of Foxp3 in non-T_{reg} cells. However, we admit that due to the potential ablation of the Foxp3 3´ UTR, Foxp3 expression in Foxp3-YFP-Cre mice might be partly deregulated, thus favoring the generation of exFoxp3 cells in general, which additionally contributes to the higher number of exFoxp3 T cells in this model compared to other Foxp3-Cre lines.

4.4.3 The Foxp3$^{YFP\text{-}Cre/Y}$ x ROSA26$^{SATB1\text{-}GFP/+}$ mouse model is not appropriate to complement the removal of SATB1 in peripheral CD4$^+$ T cells

The findings that the exFoxp3 T cells in the SATB1-KI mice presumably do not originate from SATB1-mediated reprogramming of stable T_{reg} cells, but potentially from a yet undefined subset of developing T cells in the thymus, clearly shows that this model is not suitable to complement the findings of the SATB1-Flex conditional knock-out and reporter model, as this would require a restriction of SATB1 overexpression solely to fully developed Foxp3$^+$ T_{reg} cells, which is not the case here. Besides the unspecified origin of the exFoxp3 cells in the SATB1-KI model, we could not detect any changes in the SATB1-overexpressing Foxp3$^+$ T_{reg} cells compared to WT control cells (see Figure 3.40 and Figure 3.41). This, however, is in clear contrast to our previous observations after lentiviral transfer of SATB1, which revealed a loss of the T_{reg} cell program as well as a gain of T_{eff} cell properties [113]. This discrepancy could be explained by different SATB1 expression levels between the SATB1-KI mouse model and the lentiviral overexpression. While lentiviral transfer generates expression levels of SATB1 sufficient to reprogram T_{reg} cells, the expression in the mouse model is not strong enough to elicit changes in the T_{reg} cell program. This explanation is rather likely, considering that the overexpression in the SATB1-KI mouse does not reach SATB1 levels of naive T cells (see Figure 3.37), from which effector T cell subsets normally derive.

Thus, to achieve our initial aim of SATB1 overexpression specifically in T_{reg} cells, it will be necessary to use the ROSA26-STOP-SATB1 mouse model in combination with another Cre-line restricting Cre activity solely to fully committed Foxp3$^+$ T_{reg} cells. This could be achieved by crossing the ROSA26-STOP-SATB1 model to a Foxp3-CreERT2 mouse, in which, analogous to the SATB1-Flex/CD4-CreERT2 model, the influence of cells from the thymus is minimized by induction of Cre activity, thus restricting SATB1 overexpression to fully developed T_{reg} cells in the periphery. Furthermore, the ROSA26-STOP-SATB1 allele should be homozygously present in

these mice to increase the SATB1 overexpression, as the heterozygous allele was not sufficient to induce changes in Foxp3$^+$ T_{reg} cells.

However, although SATB1-KI mice cannot be used for complementing the assessment of SATB1 function in peripheral CD4$^+$ T cells, further studying the origin and the molecular mechanisms leading to increased abundance exFoxp3 as well as to the SATB1-induced changes in these cells, might enable new insights into the processes of thymic T_{reg} cell development.

4.5 Conclusions

In conclusion, this thesis nicely demonstrates the importance of appropriate mouse models for the elucidation of the function of genes and proteins in general and for SATB1 in particular, as with the SATB1-Flex KO model we were able to refine and extend our knowledge about the function of SATB1 in CD4$^+$ T cell differentiation. Moreover, the future experiments proposed in paragraphs 4.3.1 and 4.3.2, will probably lead to quick and conclusive results, due to the specific and complete removal of SATB1 in peripheral CD4$^+$ T cells without elaborate manipulation of these cells and consequently to a comprehensive picture of the role of SATB1 for T cell differentiation *in vivo*.

However, the analysis of the SATB1-KI model in the second part of this thesis also illustrates that the results gained with mouse models have to be critically reviewed and compared to appropriate controls, since changes introduced into the genome can lead to strong deviations from the natural situation, thereby rendering the mouse model useless for the respective intention.

Nevertheless, such deviations can also be a chance to reveal new research aspects as seen with the SATB1-mediated phenotypic changes in exFoxp3 T cells (see paragraphs 3.2.3 and 4.4.2). Although these changes are probably not derived from reprogramming of T_{reg} cells, elucidating the origin of these cells as well as the molecular changes provoked by SATB1 might provide further insights into thymic T cell development.

In addition, this thesis has shown that mouse models, even with complex changes in the genome, can be generated quickly using TALENs as novel genome engineering tools. Our results as well as the considerations to improve the efficiency of TALEN-assisted gene targeting should contribute to the simplification of gene targeting and the subsequent generation of model organisms.

5 References

1. Chaplin, D.D., *Overview of the immune response.* J Allergy Clin Immunol, 2010. **125**(2 Suppl 2): p. S3-23.
2. Takeuchi, Y. and H. Nishikawa, *Roles of regulatory T cells in cancer immunity.* Int Immunol, 2016. **28**(8): p. 401-9.
3. Hirahara, K. and T. Nakayama, *CD4+ T-cell subsets in inflammatory diseases: beyond the Th1/Th2 paradigm.* Int Immunol, 2016. **28**(4): p. 163-71.
4. Starr, T.K., S.C. Jameson, and K.A. Hogquist, *Positive and negative selection of T cells.* Annu Rev Immunol, 2003. **21**: p. 139-76.
5. Klein, L., et al., *Positive and negative selection of the T cell repertoire: what thymocytes see (and don't see).* Nat Rev Immunol, 2014. **14**(6): p. 377-91.
6. Tai, X., et al., *Foxp3 transcription factor is proapoptotic and lethal to developing regulatory T cells unless counterbalanced by cytokine survival signals.* Immunity, 2013. **38**(6): p. 1116-28.
7. Lio, C.W. and C.S. Hsieh, *A two-step process for thymic regulatory T cell development.* Immunity, 2008. **28**(1): p. 100-11.
8. Burchill, M.A., et al., *Linked T cell receptor and cytokine signaling govern the development of the regulatory T cell repertoire.* Immunity, 2008. **28**(1): p. 112-21.
9. Acuto, O. and F. Michel, *CD28-mediated co-stimulation: a quantitative support for TCR signalling.* Nat Rev Immunol, 2003. **3**(12): p. 939-51.
10. Mosmann, T.R., et al., *Two types of murine helper T cell clone. I. Definition according to profiles of lymphokine activities and secreted proteins.* J Immunol, 1986. **136**(7): p. 2348-57.
11. Szabo, S.J., et al., *A novel transcription factor, T-bet, directs Th1 lineage commitment.* Cell, 2000. **100**(6): p. 655-69.
12. Finkelman, F.D., et al., *Regulation and biological function of helminth-induced cytokine responses.* Immunol Today, 1991. **12**(3): p. A62-6.
13. Swain, S.L., et al., *IL-4 directs the development of Th2-like helper effectors.* J Immunol, 1990. **145**(11): p. 3796-806.
14. Pai, S.Y., M.L. Truitt, and I.C. Ho, *GATA-3 deficiency abrogates the development and maintenance of T helper type 2 cells.* Proc Natl Acad Sci U S A, 2004. **101**(7): p. 1993-8.
15. Park, H., et al., *A distinct lineage of CD4 T cells regulates tissue inflammation by producing interleukin 17.* Nat Immunol, 2005. **6**(11): p. 1133-41.
16. O'Connor, W., Jr., L.A. Zenewicz, and R.A. Flavell, *The dual nature of T(H)17 cells: shifting the focus to function.* Nat Immunol, 2010. **11**(6): p. 471-6.
17. Bettelli, E., et al., *Reciprocal developmental pathways for the generation of pathogenic effector TH17 and regulatory T cells.* Nature, 2006. **441**(7090): p. 235-8.
18. Ivanov, II, et al., *The orphan nuclear receptor RORgammat directs the differentiation program of proinflammatory IL-17+ T helper cells.* Cell, 2006. **126**(6): p. 1121-33.
19. Dutton, R.W., L.M. Bradley, and S.L. Swain, *T cell memory.* Annu Rev Immunol, 1998. **16**: p. 201-23.
20. Sakaguchi, S., et al., *Immunologic self-tolerance maintained by activated T cells expressing IL-2 receptor alpha-chains (CD25). Breakdown of a single mechanism of self-tolerance causes various autoimmune diseases.* J Immunol, 1995. **155**(3): p. 1151-64.

21. Vignali, D.A., L.W. Collison, and C.J. Workman, *How regulatory T cells work.* Nat Rev Immunol, 2008. **8**(7): p. 523-32.
22. Williams, L.M. and A.Y. Rudensky, *Maintenance of the Foxp3-dependent developmental program in mature regulatory T cells requires continued expression of Foxp3.* Nat Immunol, 2007. **8**(3): p. 277-84.
23. Bennett, C.L., et al., *The immune dysregulation, polyendocrinopathy, enteropathy, X-linked syndrome (IPEX) is caused by mutations of FOXP3.* Nat Genet, 2001. **27**(1): p. 20-1.
24. Brunkow, M.E., et al., *Disruption of a new forkhead/winged-helix protein, scurfin, results in the fatal lymphoproliferative disorder of the scurfy mouse.* Nat Genet, 2001. **27**(1): p. 68-73.
25. Takahashi, T., et al., *Immunologic self-tolerance maintained by CD25(+)CD4(+) regulatory T cells constitutively expressing cytotoxic T lymphocyte-associated antigen 4.* J Exp Med, 2000. **192**(2): p. 303-10.
26. McHugh, R.S., et al., *CD4(+)CD25(+) immunoregulatory T cells: gene expression analysis reveals a functional role for the glucocorticoid-induced TNF receptor.* Immunity, 2002. **16**(2): p. 311-23.
27. Abbas, A.K., et al., *Regulatory T cells: recommendations to simplify the nomenclature.* Nat Immunol, 2013. **14**(4): p. 307-8.
28. Kretschmer, K., et al., *Inducing and expanding regulatory T cell populations by foreign antigen.* Nat Immunol, 2005. **6**(12): p. 1219-27.
29. Hirota, K., et al., *Fate mapping of IL-17-producing T cells in inflammatory responses.* Nat Immunol, 2011. **12**(3): p. 255-63.
30. Annunziato, F., et al., *Phenotypic and functional features of human Th17 cells.* J Exp Med, 2007. **204**(8): p. 1849-61.
31. Cosmi, L., et al., *Identification of a novel subset of human circulating memory CD4(+) T cells that produce both IL-17A and IL-4.* J Allergy Clin Immunol, 2010. **125**(1): p. 222-30 e1-4.
32. Kastirr, I., et al., *IL-21 is a central memory T cell-associated cytokine that inhibits the generation of pathogenic Th1/17 effector cells.* J Immunol, 2014. **193**(7): p. 3322-31.
33. Zhou, X., et al., *Instability of the transcription factor Foxp3 leads to the generation of pathogenic memory T cells in vivo.* Nat Immunol, 2009. **10**(9): p. 1000-7.
34. Rubtsov, Y.P., et al., *Stability of the regulatory T cell lineage in vivo.* Science, 2010. **329**(5999): p. 1667-71.
35. Miyao, T., et al., *Plasticity of Foxp3(+) T cells reflects promiscuous Foxp3 expression in conventional T cells but not reprogramming of regulatory T cells.* Immunity, 2012. **36**(2): p. 262-75.
36. Bailey-Bucktrout, S.L., et al., *Self-antigen-driven activation induces instability of regulatory T cells during an inflammatory autoimmune response.* Immunity, 2013. **39**(5): p. 949-62.
37. Murphy, E., et al., *Reversibility of T helper 1 and 2 populations is lost after long-term stimulation.* J Exp Med, 1996. **183**(3): p. 901-13.
38. Ansel, K.M., D.U. Lee, and A. Rao, *An epigenetic view of helper T cell differentiation.* Nat Immunol, 2003. **4**(7): p. 616-23.
39. Wei, G., et al., *Global mapping of H3K4me3 and H3K27me3 reveals specificity and plasticity in lineage fate determination of differentiating CD4+ T cells.* Immunity, 2009. **30**(1): p. 155-67.

40. Hegazy, A.N., et al., *Interferons direct Th2 cell reprogramming to generate a stable GATA-3(+)T-bet(+) cell subset with combined Th2 and Th1 cell functions.* Immunity, 2010. **32**(1): p. 116-28.
41. Peine, M., et al., *Stable T-bet(+)GATA-3(+) Th1/Th2 hybrid cells arise in vivo, can develop directly from naive precursors, and limit immunopathologic inflammation.* PLoS Biol, 2013. **11**(8): p. e1001633.
42. Beyer, M. and J.L. Schultze, *Regulatory T cells: major players in the tumor microenvironment.* Curr Pharm Des, 2009. **15**(16): p. 1879-92.
43. Thomas, K.R. and M.R. Capecchi, *Site-directed mutagenesis by gene targeting in mouse embryo-derived stem cells.* Cell, 1987. **51**(3): p. 503-12.
44. Bradley, A., et al., *The mammalian gene function resource: the International Knockout Mouse Consortium.* Mamm Genome, 2012. **23**(9-10): p. 580-6.
45. International Mouse Knockout, C., et al., *A mouse for all reasons.* Cell, 2007. **128**(1): p. 9-13.
46. Skarnes, W.C., et al., *A conditional knockout resource for the genome-wide study of mouse gene function.* Nature, 2011. **474**(7351): p. 337-42.
47. Folger, K.R., et al., *Patterns of integration of DNA microinjected into cultured mammalian cells: evidence for homologous recombination between injected plasmid DNA molecules.* Mol Cell Biol, 1982. **2**(11): p. 1372-87.
48. Smithies, O., et al., *Insertion of DNA sequences into the human chromosomal beta-globin locus by homologous recombination.* Nature, 1985. **317**(6034): p. 230-4.
49. Thomas, K.R., K.R. Folger, and M.R. Capecchi, *High frequency targeting of genes to specific sites in the mammalian genome.* Cell, 1986. **44**(3): p. 419-28.
50. Jasin, M. and R. Rothstein, *Repair of strand breaks by homologous recombination.* Cold Spring Harb Perspect Biol, 2013. **5**(11): p. a012740.
51. Evans, M.J. and M.H. Kaufman, *Establishment in culture of pluripotential cells from mouse embryos.* Nature, 1981. **292**(5819): p. 154-6.
52. Bradley, A., et al., *Formation of germ-line chimaeras from embryo-derived teratocarcinoma cell lines.* Nature, 1984. **309**(5965): p. 255-6.
53. Mansour, S.L., K.R. Thomas, and M.R. Capecchi, *Disruption of the proto-oncogene int-2 in mouse embryo-derived stem cells: a general strategy for targeting mutations to non-selectable genes.* Nature, 1988. **336**(6197): p. 348-52.
54. McCarrick, J.W., 3rd, et al., *Positive-negative selection gene targeting with the diphtheria toxin A-chain gene in mouse embryonic stem cells.* Transgenic Res, 1993. **2**(4): p. 183-90.
55. Lewandoski, M., *Conditional control of gene expression in the mouse.* Nat Rev Genet, 2001. **2**(10): p. 743-55.
56. Guo, F., D.N. Gopaul, and G.D. van Duyne, *Structure of Cre recombinase complexed with DNA in a site-specific recombination synapse.* Nature, 1997. **389**(6646): p. 40-6.
57. Kano, M., et al., *Cre-loxP-mediated DNA flip-flop in mammalian cells leading to alternate expression of retrovirally transduced genes.* Biochem Biophys Res Commun, 1998. **248**(3): p. 806-11.
58. Sauer, B. and N. Henderson, *Cre-stimulated recombination at loxP-containing DNA sequences placed into the mammalian genome.* Nucleic Acids Res, 1989. **17**(1): p. 147-61.
59. Araki, K., M. Araki, and K. Yamamura, *Targeted integration of DNA using mutant lox sites in embryonic stem cells.* Nucleic Acids Res, 1997. **25**(4): p. 868-72.

60. Gu, H., et al., *Deletion of a DNA polymerase beta gene segment in T cells using cell type-specific gene targeting.* Science, 1994. **265**(5168): p. 103-6.
61. Orban, P.C., D. Chui, and J.D. Marth, *Tissue- and site-specific DNA recombination in transgenic mice.* Proc Natl Acad Sci U S A, 1992. **89**(15): p. 6861-5.
62. Giraldo, P. and L. Montoliu, *Size matters: use of YACs, BACs and PACs in transgenic animals.* Transgenic Res, 2001. **10**(2): p. 83-103.
63. Rickert, R.C., J. Roes, and K. Rajewsky, *B lymphocyte-specific, Cre-mediated mutagenesis in mice.* Nucleic Acids Res, 1997. **25**(6): p. 1317-8.
64. Rubtsov, Y.P., et al., *Regulatory T cell-derived interleukin-10 limits inflammation at environmental interfaces.* Immunity, 2008. **28**(4): p. 546-58.
65. Metzger, D., et al., *Conditional site-specific recombination in mammalian cells using a ligand-dependent chimeric Cre recombinase.* Proc Natl Acad Sci U S A, 1995. **92**(15): p. 6991-5.
66. Feil, R., et al., *Regulation of Cre recombinase activity by mutated estrogen receptor ligand-binding domains.* Biochem Biophys Res Commun, 1997. **237**(3): p. 752-7.
67. Lakso, M., et al., *Targeted oncogene activation by site-specific recombination in transgenic mice.* Proc Natl Acad Sci U S A, 1992. **89**(14): p. 6232-6.
68. Zambrowicz, B.P., et al., *Disruption of overlapping transcripts in the ROSA beta geo 26 gene trap strain leads to widespread expression of beta-galactosidase in mouse embryos and hematopoietic cells.* Proc Natl Acad Sci U S A, 1997. **94**(8): p. 3789-94.
69. Soriano, P., *Generalized lacZ expression with the ROSA26 Cre reporter strain.* Nat Genet, 1999. **21**(1): p. 70-1.
70. Schnutgen, F., et al., *A directional strategy for monitoring Cre-mediated recombination at the cellular level in the mouse.* Nat Biotechnol, 2003. **21**(5): p. 562-5.
71. Senecoff, J.F. and M.M. Cox, *Directionality in FLP protein-promoted site-specific recombination is mediated by DNA-DNA pairing.* J Biol Chem, 1986. **261**(16): p. 7380-6.
72. Buchholz, F., et al., *Different thermostabilities of FLP and Cre recombinases: implications for applied site-specific recombination.* Nucleic Acids Res, 1996. **24**(21): p. 4256-62.
73. Buchholz, F., P.O. Angrand, and A.F. Stewart, *Improved properties of FLP recombinase evolved by cycling mutagenesis.* Nat Biotechnol, 1998. **16**(7): p. 657-62.
74. Rohozinski, J., et al., *Successful targeting of mouse Y chromosome genes using a site-directed insertion vector.* Genesis, 2002. **32**(1): p. 1-7.
75. Wang, H., et al., *TALEN-mediated editing of the mouse Y chromosome.* Nat Biotechnol, 2013. **31**(6): p. 530-2.
76. Carroll, D., *Genome engineering with targetable nucleases.* Annu Rev Biochem, 2014. **83**: p. 409-39.
77. Lieber, M.R., *The mechanism of double-strand DNA break repair by the nonhomologous DNA end-joining pathway.* Annu Rev Biochem, 2010. **79**: p. 181-211.
78. Maeder, M.L., et al., *Rapid "open-source" engineering of customized zinc-finger nucleases for highly efficient gene modification.* Mol Cell, 2008. **31**(2): p. 294-301.
79. Sander, J.D. and J.K. Joung, *CRISPR-Cas systems for editing, regulating and targeting genomes.* Nat Biotechnol, 2014. **32**(4): p. 347-55.

80. Boch, J., et al., *Breaking the code of DNA binding specificity of TAL-type III effectors.* Science, 2009. **326**(5959): p. 1509-12.
81. Christian, M., et al., *Targeting DNA double-strand breaks with TAL effector nucleases.* Genetics, 2010. **186**(2): p. 757-61.
82. Briggs, A.W., et al., *Iterative capped assembly: rapid and scalable synthesis of repeat-module DNA such as TAL effectors from individual monomers.* Nucleic Acids Res, 2012. **40**(15): p. e117.
83. Cermak, T., et al., *Efficient design and assembly of custom TALEN and other TAL effector-based constructs for DNA targeting.* Nucleic Acids Res, 2011. **39**(12): p. e82.
84. Kim, Y., et al., *A library of TAL effector nucleases spanning the human genome.* Nat Biotechnol, 2013. **31**(3): p. 251-8.
85. Liang, J., et al., *FairyTALE: a high-throughput TAL effector synthesis platform.* ACS Synth Biol, 2014. **3**(2): p. 67-73.
86. Miller, J.C., et al., *A TALE nuclease architecture for efficient genome editing.* Nat Biotechnol, 2011. **29**(2): p. 143-8.
87. Reyon, D., et al., *FLASH assembly of TALENs for high-throughput genome editing.* Nat Biotechnol, 2012. **30**(5): p. 460-5.
88. Sanjana, N.E., et al., *A transcription activator-like effector toolbox for genome engineering.* Nat Protoc, 2012. **7**(1): p. 171-92.
89. Schmid-Burgk, J.L., et al., *A ligation-independent cloning technique for high-throughput assembly of transcription activator-like effector genes.* Nat Biotechnol, 2013. **31**(1): p. 76-81.
90. Davies, B., et al., *Site specific mutation of the Zic2 locus by microinjection of TALEN mRNA in mouse CD1, C3H and C57BL/6J oocytes.* PLoS One, 2013. **8**(3): p. e60216.
91. Li, C., et al., *Simultaneous gene editing by injection of mRNAs encoding transcription activator-like effector nucleases into mouse zygotes.* Mol Cell Biol, 2014. **34**(9): p. 1649-58.
92. Wefers, B., et al., *Direct production of mouse disease models by embryo microinjection of TALENs and oligodeoxynucleotides.* Proc Natl Acad Sci U S A, 2013. **110**(10): p. 3782-7.
93. Jones, J.M. and M.H. Meisler, *Modeling human epilepsy by TALEN targeting of mouse sodium channel Scn8a.* Genesis, 2014. **52**(2): p. 141-8.
94. Kanno, Y., et al., *Transcriptional and epigenetic control of T helper cell specification: molecular mechanisms underlying commitment and plasticity.* Annu Rev Immunol, 2012. **30**: p. 707-31.
95. Dickinson, L.A., et al., *A tissue-specific MAR/SAR DNA-binding protein with unusual binding site recognition.* Cell, 1992. **70**(4): p. 631-45.
96. Nakayama, Y., et al., *A nuclear targeting determinant for SATB1, a genome organizer in the T cell lineage.* Cell Cycle, 2005. **4**(8): p. 1099-106.
97. de Belle, I., S. Cai, and T. Kohwi-Shigematsu, *The genomic sequences bound to special AT-rich sequence-binding protein 1 (SATB1) in vivo in Jurkat T cells are tightly associated with the nuclear matrix at the bases of the chromatin loops.* J Cell Biol, 1998. **141**(2): p. 335-48.
98. Alvarez, J.D., et al., *The MAR-binding protein SATB1 orchestrates temporal and spatial expression of multiple genes during T-cell development.* Genes Dev, 2000. **14**(5): p. 521-35.
99. Kondo, M., et al., *SATB1 Plays a Critical Role in Establishment of Immune Tolerance.* J Immunol, 2016. **196**(2): p. 563-72.

100. Hao, B., et al., *An anti-silencer- and SATB1-dependent chromatin hub regulates Rag1 and Rag2 gene expression during thymocyte development.* J Exp Med, 2015. **212**(5): p. 809-24.
101. Kakugawa, K., et al., *Essential Roles of SATB1 in Specifying T Lymphocyte Subsets.* Cell Rep, 2017. **19**(6): p. 1176-1188.
102. Kitagawa, Y., et al., *Guidance of regulatory T cell development by Satb1-dependent super-enhancer establishment.* Nat Immunol, 2017. **18**(2): p. 173-183.
103. Seo, J., M.M. Lozano, and J.P. Dudley, *Nuclear matrix binding regulates SATB1-mediated transcriptional repression.* J Biol Chem, 2005. **280**(26): p. 24600-9.
104. Purbey, P.K., et al., *PDZ domain-mediated dimerization and homeodomain-directed specificity are required for high-affinity DNA binding by SATB1.* Nucleic Acids Res, 2008. **36**(7): p. 2107-22.
105. Purbey, P.K., et al., *Acetylation-dependent interaction of SATB1 and CtBP1 mediates transcriptional repression by SATB1.* Mol Cell Biol, 2009. **29**(5): p. 1321-37.
106. Galande, S., et al., *The third dimension of gene regulation: organization of dynamic chromatin loopscape by SATB1.* Curr Opin Genet Dev, 2007. **17**(5): p. 408-14.
107. Cai, S., H.J. Han, and T. Kohwi-Shigematsu, *Tissue-specific nuclear architecture and gene expression regulated by SATB1.* Nat Genet, 2003. **34**(1): p. 42-51.
108. Cai, S., C.C. Lee, and T. Kohwi-Shigematsu, *SATB1 packages densely looped, transcriptionally active chromatin for coordinated expression of cytokine genes.* Nat Genet, 2006. **38**(11): p. 1278-88.
109. Spilianakis, C.G. and R.A. Flavell, *Long-range intrachromosomal interactions in the T helper type 2 cytokine locus.* Nat Immunol, 2004. **5**(10): p. 1017-27.
110. Yasui, D., et al., *SATB1 targets chromatin remodelling to regulate genes over long distances.* Nature, 2002. **419**(6907): p. 641-5.
111. Ahlfors, H., et al., *SATB1 dictates expression of multiple genes including IL-5 involved in human T helper cell differentiation.* Blood, 2010. **116**(9): p. 1443-53.
112. Classen, S., *Novel aspects of TGFβ in human CD4+ T cell biology.* Unpublished Dissertation, 2008, University of Bonn.
113. Beyer, M., et al., *Repression of the genome organizer SATB1 in regulatory T cells is required for suppressive function and inhibition of effector differentiation.* Nat Immunol, 2011. **12**(9): p. 898-907.
114. Doyle, E.L., et al., *TAL Effector-Nucleotide Targeter (TALE-NT) 2.0: tools for TAL effector design and target prediction.* Nucleic Acids Res, 2012. **40**(Web Server issue): p. W117-22.
115. T., W., *Regulation of SATB1 in CD4⁺ T cells.* Unpublished Master Thesis, 2012, University of Bonn.
116. *Guide for the Care and Use of Laboratory Animals.*, in *Guide for the Care and Use of Laboratory Animals*. 2011, National Research Council (US) Committee for the Update of the Guide for the Care and Use of Laboratory Animals.: Washington (DC).
117. Guschin, D.Y., et al., *A rapid and general assay for monitoring endogenous gene modification.* Methods Mol Biol, 2010. **649**: p. 247-56.
118. Morrissey, P.J., et al., *CD4+ T cells that express high levels of CD45RB induce wasting disease when transferred into congenic severe combined*

immunodeficient mice. Disease development is prevented by cotransfer of purified CD4+ T cells. J Exp Med, 1993. **178**(1): p. 237-44.
119. Ostanin, D.V., et al., *T cell transfer model of chronic colitis: concepts, considerations, and tricks of the trade.* Am J Physiol Gastrointest Liver Physiol, 2009. **296**(2): p. G135-46.
120. Lund, R., et al., *Identification of genes involved in the initiation of human Th1 or Th2 cell commitment.* Eur J Immunol, 2005. **35**(11): p. 3307-19.
121. Ahern, P.P., et al., *Interleukin-23 drives intestinal inflammation through direct activity on T cells.* Immunity, 2010. **33**(2): p. 279-88.
122. Wefers, B., et al., *Generation of targeted mouse mutants by embryo microinjection of TALEN mRNA.* Nat Protoc, 2013. **8**(12): p. 2355-79.
123. Panda, S.K., et al., *Highly efficient targeted mutagenesis in mice using TALENs.* Genetics, 2013. **195**(3): p. 703-13.
124. Hermann, M., et al., *Evaluation of OPEN zinc finger nucleases for direct gene targeting of the ROSA26 locus in mouse embryos.* PLoS One, 2012. **7**(9): p. e41796.
125. Cui, X., et al., *Targeted integration in rat and mouse embryos with zinc-finger nucleases.* Nat Biotechnol, 2011. **29**(1): p. 64-7.
126. Sung, Y.H., et al., *Knockout mice created by TALEN-mediated gene targeting.* Nat Biotechnol, 2013. **31**(1): p. 23-4.
127. Pierce, A.J., et al., *Ku DNA end-binding protein modulates homologous repair of double-strand breaks in mammalian cells.* Genes Dev, 2001. **15**(24): p. 3237-42.
128. Auer, T.O., et al., *Highly efficient CRISPR/Cas9-mediated knock-in in zebrafish by homology-independent DNA repair.* Genome Res, 2014. **24**(1): p. 142-53.
129. Maresca, M., et al., *Obligate ligation-gated recombination (ObLiGaRe): custom-designed nuclease-mediated targeted integration through nonhomologous end joining.* Genome Res, 2013. **23**(3): p. 539-46.
130. Yoshimi, K., et al., *ssODN-mediated knock-in with CRISPR-Cas for large genomic regions in zygotes.* Nat Commun, 2016. **7**: p. 10431.
131. Ma, Y., et al., *Increasing the efficiency of CRISPR/Cas9-mediated precise genome editing in rats by inhibiting NHEJ and using Cas9 protein.* RNA Biol, 2016. **13**(7): p. 605-12.
132. Maruyama, T., et al., *Increasing the efficiency of precise genome editing with CRISPR-Cas9 by inhibition of nonhomologous end joining.* Nat Biotechnol, 2015. **33**(5): p. 538-42.
133. Chu, V.T., et al., *Increasing the efficiency of homology-directed repair for CRISPR-Cas9-induced precise gene editing in mammalian cells.* Nat Biotechnol, 2015. **33**(5): p. 543-8.
134. Nie, H., et al., *A role for SATB1, a nuclear matrix association region-binding protein, in the development of CD8SP thymocytes and peripheral T lymphocytes.* J Immunol, 2005. **174**(8): p. 4745-52.
135. Egerton, M., R. Scollay, and K. Shortman, *Kinetics of mature T-cell development in the thymus.* Proc Natl Acad Sci U S A, 1990. **87**(7): p. 2579-82.
136. Huesmann, M., et al., *Kinetics and efficacy of positive selection in the thymus of normal and T cell receptor transgenic mice.* Cell, 1991. **66**(3): p. 533-40.
137. Sledzinska, A., et al., *TGF-beta signalling is required for CD4(+) T cell homeostasis but dispensable for regulatory T cell function.* PLoS Biol, 2013. **11**(10): p. e1001674.

138. Atasoy, D., et al., *A FLEX switch targets Channelrhodopsin-2 to multiple cell types for imaging and long-range circuit mapping.* J Neurosci, 2008. **28**(28): p. 7025-30.
139. Vooijs, M., J. Jonkers, and A. Berns, *A highly efficient ligand-regulated Cre recombinase mouse line shows that LoxP recombination is position dependent.* EMBO Rep, 2001. **2**(4): p. 292-7.
140. McInnes, N., et al., *FOXP3 and FOXP3-regulated microRNAs suppress SATB1 in breast cancer cells.* Oncogene, 2012. **31**(8): p. 1045-54.
141. Morrison, P.J., S.J. Ballantyne, and M.C. Kullberg, *Interleukin-23 and T helper 17-type responses in intestinal inflammation: from cytokines to T-cell plasticity.* Immunology, 2011. **133**(4): p. 397-408.
142. Krausgruber, T., et al., *T-bet is a key modulator of IL-23-driven pathogenic CD4(+) T cell responses in the intestine.* Nat Commun, 2016. **7**: p. 11627.
143. Bending, D., et al., *Highly purified Th17 cells from BDC2.5NOD mice convert into Th1-like cells in NOD/SCID recipient mice.* J Clin Invest, 2009. **119**(3): p. 565-72.
144. Kebir, H., et al., *Preferential recruitment of interferon-gamma-expressing TH17 cells in multiple sclerosis.* Ann Neurol, 2009. **66**(3): p. 390-402.
145. Lee, Y.K., et al., *Late developmental plasticity in the T helper 17 lineage.* Immunity, 2009. **30**(1): p. 92-107.
146. Nurieva, R., et al., *Cutting edge: in vitro generated Th17 cells maintain their cytokine expression program in normal but not lymphopenic hosts.* J Immunol, 2009. **182**(5): p. 2565-8.
147. Izcue, A., et al., *Interleukin-23 restrains regulatory T cell activity to drive T cell-dependent colitis.* Immunity, 2008. **28**(4): p. 559-70.
148. Burkett, P.R., G. Meyer zu Horste, and V.K. Kuchroo, *Pouring fuel on the fire: Th17 cells, the environment, and autoimmunity.* J Clin Invest, 2015. **125**(6): p. 2211-9.
149. Feng, T., et al., *Th17 cells induce colitis and promote Th1 cell responses through IL-17 induction of innate IL-12 and IL-23 production.* J Immunol, 2011. **186**(11): p. 6313-8.
150. Harbour, S.N., et al., *Th17 cells give rise to Th1 cells that are required for the pathogenesis of colitis.* Proc Natl Acad Sci U S A, 2015. **112**(22): p. 7061-6.
151. Krawczyk, C.M., H. Shen, and E.J. Pearce, *Functional plasticity in memory T helper cell responses.* J Immunol, 2007. **178**(7): p. 4080-8.
152. Franckaert, D., et al., *Promiscuous Foxp3-cre activity reveals a differential requirement for CD28 in Foxp3(+) and Foxp3(-) T cells.* Immunol Cell Biol, 2015. **93**(4): p. 417-23.
153. Zhou, X., et al., *Selective miRNA disruption in T reg cells leads to uncontrolled autoimmunity.* J Exp Med, 2008. **205**(9): p. 1983-91.
154. Fayyad-Kazan, H., et al., *MicroRNA profile of circulating CD4-positive regulatory T cells in human adults and impact of differentially expressed microRNAs on expression of two genes essential to their function.* J Biol Chem, 2012. **287**(13): p. 9910-22.
155. Rouas, R., et al., *Human natural Treg microRNA signature: role of microRNA-31 and microRNA-21 in FOXP3 expression.* Eur J Immunol, 2009. **39**(6): p. 1608-18.

6 Appendix

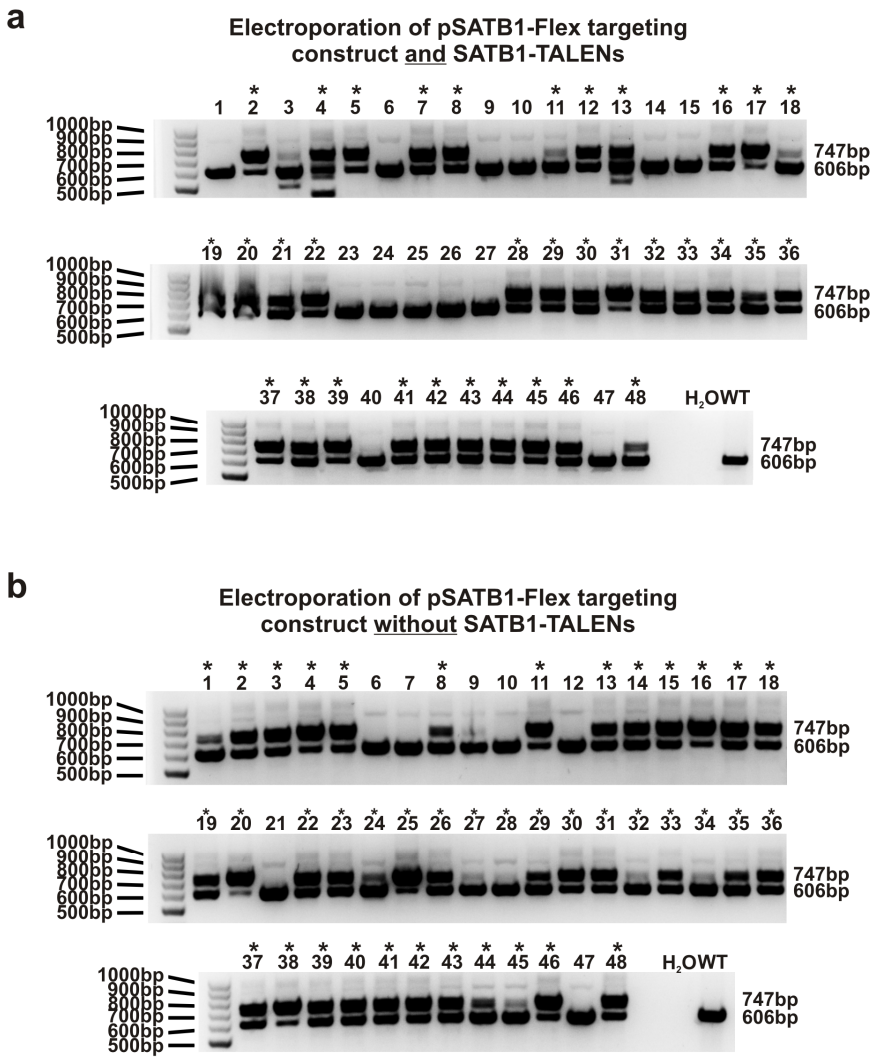

Figure 6.1 Analysis of genomic integration of the pSATB1-Flex targeting construct in ES cells treated with or without SATB1-TALENs
Agarose gel electrophoresis of the genotyping PCR (see Figure 3.9a) performed on genomic DNA of ES cell clones electroporated with or without TALEN plasmids (48 representative clones of each condition are shown).

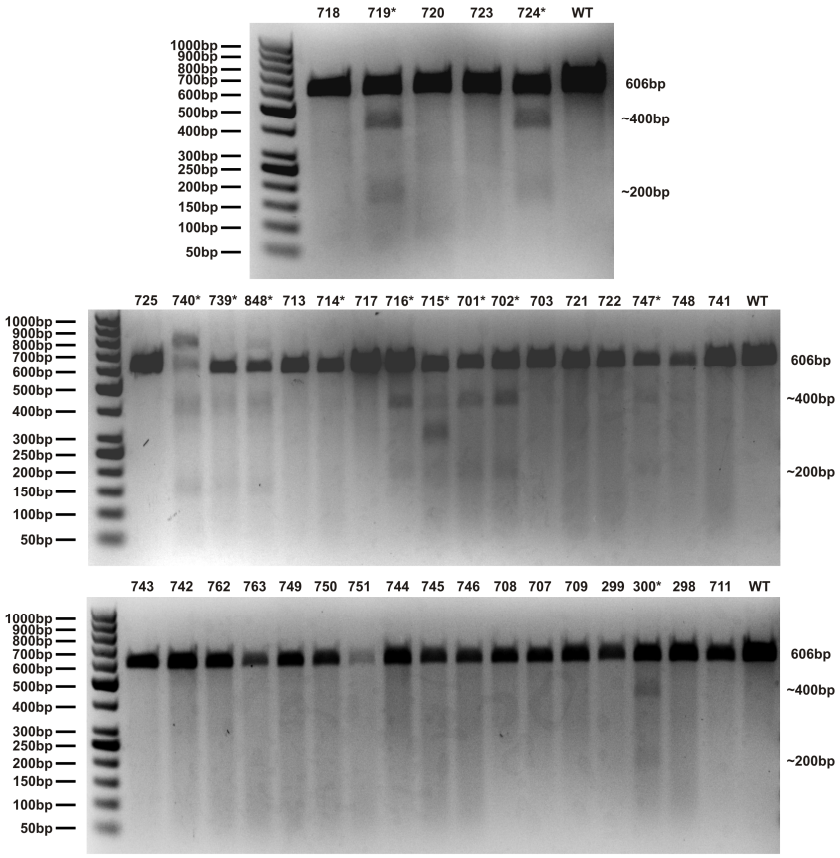

Figure 6.2 SATB1 mutation screening by Surveyor nuclease I assay of the first 39 mice derived from oocyte injections
Samples marked with an asterisk denote mice with TALEN-induced mutations determined by Surveyor assay.

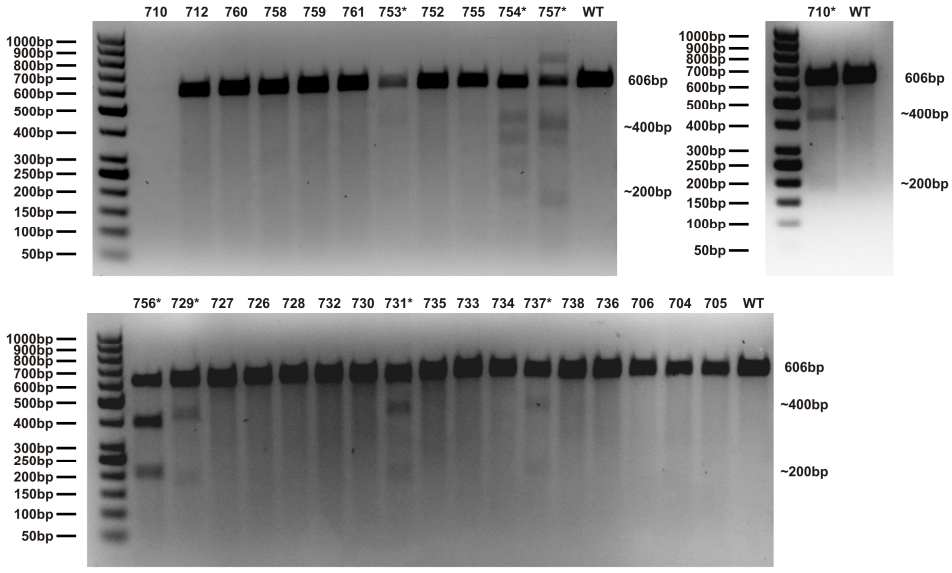

Figure 6.3 SATB1 mutation screening by Surveyor nuclease I assay of the remaining 28 mice derived from oocyte injections
Samples marked with an asterisk denote mice with TALEN-induced mutations determined by Surveyor assay

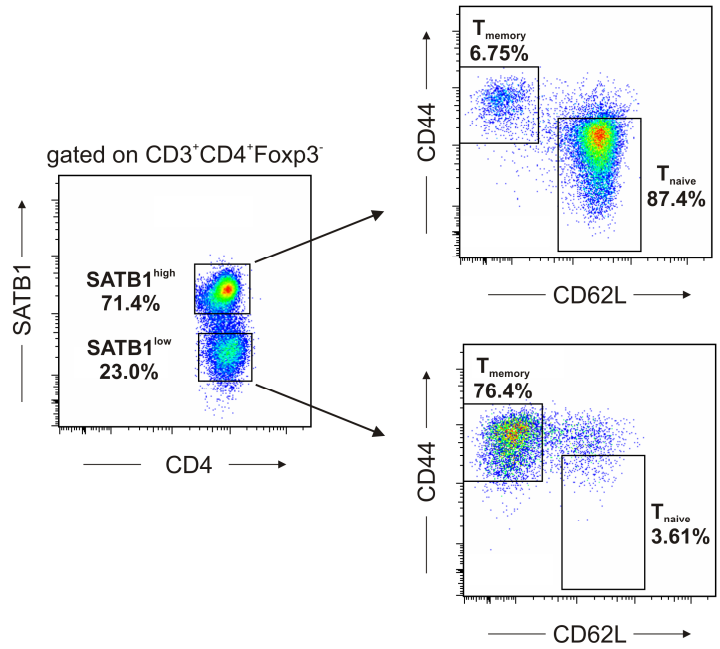

Figure 6.4 SATB1 expression in naive and memory T cells
Assessment of SATB1, CD44 and CD62L expression in murine conventional CD4⁺ WT T cells by flow cytometry. Representative dot plots illustrating SATB1 expression in Foxp3⁻ CD4⁺ conventional T cells (left panel) and expression of the naive and effector/memory T cell markers CD62L and CD44 in the respective SATB1 expressing cell subsets (right panels).

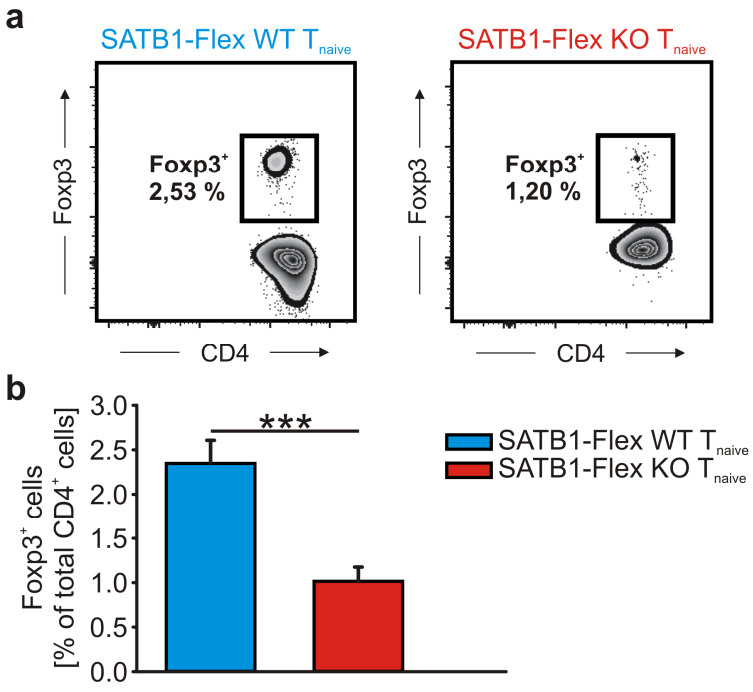

Figure 6.5 Development of SATB1-Flex KO T_{naive} cells into T_{reg} cells *in vivo*
Assessment of Foxp3 expression in CD4⁺ T cells isolated from mLNs of RAG2$^{-/-}$ mice injected with SATB1-sufficient or -deficient CD4⁺ T_{naive} cells. (a) Representative dot plots of Foxp3 staining in CD4⁺ T cells; (b) Quantification of Foxp3⁺ cells (n=4-5 per cohort; mean and standard deviation; ***P<0.001, n.s.: not significant, Student´s t-test)